



UCGE Reports
Number 20237

Department of Geomatics Engineering

**Performance Comparison of Kinematic GPS Integrated
with Different Tactical Grade IMUs**

(URL: <http://www.geomatics.ucalgary.ca/research/publications/GradTheses.html>)

by

Hai Tao (Haitao) Zhang

Jan 2006



THE UNIVERSITY OF CALGARY

**Performance Comparison of Kinematic GPS Integrated
with Different Tactical Grade IMUs**

By

Hai Tao(Haitao) Zhang

A THESIS

SUBMITTED TO THE FACULTY OF GRADUATE STUDIES
IN PARTIAL FULFILMENT OF THE REQUIREMENTS FOR THE
DEGREE OF MASTER OF SCIENCE

DEPARTMENT OF GEOMATICS ENGINEERING

CALGARY, ALBERTA

January, 2006

© Hai Tao(Haitao) Zhang 2006

ABSTRACT

With the decreasing cost of inertial measurement units (IMUs), the use of integrated GPS/INS (Global Positioning System/Inertial Navigation System) systems becomes more feasible for high-accuracy navigation. Improvements from the integration of GPS and tactical-grade inertial navigation systems have previously been investigated using the Honeywell HG1700 for high-accuracy vehicular applications. However, side-by-side testing of other tactical-grade inertial measurement units (IMUs) has not been done to assess whether the same improvements can be achieved when using the data collected simultaneously using more than one IMU. In this thesis, Honeywell HG1700 and Litton LN200 IMUs are independently integrated with a NovAtel OEM4 dual-frequency GPS receiver in the same test vehicle for high-accuracy positioning using GPS carrier phase observables. Improvements realized through the integration of GPS and these two tactical-grade INS's using different integration strategies are investigated. The performance in the position domain is measured through the system accuracy during complete GPS data outages of up to 100 seconds. The times to fix ambiguities after complete data outages are then used to measure the improvement in the ambiguity domain to assess how INS aiding affects the ambiguity resolution process, relative to the GPS-only solution. Initial results show that both integrated systems are capable of providing 2 to 4 centimetre accuracy with good GPS coverage with more than six GPS satellites

available and less than 4 GDOP values. Furthermore, a quantitative relationship between the free-inertial positioning accuracy after a GPS outage and the respective ambiguity resolution improvements with the aiding of inertial data is presented. In this thesis, a Rauch-Tung-Striebel (RTS) smoothing method is implemented and tested during different periods of GPS outages as well to investigate the smoothing technique in minimizing the position error during outages. Initial results show that smoothing can reduce the 3D RMS position errors by up to 96% for 100-second GPS data outages.

The assessment of the use of different ambiguity strategies on short baselines (less than 10 km) and long baselines (more than 50 km), in terms of position accuracy, will provide insight as to which ambiguity strategy is best suited in the presence of large differential errors. To give the criteria for ambiguity strategy selection under different scenarios, the ambiguity resolution strategies and their advantages and disadvantages under short and long baseline conditions were investigated.

ACKNOWLEDGEMENTS

The happiness of the crown of the year, in many ways, is not only attributed to the seeders but also to the many others who have helped seeders along their journey, both directly and indirectly. I would like to take this opportunity to express my gratitude to all of the people who have helped me during my studies at the University of Calgary. My only sorrow is not being able to thank everyone explicitly.

Firstly, I would like to express my heartfelt thanks and gratitude to my supervisor, Dr. Elizabeth Cannon for her continuous financial support, encouragement and confidence in me. Her help not only in academic, but also in life, during my studies made me enjoy my studies here.

Secondly, Dr. Gérard Lachapelle, Dr. Yang Gao, and Dr Mike Potter, members of my examining committee, are greatly appreciated for their efforts in reading through this thesis.

Thirdly, I would like to thank Dr. Mark Petovello, for his patience and understanding in answering my numerous questions. Other members in the PLAN group are also thanked including Dr. Gérard Lachapelle, John Schleppe

and Scott Crawford to name a few. Everyone who helped with my data collection for my thesis is thanked and these efforts are highly appreciated.

Fourthly, I would like to thank Dr. Naser El-Sheimy for sharing equipment and data that his group collected with NovAtel. Many members of Dr. El-Sheimy's group, especially Dr. Xiaoji Niu, and Mr. Haiying Hou are thanked for thoroughly teaching me how to operate the Applanix system.

Also, I would like to thank many friends and fellow graduate students - Zhi Jiang, Changlin Ma, Lei Dong, Bo Zheng, Dharshaka Karunanayake, Jianchen Gao, and Ning Luo for their help in many ways.

Finally, and most of all, I would like to thank my best love Yanmei who makes my life colourful and meaningful, due to her continuous encouragement support and belief in me; and for taking care of our baby.

DEDICATION

To my parents, my wife
and especially my baby Amey

The world is meaningful when my parents have me; the world is meaningful
when we have you, Amey.

TABLE OF CONTENTS

ABSTRACT.....	III
ACKNOWLEDGEMENTS.....	V
DEDICATION.....	VII
TABLE OF CONTENTS.....	VIII
LIST OF TABLES	XII
LIST OF FIGURES	XIV
NOTATION.....	XVIII
CHAPTER ONE - INTRODUCTION	1
1.1 BACKGROUND AND OBJECTIVES	2
1.1.1 Global Positioning System (GPS)	3
1.1.2 Inertial Navigation Systems (INS).....	7
1.1.3 INS/GPS Integration	8
1.1.4 Backward Smoothing.....	11
1.1.5 Objectives.....	14
1.2 THESIS OUTLINE	17
CHAPTER TWO - OVERVIEW OF GPS AND INS	20
2.1 OVERVIEW OF THE GLOBAL POSITIONING SYSTEM.....	20
2.1.1 Basic Concepts.....	21
2.1.2 GPS Observables	25
2.1.3 GPS Error Sources.....	29
2.2 INS CONCEPTS.....	41

2.2.1	<i>Principles of INS</i>	41
2.2.2	<i>INS Mechanization</i>	44
2.2.3	<i>Inertial Sensor Error Equations</i>	45
2.3	GPS/INS INTEGRATION	48
2.3.1	<i>GPS/INS Integration Architectures</i>	49
CHAPTER THREE - OVERVIEW OF CARRIER PHASE INTEGER AMBIGUITY		
	RESOLUTION	54
3.1	OVERVIEW OF AMBIGUITY RESOLUTION	54
3.2	OVERVIEW OF AMBIGUITY SEARCH TECHNIQUES	60
3.3	AMBIGUITY SEARCH TECHNIQUES	63
3.3.1	<i>Classification of Ambiguity Search Techniques</i>	63
3.3.2	<i>LAMBDA Method</i>	66
3.3.3	<i>Ambiguity Resolution Improvements with Aiding of Inertial Data</i>	71
3.4	OVERVIEW OF GPS OBSERVABLES – GPS INTER-FREQUENCY CARRIER PHASE COMBINATION	78
3.5	AMBIGUITY ESTIMATION PROCESSING STRATEGIES	84
CHAPTER FOUR - OPTIMAL BACKWARD SMOOTHING FOR BRIDGING POSITION		
	ERROR DURING GPS OUTAGES	88
4.1	INS/GPS EXTENDED KALMAN FILTER	88
4.2	BACKWARD SMOOTHING ALGORITHMS	91
4.2.1	<i>Smoother Basic</i>	92
4.3	RAUCH-TUNG-STRIEBEL (RTS) SMOOTHER	95
CHAPTER FIVE - FIELD TESTING DESCRIPTION AND DATA PROCESSING100		
5.1	SYSTEMS OVERVIEW	100

5.1.1	<i>Equipment and Field Testing</i>	100
5.1.2	<i>Processing Software</i>	108
5.2	REFERENCE TRAJECTORY GENERATION.....	110
5.2.1	<i>Short Baseline GPS-Only Solution</i>	111
5.2.2	<i>Short Baseline INS/CDGPS Integration Solution</i>	114
5.2.3	<i>GPS Data Outage Simulation</i>	118
5.2.4	<i>Data Analysis Strategy</i>	120
CHAPTER SIX - PERFORMANCE COMPARISON OF TWO INTEGRATED SYSTEMS.....		123
6.1	COMPARISON IN POSITION DOMAIN	123
6.2	COMPARISON IN THE AMBIGUITY RESOLUTION DOMAIN	129
6.3	AMBIGUITY RESOLUTION IMPROVEMENTS WITH AIDING OF INERTIAL DATA	135
6.4	RTS BACKWARD SMOOTHING TEST RESULTS	142
CHAPTER SEVEN - AMBIGUITY PROCESSING STRATEGY PERFORMANCE		
COMPARISON		147
7.1	DEFINITION OF EACH AMBIGUITY PROCESSING STRATEGIES	149
7.1.1	<i>Strategy 1 (L1)</i>	149
7.1.2	<i>Strategy 2 (WL)</i>	149
7.1.3	<i>Strategy 3 (L1L2)</i>	150
7.1.4	<i>Strategy 4 (L1WL)</i>	150
7.1.5	<i>Strategy 5 (IF)</i>	151
7.1.6	<i>Strategy 6 (L1WL+I)</i>	152
7.1.7	<i>Strategy 7 (L1L2+I)</i>	153
7.2	SHORT BASELINE TESTS AND RESULTS.....	155
7.2.1	<i>Ambiguity Processing Strategy Differences in Position Domain</i>	155
7.2.2	<i>Ambiguity Processing Strategy Differences in the Ambiguity Domain</i>	165

7.3	LONG BASELINE TESTS AND RESULTS	167
CHAPTER EIGHT - CONCLUSIONS AND RECOMMENDATIONS		178
REFERENCES.....		186
APPENDIX A		194
APPENDIX B		196
APPENDIX C		206
C.1	PROCESSING STRATEGY AND GPS MEASUREMENTS PARAMETERS	206
C.2	INS ERROR MODEL PARAMETERS	207
C.3	GPS DYNAMIC MODEL PARAMETERS	208
APPENDIX D		209
APPENDIX E		212

LIST OF TABLES

2.1	MAGNITUDES OF SPATIALLY CORRELATED DD ERROR SOURCES.....	37
2.2	MAGNITUDES OF NON-SPATIALLY CORRELATED GPS ERROR SOURCES	40
3.1	ACHIEVABLE ACCURACY VS. DIFFERENT POSITIONING CHOICE	56
3.2	INTER-FREQUENCY CARRIER PHASE COMBINATION CHARACTERISTICS	84
3.3	PROCESSING STRATEGY SUMMARY.....	85
5.1	IMU SPECIFICATIONS.....	107
5.2	SAINTTM AMBIGUITY PROCESSING STRATEGY SUMMARY.....	109
5.3	RMS OF CORRECTIONS TO INS POSITION AND VELOCITY ERRORS STATES USING A TIGHT INTEGRATION WITHOUT DATA OUTAGES	115
5.4	RMS DIFFERENCE BETWEEN POSITIONS COMPUTED USING LOOSE AND TIGHT INTEGRATION STRATEGIES WITHOUT DATA OUTAGE	116
5.5	MEAN OF ABSOLUTE FIXED L1 CARRIER PHASE RESIDUALS COMPUTED USING DIFFERENT INTEGRATION STRATEGIES.....	117
6.1	AVERAGE PERCENT IMPROVEMENT IN L1 AMBIGUITY RESOLUTION TIMES AFTER COMPLETE DATA OUTAGES USING DIFFERENT APPROACHES.....	135
6.2	AVERAGE MAXIMUM VALUE OF POSITION ERROR CROSS ALL 9 SIMULATED 100-SECOND GPS OUT-AGES BEFORE AND AFTER RTS SMOOTHING (HG1700/GPS).....	145
6.3	AVERAGE MAXIMUM VALUE OF POSITION ERROR CROSS ALL 9 SIMULATED 100-SECONDS GPS OUTAGES BEFORE AND AFTER RTS SMOOTHING (LN200/GPS)	145
7.1	ESTIMATOR CONVERGENCE SPEED COMPARISON USING EACH AMBIGUITY PROCESSING STRATEGY.....	154
7.2	RMS OF OVERALL POSITION DIFFERENCE COMPARE TO SHORT BASELINE TIGHT INTEGRATION L1 SOLUTION (HG1700/CDGPS SYSTEM, SHORT BASELINE)	157
7.3	RMS OF OVERALL POSITION DIFFERENCE COMPARE TO SHORT BASELINE TIGHT	

	INTEGRATION L1 SOLUTION (LN200/CDGPS SYSTEM, SHORT BASELINE).....	157
7.4	RMS OF OVERALL POSITION DIFFERENCE COMPARE TO SHORT BASELINE TIGHT	
	INTEGRATION L1 SOLUTION (HG1700/CDGPS SYSTEM, LONG BASELINE).....	169
C.1	OBSERVATION STANDARD DEVIATIONS.....	207
C.2	ESTIMATED ERROR MODEL PARAMETERS.....	208

LIST OF FIGURES

2.1	GPS SATELLITES CONSTELLATION	23
2.2	GPS CONTROL SEGMENT	24
2.3	DOUBLE DIFFERENCING CONCEPT	27
2.4	REFRACTION OF GPS SIGNALS IN THE EARTH'S ATMOSPHERE	31
2.5	MULTIPATH SKETCH MAP	38
2.6	MECHANIZATION IN EARTH CENTER EARTH FIXED FRAME	44
2.7	GPS/INS INFORMATION FLOW DIAGRAM USING LOOSE INTEGRATION STRATEGY	51
2.8	GPS/INS INFORMATION FLOW DIAGRAM USING TIGHT INTEGRATION STRATEGY	52
3.1	GEOMETRICAL INTERPRETATION OF AMBIGUITY	55
3.2	AMBIGUITY SEARCH TECHNIQUES CLASSIFICATION	65
4.1	FORWARD AND BACKWARD KALMAN FILTER.....	93
5.1	SOUTHERN ALBERTA NETWORK, LOCAL AND REMOTE BASE.....	102
5.2	REMOTE AND LOCAL GPS REFERENCE STATION SETUP (LEFT IS REMOTE).....	103
5.3	KP INDEX BEFORE AND AFTER DATA COLLECTION PERIOD.....	104
5.4	TEST HARDWARE SETUP SHOWING THE ROVER ANTENNA, HG1700 IMU AND LN200 IMU.....	104
5.5	TEST TRAJECTORY WRT LOCAL REFERENCE STATION	105
5.6	ESTIMATED VEHICLE VELOCITIES USING TIGHT COUPLING SHORT BASELINE SOLUTION	106
5.7	ABSOLUTE VALUE OF GPS-ONLY SOLUTION FIXED AMBIGUITY L1 CARRIER PHASE RESIDUALS VS. BASELINE LENGTH WITHOUT DATA OUTAGES (UPPER PLOT); NUMBER OF SATELLITES VISIBLE, AND NUMBER OF SATELLITES WITH AMBIGUITIES FIXED (LOWER PLOT)	114
5.8	BASELINE LENGTH AND THE STARTING POINTS OF EACH OF THE SIMULATED GPS OUTAGES.....	119
6.1	GPS/HG1700 INTEGRATED SYSTEM 3-D RMS ERRORS AND AVERAGE ESTIMATED STANDARD DE-VIATIONS DURING ALL COMPLETE DATA OUTAGES USING L1 CARRIER PHASE UPDATES AND A TIGHT INTEGRATION.....	125

6.2	GPS/LN200 INTEGRATED SYSTEM 3-D RMS ERRORS AND AVERAGE ESTIMATED STANDARD DEVIATIONS DURING ALL COMPLETE DATA OUTAGES USING L1 CARRIER PHASE UPDATES AND A TIGHT INTEGRATION.....	126
6.3	AVERAGE TIME TO FIX L1 CARRIER PHASE AMBIGUITIES AFTER COMPLETE DATA OUTAGES FOR CDGPS/HG1700	130
6.4	AVERAGE TIME TO FIX L1 CARRIER PHASE AMBIGUITIES AFTER COMPLETE DATA OUTAGES FOR CDGPS/LN200.....	131
6.5	TIME TO FIX L1 AMBIGUITIES AFTER EACH COMPLETE GPS DATA OUTAGES (CDGPS/HG1700).....	132
6.6	TIME TO FIX L1 AMBIGUITIES AFTER EACH COMPLETE GPS DATA OUTAGES (CDGPS/LN200)	133
6.7	TIME TO FIX L1 AMBIGUITY IMPROVEMENTS AFTER EACH COMPLETE GPS OUTAGES AND EACH DURATION VS. CORRESPONDING ESTIMATED STD OF FILTER USING TIGHT COUPLING	137
6.8	TIME TO FIX L1 AMBIGUITY IMPROVEMENTS AFTER EACH COMPLETE GPS OUTAGES AND EACH DURATION VS. CORRESPONDING ESTIMATED STD OF FILTER USING LOOSE COUPLING	138
6.9	TIME TO FIX L1 AMBIGUITY IMPROVEMENTS AFTER EACH COMPLETE GPS OUTAGES AND EACH DURATION VS. CORRESPONDING ESTIMATED STD OF FILTER USING TIGHT COUPLING	140
6.10	TIME TO FIX L1 AMBIGUITY IMPROVEMENTS AFTER EACH COMPLETE GPS OUTAGES AND EACH DURATION VS. CORRESPONDING ESTIMATED STD OF FILTER USING LOOSE COUPLING	141
6.11	AVERAGE ABSOLUTE POSITION ERROR ACROSS ALL 9 SIMULATED GPS OUTAGES BEFORE AND AFTER RTS SMOOTHING (HG1700/GPS SYSTEM).....	143
6.12	AVERAGE ABSOLUTE POSITION ERROR ACROSS ALL 9 SIMULATED GPS OUTAGES BEFORE AND AFTER RTS SMOOTHING (LN200/GPS SYSTEM)	144
7.1	POSITION DIFFERENCE L1L2 STRATEGY COMPARED TO REFERENCE TRAJECTORY	160
7.2	POSITION DIFFERENCE L1WL STRATEGY COMPARED TO REFERENCE TRAJECTORY.....	161
7.3	POSITION DIFFERENCE L1L2+I STRATEGY COMPARED TO REFERENCE TRAJECTORY.....	162

7.4	POSITION DIFFERENCE L1WL+I STRATEGY COMPARED TO REFERENCE TRAJECTORY	163
7.5	POSITION DIFFERENCE WL STRATEGY COMPARED TO REFERENCE TRAJECTORY	164
7.6	POSITION DIFFERENCE IF STRATEGY COMPARED TO REFERENCE TRAJECTORY	165
7.7	TIME TO FIX CORRESPONDING AMBIGUITIES AFTER 9, 20, 50 AND 100 SECONDS OUTAGE AT OUTAGE NUMBER 2 USING DIFFERENT AMBIGUITY PROCESSING STRATEGIES (HG1700/CDGPS SYSTEM, GPS- ONLY).....	166
7.8	POSITION DIFFERENCE L1 STRATEGY COMPARED TO REFERENCE TRAJECTORY	171
7.9	POSITION DIFFERENCE L1L2 STRATEGY COMPARED TO REFERENCE TRAJECTORY	172
7.10	POSITION DIFFERENCE L1L2+I STRATEGY COMPARED TO REFERENCE TRAJECTORY	173
7.11	POSITION DIFFERENCE WL STRATEGY COMPARED TO REFERENCE TRAJECTORY	174
7.12	POSITION DIFFERENCE L1WL STRATEGY COMPARED TO REFERENCE TRAJECTORY	175
7.13	POSITION DIFFERENCE L1WL+I STRATEGY COMPARED TO REFERENCE TRAJECTORY	176
7.12	POSITION DIFFERENCE IF STRATEGY COMPARED TO REFERENCE TRAJECTORY	177
A.1	DOP VALUE DURING DATA COLLECTION	194
A.2	SATELLITE ELEVATION ANGLE DURING DATA COLLECTION.....	195
B.1	POSITION ERROR AT GPS OUTAGE #1 (HG1700/CDGPS).....	196
B.2	POSITION ERROR AT GPS OUTAGE #2 (HG1700/CDGPS).....	197
B.3	POSITION ERROR AT GPS OUTAGE #3 (HG1700/CDGPS).....	197
B.4	POSITION ERROR AT GPS OUTAGE #4 (HG1700/CDGPS).....	198
B.5	POSITION ERROR AT GPS OUTAGE #5 (HG1700/CDGPS).....	198
B.6	POSITION ERROR AT GPS OUTAGE #6 (HG1700/CDGPS).....	199
B.7	POSITION ERROR AT GPS OUTAGE #7 (HG1700/CDGPS).....	199
B.8	POSITION ERROR AT GPS OUTAGE #8 (HG1700/CDGPS).....	200
B.9	POSITION ERROR AT GPS OUTAGE #9 (HG1700/CDGPS).....	200
B.10	POSITION ERROR AT GPS OUTAGE #1 (LN200/CDGPS)	201
B.11	POSITION ERROR AT GPS OUTAGE #2 (LN200/CDGPS)	201

B.12 POSITION ERROR AT GPS OUTAGE #3 (LN200/CDGPS)	202
B.13 POSITION ERROR AT GPS OUTAGE #4 (LN200/CDGPS)	202
B.14 POSITION ERROR AT GPS OUTAGE #5 (LN200/CDGPS)	203
B.15 POSITION ERROR AT GPS OUTAGE #6 (LN200/CDGPS)	203
B.16 POSITION ERROR AT GPS OUTAGE #7 (LN200/CDGPS)	204
B.17 POSITION ERROR AT GPS OUTAGE #8 (LN200/CDGPS)	204
B.18 POSITION ERROR AT GPS OUTAGE #9 (LN200/CDGPS)	205
D.1 ESTIMATED DD IONOSPHERIC DELAY VS. BASELINE LENGTH VS. GPS TIME	210
D.2 ESTIMATED DD IONOSPHERIC DELAY VS. BASELINE LENGTH VS. GPS TIME	211

NOTATION

Symbols

c	speed of light (m/s)
P	pseudorange observation (m)
CP	carrier phase observation (cycle)
ρ	true range between GPS satellite and receiver (m)
$d\rho$	orbital error (m)
T	tropospheric effect (m)
I	ionospheric effect (m)
dT_u^0	receiver clock error (s)
dT_0^s	satellite clock error (s)
λ	carrier wavelength (m)
N	integer carrier phase ambiguities (cycles)
ε_p	measurement noise and multipath on pseudorange (m)
ε_{CP}	measurement noise and multipath on carrier phase (cycle)
$\Delta, \nabla\Delta$	single difference (D) and double difference (DD) operators
$\delta\mathbf{p}$	3 position errors
$\delta\mathbf{v}$	3 velocity errors
\mathbf{F}	skew-symmetric matrix of specific force
ε	3 attitude errors (misalignments)

N	tensor of gravitational gradients
Ω_{in}^n	skew-symmetric matrix of the rotation rate of the navigation frame relative to inertial space seen from navigation frame
\mathbf{R}_b^n	rotation matrix from the body frame to the navigation frame
d	3 gyro drifts
b	3 accelerometer biases
α, β	parameters for modeling the drift and bias terms as first-order Gauss-Markov process
$\mathbf{w}_{i=1,2,3,4}$	noise term
p	position vector
v	velocity vector
$\boldsymbol{\omega}$	rotation rate vector
$\boldsymbol{\Omega}$	skew-symmetric form of the rotation rate vector
\mathbf{f}^b	specific force measurements
$\boldsymbol{\omega}_{ib}^b$	angular rate measurements

Abbreviations and Acronyms

C/A	Coarse Acquisition
CDGPS	Carrier phase Differential GPS
DD	Double Difference
DGPS	Differential GPS

FASF	Fast Ambiguity Search Filter
GM	Gauss-Markov
GPS	Global Positioning System
IF	Ionospheric Free
IMU	Inertial Measurement Units
INS	Inertial Navigation System
LAMBDA	Least Squares Ambiguity Search Adjustment
MultiRef	Multiple Reference
NL	Narrowlane
P-Code	Precise Code
PPS	Precise Positioning Service
PRN	Pseudorandom Noise
RF	Radio Frequency
RMS	Root Mean Square
RTK	Real Time Kinematic
RTS	Rauch-Tung-Striebel
SA	Selective Availability
SD	Single Difference
SPS	Standard Positioning Service
STD	Standard Deviation
TEC	Total Electron Content
VC	Variance Covariance

VRS	Virtual Reference Station
WAAS	Wide Area Augmentation System
WGS84	World Geodetic System of 1984
WL	Widelane
ZUPTS	Zero Velocity Updates

CHAPTER ONE - INTRODUCTION

With the ever-increasing demand for precise position and navigation information, much effort has been invested in improving positioning systems in terms of extending the achievable precision as well as mitigating signal disturbances. The integration of a tactical-grade inertial measurement unit (IMU), such as the Honeywell HG1700, with kinematic carrier phase differential Global Positioning System (CDGPS) has successfully achieved centimetre-level positioning accuracy for vehicular applications (Scherzinger, 2000; Petovello *et al.*, 2001; Leach *et al.*, 2003; Petovello, 2003a). Furthermore, these results demonstrate a 50% to 80% average improvement in the time needed to re-fix L1 integer ambiguities after complete GPS data outages of 40 seconds using loose and tight coupling integration approaches, respectively (Petovello, 2003a). However, to this point, no quantitative measure of how different quality IMUs affect the integrated system performance in terms of position accuracy and ambiguity resolution improvements has been done using side-by-side testing.

This thesis aims to evaluate the performance of kinematic GPS integrated with two different tactical-grade IMUs in terms of free-inertial (INS alone) position accuracy during - and ambiguity resolution performance after - GPS data outages. As part of the investigation, various integration strategies are also

considered to determine if the integration strategy affects the system performance. The research to be conducted proposes to evaluate the performance of kinematic GPS integrated with two different tactical grade IMUs, namely the LN200 and the HG1700. The performance of these two integrated systems will be compared in terms of position, and ambiguity resolution. The ambiguity resolution strategies given in Liu (2003) will be augmented by implementing various approaches which will be further investigated in Chapters Three and Seven. Since Petovello (2003a, 2003b) looked only at relatively short baselines (less than 8 km), the impact of long baselines (longer than 60 km) on the performance of the integrated system will also be evaluated in this research. In addition, the application of backward smoothing to improve the accuracy of the integrated system during GPS data outages in post-mission will also be investigated.

The following section describes some of the work done previously in this area and further details on the proposed objectives and approaches.

1.1 BACKGROUND AND OBJECTIVES

The following subsections review the advantages and disadvantages of GPS and INS technologies. That will further provide motivation for an integrated

approach. Some GPS and INS related concepts and applications are also described.

1.1.1 GLOBAL POSITIONING SYSTEM (GPS)

The Global Positioning System (GPS), composed of a constellation of satellites, broadcasts signals that can be used to derive precise time, location, and velocity information. Standard GPS position estimates can achieve accuracy on the order of metres to centimetres (Lachapelle, 2003), depending on the measurements and methods employed. To this end, GPS position estimates can achieve accuracies at the centimetre level by using carrier phase observables combined with differential GPS techniques involving two (or more) GPS receivers. This high accuracy positioning capability is required by many applications such as automated vehicle position control sub-systems within an automated highway system (AHS). However, a navigation system based solely on GPS still has some issues to be resolved to achieve such a high accuracy.

The first issue is to resolve the initially unknown number of cycles between the receiver and a satellite, which is referred to as the ambiguity. Only after these ambiguities are resolved to their integer values is centimetre-level positioning possible (Kaplan, 1996; Lachapelle, 2003). Much research has therefore been focused on resolving the integer ambiguities in as short a time as possible, and

several algorithms have been developed such as the Fast Ambiguity Search Filter (FASF) (Chen, 1994) and Least-squares Ambiguity Decorrelation Adjustment (LAMBDA) (Teunissen *et al.*, 1994). Han and Rizos (1997), Hein and Werner (1995) and Hatch (1994) discussed the performance of these and other algorithms. Further information about ambiguity search techniques will be investigated in Chapter Three.

The second issue is to eliminate errors affecting carrier phase measurements such as atmospheric, satellite-based, and receiver clock errors and, in this case, double-differencing provides an effective way of eliminating or mitigating the effects of such errors (Lachapelle, 2003). Although it can eliminate satellite and receiver clock error, double differencing reduces only the spatially correlated atmospheric and orbital errors with the residual error being a function of user-reference station separation. Multipath and receiver noise cannot be reduced by double differencing but are, instead, amplified. Therefore, errors will remain after double differencing which will affect integer ambiguity resolution. De Jong *et al.* (2002) have identified the general rule of thumb that instantaneous ambiguity resolution is possible if the position accuracy (along the line-of-sight to the satellite) is known to better than half of the wavelength of the ambiguities being resolved.

Research has been conducted to reduce the spatially correlated atmospheric

errors, including modeling of the ionospheric error (Skone, 1998), the tropospheric error (Zhang, 1999) and composite error effects (Raquet, 1998). Extensive research on mitigating carrier phase multipath has also been conducted, including the development of an antenna array method (Ray, 2000) and a signal processing-based method (Axelard *et al.*, 1996; Comp and Axelard, 1998). However, despite such efforts, problems remain; for example, because both the ionospheric error modeling method given by Skone (1998), and the tropospheric error modeling method given by Zhang (1999), require more than one reference station to predict the corresponding atmospheric error, many of the techniques developed are inapplicable to kinematic positioning using a single reference station.

The third issue is maintaining carrier phase lock. Precise kinematic positioning requires continuous tracking of the carrier phase. The loss of phase lock, which leads to discontinuous phase measurements, generates cycle slips. If a cycle slip is detected, the first option is to try to correct the ambiguity by the number of cycles slipped (Cannon, 1991). If this approach is unsuccessful, the associated ambiguity can be estimated as a real value and determined using one of the appropriate search techniques (Cannon, 1990). However, for the processing of GPS-only measurements, detection and correction of cycle slips require sophisticated algorithms that track a large number of satellites for detection and correction.

Fourthly, the use of GPS-only measurements is possible only if four or more satellites can be tracked at the same time to get a position estimation. However, the maximum expected power of a satellite's signal, after traveled more than 20,000 km from a satellite orbit all the way to the Earth, are in the order of only -153 dBW (Spilker, 1996; Misra and Enge, 2001). Hence, loss of lock is common in certain applications such as vehicular navigation in urban areas. This can result in poor positioning accuracy and/or position unavailability because of measurement outages. In order to improve the position accuracy in case of a GPS outage, Nassar (2003), and Shin and El-Sheimy (2002) tried backward smoothing techniques to bridge the position accuracy during GPS outages in post-mission.

Finally, since exploitation of the integer nature of the ambiguities allows for high-accuracy position estimates, recent efforts have focused on decreasing the time needed for re-determining integer ambiguities after loss of lock. The faster the ambiguity resolution process, the faster the system will be able to return to the highest accuracy level. So the efforts using aiding information, e.g. INS, to help re-determine integer ambiguities after GPS outages have been made recently. More than a 50% to 80% average improvement in L1 ambiguity resolution times after complete data outages has been achieved using a loosely and tightly coupled GPS/INS integration approach, respectively compared to a GPS-only

approach (Petovello, 2003a).

1.1.2 INERTIAL NAVIGATION SYSTEMS (INS)

Unlike GPS, which typically updates position and velocity at 1 Hz intervals (although some receivers have 10 Hz and higher capabilities), an inertial navigation system (INS) can provide the vehicle state information at rates of at least 10 Hz. However, an INS has its disadvantages as well.

The main disadvantage of an unaided INS is unbounded growth in the position estimation error owing to the nature of an INS. System inaccuracies, such as gyro drifts and accelerometer biases, cause a rapid degradation in position quality. The degradation speed is dependent on the sensor quality. To overcome this drawback, the use of higher quality units, which exhibit significantly lower position degradation, is one option. However, higher quality units are very expensive. Therefore, providing an INS with regular updates in order to limit the errors to a reasonable level – a task that is commonly achieved through the use of zero velocity updates (ZUPTS) – is another option (Jekeli, 2000; Masson *et al.*, 1996). However, in many applications such as aviation, periodic stops of the carrier are impractical. Many other means of bounding INS errors have been developed over the past few decades, such as position markers that are sensed by the vehicle to be positioned (Ebert *et al.*, 1994), and external velocity sensors

such as Electromagnetic (EM) logs (Carvill, 1993). Generally, an INS system used in conjunction with aiding sensors can provide the state estimate at the desired control frequency more accurately than either technique used independently. Most recently, much research has been focused on using GPS position and velocity (or measurement) updates to bound INS errors, despite the fact that GPS has high frequency errors while an INS typically does not.

1.1.3 INS/GPS INTEGRATION

As described in the previous sections, INS and GPS possess complementary characteristics (Greenspan, 1996; Škaloud, 1998) that makes integration in a common positioning system ideal (Greenspan, 1996). Each system compensates for the other's shortcomings. However, most research conducted to date has focused on the use of high-end inertial equipment. Although these allow for good navigation performance, their high cost is a serious limitation. Therefore lower cost and, hence, poorer quality IMUs must be investigated as possible alternatives. Extensive research has been performed to investigate the potential benefits when GPS is integrated with poorer quality IMUs (Petovello *et al.*, 2001; Scherzinger, 2002; Petovello, 2003a; Leach *et al.*, 2003). The aiding of INS can improve GPS performance in many aspects.

The first obvious performance improvements delivered by GPS aiding of an INS

are smooth, high data rate, and high accuracy data updates. Kinematic carrier phase GPS, with a 1 to 10 Hz update rate, provides high accuracy (centimetre level to this end) position and velocity information. The INS estimates states without differentiation (low sensitivity to high-frequency noise) at a very high data update rate.

The second GPS aiding technique for INS performance improvement is carrier phase ambiguity resolution. Generally speaking, the size of the search space is an important predictor of ambiguity resolution, and relates directly to the success of the ambiguity resolution process. An INS can provide position and velocity information to GPS, following which the INS can influence the size of the ambiguity search space. Škaloud (1998), Teunissen (1996), and Scherzinger (2000, 2002) describe how the inclusion of high-quality inertial measurements affects the size of the ambiguity search space in such a way that the ambiguity resolution process benefits. Petovello (2003a) achieved more than a 50% to 80% average improvement in L1 ambiguity resolution times after complete data outages using loosely and tightly coupled integration approaches, respectively, through GPS aiding of an HG1700 IMU. In most cases, using inertial data will result in greater applicability of the on-the-fly (OTF) search algorithm since the ambiguities can be determined over shorter time spans and with fewer satellites. The availability of INS position and velocity information can shorten the ambiguity search time, if such a search is even necessary, after short GPS data

outages. Reduction of the on-the-fly ambiguity search space can be accomplished using the INS to bridge GPS gaps (Söhne *et al.*, 1994; Škaloud, 1998; Grejner-Brzezinska *et al.*, 1998; Scherzinger, 2000; Petovello, 2003a).

The third performance improvement is reliability enhancement. Both GPS and INS can provide three-dimensional position and velocity information. Thus, redundant measurements are available for the determination of the vehicle trajectory parameters which greatly enhances the reliability of the system, as the two systems can act as checks on one another using redundant measurements (Brenner, 1995). The minimum detectable blunder (MDB) of the Doppler and L1 carrier phase measurements have shown to be reduced by decimetres per second and several centimetres, respectively, by the use of a tightly coupled CDGPS/INS system (Petovello, 2003a). GPS cycle slip identification and correction with the help of an INS solution computed between GPS epochs is another important improvement in GPS reliability (Cannon, 1991; Schwarz *et al.*, 1994a; Colombo *et al.*, 1999). After a cycle slip, with the help of the INS solution, a search process need not be implemented if ambiguities are already fixed. Similarly, the search process need not be reset if ambiguities have to be resolved to their integer values.

Finally, in addition to improvements in position accuracy, ambiguity resolution, reliability and availability GPS/INS integration can improve system performance

in many other respects. A deeply coupled integration approach has been developed by Sennott and Senffner (1997) and Bye *et al.* (1997) which improved GPS receiver tracking performance by feeding the INS information (predicted range and range rates) to the receiver to aid the code and carrier phase tracking loops.

1.1.4 BACKWARD SMOOTHING

Reference trajectory generation is needed for many applications and in some cases this requires centimetre-level position accuracy. However, in many cases (such as in urban canyons or GPS blocked conditions), the position error associated with the free inertial position solution using tactical-grade IMUs will be worse than 10 centimetres after a 10 to 15-second GPS data outage. To improve the accuracy attained through stand-alone INS or INS/GPS integration, several methods have been investigated, as described below.

The first of these entails maximizing the GPS data quality since GPS provides the update information. This, in turn, can be achieved by using short reference to rover baselines (Schwarz *et al.*, 1994b), more sophisticated ionospheric and tropospheric correction models (Abdullah, 1997), and so on. The use of high quality inertial sensor technologies, such as those used in airborne gravimetry (Bruton, 2000), is another option.

The third strategy usually involves applying optimal procedures for the overall system calibration and/or sensor placement, e.g. in direct georeferencing applications to name a few (Škaloud, 1999).

The fourth method is to use optimized INS mathematical modeling and error compensation techniques, especially in INS stand-alone applications and INS/GPS applications with frequent GPS outages. For example, as compared to the Gauss-Markov process, in terms of modeling the INS error, the use of an autoregressive (AR) process (Nassar, 2003) that predicts current states based on a linear combination of previous states can improve the results by 40% to 60% in INS stand-alone positioning and by 15% to 35% in INS/DGPS applications during DGPS outages (Nassar, 2003). The Gauss-Markov process is a special class of random processes which can be generated by passing white noise through simple filters. If a continuous process $x(t)$ is a first-order Gauss-Markov process, then it can be represented by the differential equation $\dot{x} + \beta x = w$ where w represents white noise (a random process with constant power spectrum density), and $1/\beta$ is the so-called correlation time. The use of de-noised INS data can improve positioning performance by 55% in INS stand-alone positioning and by 35% during DGPS outages in INS/DGPS applications (ibid).

However, many applications such as vehicular navigation, a low cost IMU integrated with carrier phase GPS is a typical selection to achieve high accuracy navigation solutions. In this situation, to improve positions obtained during GPS outages in INS/GPS applications, two different bridging methods have been investigated by Nassar (2003): backward smoothing and Strap-down Inertial Navigation System (SINS) parametric error modeling. When applying either of these bridging approaches during GPS outages, position errors are decreased by 85% to 93% (Nassar, 2003), while 60% to 90% improvements in maximum position accuracy have also been achieved by Shin and El-Sheimy (2002). In the latter case, the complete vcv information produced by forward Kalman filtering was not used so further improvement in position accuracy could not be done, despite a reduction in time needed to store the results.

In this research, the Rauch-Tung-Striebel (RTS) backward smoothing method is implemented to improve position accuracy during GPS outages in INS/CDGPS application (Rauch *et al.* 1965; Nassar, 2003). The application of backward smoothing to improve the integrated system performance in terms of position accuracy during CDGPS data outages for post-mission can provide more accurate trajectory information in case of any GPS data outages during data collection.

1.1.5 OBJECTIVES

The overall objective of this thesis is to investigate the integration of two tactical grade IMUs with a GPS. The sub-objectives are below.

1. *Compare the performance of two tactical-grade IMUs integrated with GPS.* Free inertial solution during GPS outages can best represent the performance of each IMU. Meanwhile, the re-fix time after GPS outages with inertial aiding can be used to assess the improvements of ambiguity resolution with inertial aiding. Simulation of complete GPS outages with varying duration is used to assess the performance of kinematic GPS integrated with two different tactical-grade IMUs in terms of free-inertial position accuracy during - and ambiguity resolution performance after - GPS data outages. As part of the investigation, various integration strategies are also considered to determine if the integration strategy affects the system performance.
2. *Quantify improvement in ambiguity resolution performance over GPS-only case.* Once the carrier phase observables become available in the aftermath of a GPS outage, the integer ambiguities must be re-determined as quickly as possible to enable the system to regain the highest possible accuracy level. The time taken to re-fix the ambiguities in the integrated system, as compared to the GPS-only case, will be

compared and correlated to the free-inertial accuracy to derive the relationship of quantity improvements to free-inertial accuracy.

3. *Evaluate the application of backward smoothing to improve the accuracy of the integrated system during GPS data outages in post-mission phase.*
4. *Assess the performance of various ambiguity processing strategies for short baseline (less than 10 km) and long baseline (longer than 60 km) conditions. The performance is judged on the basis of the maximum achievable position accuracy for both short and long baselines, and by the time to re-fix an ambiguity for short baseline since it is possible to resolve ambiguities only in the short baseline case.*

This thesis aims to evaluate the performance of kinematic GPS integrated with two different tactical-grade IMUs in terms of free-inertial position accuracy during - and ambiguity resolution performance after - GPS data outages. As part of the investigation, various integration strategies are also considered to determine if the integration strategy affects the system performance. Since Petovello (2003a, 2003b) looked only at relatively short baselines (less than 8 km), the impact of long baselines (longer than 60 km) on the performance of the integrated system will also be evaluated in this research. In addition, the application of backward smoothing to improve the accuracy of the integrated system during GPS data outages in post-mission will also be investigated. An assessment using different

ambiguity resolution strategies under long baseline (about 80 km) conditions, as measured by the achievable position accuracy, is tested to provide a general idea of which ambiguity strategy is more suitable in the presence of larger differential errors, as compared to the short baseline case.

The major contributions of this thesis are:

1. *The performance comparison of kinematic GPS integrated with two different tactical-grade IMUs in terms of free-inertial position accuracy during - and ambiguity resolution performance after - GPS data outages.*
The comparison is measured by free inertial position accuracy and time to re-fix ambiguities after GPS outage. The influence of each integration strategy, namely loosely coupled and tightly coupled, was investigated by comparing the overall position solution of each strategy.
2. *A relationship between ambiguity resolution improvements, in terms of time to re-fix ambiguities, and INS variance seeding after a complete GPS outage has been developed.* This knowledge will simplify the selection of an IMU needed to obtain a certain level of navigation performance in terms of ambiguity resolution (e.g. the ambiguity re-fixing time after a GPS complete outage with inertial aiding). This will provide another “tool” for designing and assessing GPS/INS systems and/or system requirements

3. *A backward smoothing method - namely the RTS smoother - is implemented in this particular research. The implementation and application of backward smoothing is intended to improve the performance of the integrated system in terms of position accuracy during GPS data outages in post-mission, thus providing a more accurate position solution in case of any GPS data outages during data collection.*
4. *The ambiguity resolution strategies given in Liu (2003) has been augmented by implementing various approaches in current Satellite And Inertial Navigation Technology (SAINTTM) software (Petovello et al. 2003).*
5. *Augmentation of the Satellite And Inertial Navigation Technology (SAINTTM) software (Petovello et al. 2003) developed in the Position, Location and Navigation (PLAN) Group in the Department of Geomatics Engineering, University of Calgary is employed to implement the proposed methods.*

1.2 THESIS OUTLINE

The thesis is composed of eight chapters and two appendices which are organized as described below.

Chapter One presents the background, objectives and motivation. The research to be performed along with the methodology used are presented in Chapters Two, Three and Four. Chapter Two gives an overview of the positioning principles of GPS and INS as well as the error sources relevant to GPS positioning. It also describes the different INS/CDGPS integration strategies which are used in the existing software system.

An overview of ambiguity resolution in terms of concepts, search techniques, observables and processing strategies are given in Chapter Three.

Chapter Four is devoted to the subject of bridging CDGPS outages in INS/CDGPS integration applications. Optimal backward smoothing is applied as the bridging method and the concepts and modifications of the backward smoothing equations required for the case of bridging GPS outages are developed.

Chapter Five gives a description of a field test and the corresponding GPS solutions, along with INS/CDGPS integration results to verify the quality of the reference trajectory.

Chapter Six provides short baseline results of the integrated system which are

produced off-line; specifically, position accuracy during complete data outages, ambiguity resolution performance produced by use of inertial data, as well as position improvements during GPS outages using backward smoothing methods are investigated. An assessment of the ambiguity processing strategy under long baseline (about 80 km) conditions in terms of position accuracy is given in Chapter Seven using field data.

Chapter Eight concludes the major results and findings obtained in the previous chapters with reference to the objectives listed in Section 1.1.5.

CHAPTER TWO - OVERVIEW OF GPS AND INS

This chapter reviews the GPS and INS systems separately, and the integration of GPS and INS. GPS is reviewed firstly focusing on the various error sources and their magnitudes. The GPS observables are reviewed and the principles of inertial navigation systems are detailed through a focus on the relevant equations. A review of the most common GPS/INS integration strategies realized in the existing software system is presented with more detail given to those strategies used in subsequent chapters.

2.1 OVERVIEW OF THE GLOBAL POSITIONING SYSTEM

For military users to accurately and instantaneously determine their position, velocity, and time in a common reference coordinate system anywhere on or near the Earth on a continuous basis (Parkinson *et al.*, 1995), the GPS was originally designed for metre-level accuracies (Parkinson, 1996); developed by the United States Department of Defense (DoD); and first declared operational in 1993 (Leick, 1995). The developments from there, produced primarily by the civil community, have made centimetre-level accuracies more common. The realization and revolution of GPS gives modern positioning and navigation the ability to provide a wide range of positioning accuracies under all weather

conditions. An overview of GPS concepts focusing on GPS architecture, observables and error sources is presented in this section.

2.1.1 BASIC CONCEPTS

The Navigation System with Timing And Ranging (NAVSTAR) Global Positioning System is a satellite-based radio-navigation system developed and maintained by the Joint Program Office (JPO), which is directed by the United States Department of Defense (DoD). The GPS system consists of three segments: the Space Segment, the Control Segment, and the User Segment. The Space Segment comprises the satellites which broadcast signals; the Control Segment manages the satellite operations; and the User Segment covers activities related to the development of military and civil GPS user equipment (i.e., receivers). The DoD is responsible for both the Space and Control Segments, while the development of receivers and services in the civil sector is essentially conducted by market forces.

Currently there are twenty-nine Block II/IIA/IIR satellites (24 operational, 3 spares, and 2 newly launched) in the Space Segment (U.S. Naval Observatory, 2005). GPS satellites operate in near-circular 20,200 km, 12-hour orbits at an inclination of 55 degrees and with stationary ground tracks (as shown in Figure 2.1). This constellation of satellites provides continuous GPS coverage

anywhere on Earth at any time of the day. Each satellite in the constellation continuously broadcasts signals on two L-band carrier phase frequencies. One is the L1 frequency at 1575.42 MHz (wavelength 19 cm) and the other is the L2 frequency at 1227.6 MHz (wavelength 24 cm). Two pseudo-random noise (PRN) codes, which are used to achieve the pseudorange from a receiver to a corresponding satellite, are modulated onto corresponding base carriers. The first code, the Coarse/Acquisition code (C/A-code), is modulated only on L1. However, the second code, the Precise code (P-code), is modulated on both L1 and L2 carriers. The navigation message which includes the satellite ephemeris, the satellite clock bias and the satellite status is modulated onto both the L1 and L2 carriers. According to the GPS modernization plan, a C-Code will be added on L2, a Military M-Code will be added both on L1 and L2, and another frequency (L5 = 1176.45 MHz) will be introduced in the future. The first satellite containing the L2 C-code was launched on September 21, 2005 (Lockheed Martin Corporation, 2005).

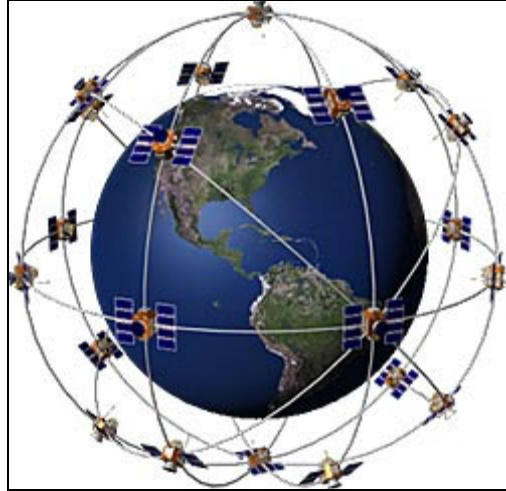


Figure 2.1 GPS Satellites Constellation ([Garmin](#), 2005)

The Control Segment consists of a Master Control Station located at the Schriever Air Force Base in Colorado Springs, and five monitoring stations which are located at the Falcon Air Force Base (Colorado), Hawaii, Ascension Island (the Atlantic Ocean), Diego Garcia Atoll (the Indian Ocean), and Kwajalein Island (the South Pacific Ocean) (as shown in Figure 2.2). The major responsibility of each of the monitoring stations is to check the exact altitude, position, speed, and overall health of the orbiting satellites. The stations will also pay attention to any variations that are caused by the gravity of the Moon, the Sun and the pressure of solar radiation. All of this information is passed along to, and processed by, the Control Station, which then corrects and updates the navigational messages of the satellites. Ground antennas monitor and track the satellites from horizon to horizon to further enhance control measures. These ground antennas can also transmit correction information to any individual

satellites.

The user segment is comprised of the equipment for military personnel and civilians who determine their position by receiving GPS signals. Military equipment has been integrated with GPS user equipment in many ways, e.g. fighter jets, bombers, tankers, helicopters, ships, tanks, jeeps, and soldiers' equipment. Furthermore, military applications of GPS also include target designation, close air support, "smart" weapons, etc (ibid). In the civilian community, GPS users come from many different sectors such as surveying, agriculture, shipping (land and sea), in-car navigation, recreation and other outdoor-related activities (ibid).

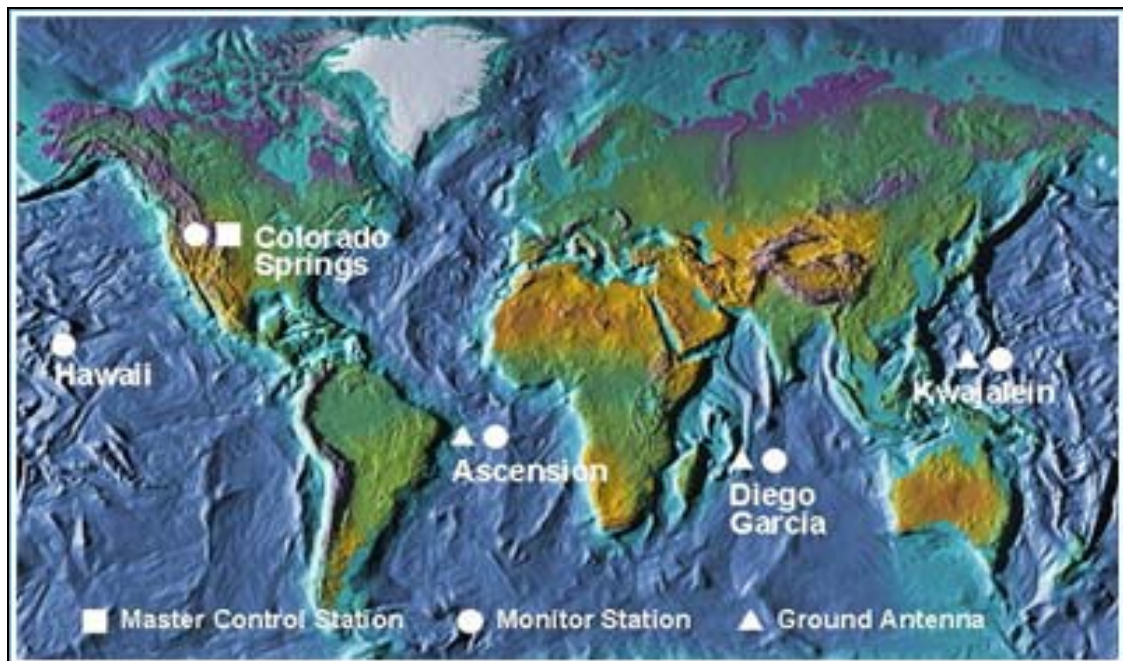


Figure 2.2 GPS Control Segment ([Federal Aviation Administration, 2005](#))

2.1.2 GPS OBSERVABLES

GPS observables consist mainly of pseudorange (code), carrier phase (phase) and the instantaneous Doppler frequency. Lower precision applications, such as most navigation applications, use pseudoranges. Carrier phase observations are used to achieve the high precision required in applications such as geodetic surveying and large scale airborne mapping. Pseudorange observables are derived from the PRN-codes by comparing the replica PRN-code generated in the receiver with the PRN-code transmitted from the satellite to determine the time shift through an autocorrelation analysis. Consequently, pseudorange observables are accordingly classified by code and frequency as L1-C/A, L1-P and L2-P code observable; carrier phase (phase) observables are derived from the accumulation of phase offset between the replica carrier signal and the received satellite carrier signal. Therefore, the initial number of integer cycles in the carrier phase (referred to as the “ambiguities”) is unknown (Wells *et al.*, 1987).

The basic pseudorange and carrier phase observation equations in metres and cycles can be expressed as follows (Misra and Enge, 2001):

$$P = \rho + d\rho + T + I + c(dT_u - dT^s) + \varepsilon_p \quad (2.1)$$

$$CP = \rho + d\rho + T - I + c(dT_u - dT^s) + \lambda N + \varepsilon_{CP} \quad (2.2)$$

where

- P is the pseudorange observation (m),
- CP is the carrier phase observation (cycles),
- ρ is the true range between GPS satellite and receiver (m),
- $d\rho$ is the orbital error (m),
- T is the tropospheric effect (m),
- I is the ionospheric effect (m),
- c is the speed of light (m/s),
- dT_u is the receiver clock error (s),
- dT^s is the satellite clock error (s),
- λ is the carrier wavelength (m),
- N is the carrier phase integer ambiguities (cycles)
- ε_p is the measurement noise and multipath on pseudorange (m), and
- ε_{CP} is the measurement noise and multipath on carrier phase (cycles).

As can be seen in Equations (2.1) and (2.2), some common error sources can be reduced and mitigated using differential techniques. In the context of this

thesis, the double-differenced (DD) processing technique is used. The double-differenced observation equation and error sources are therefore discussed in detail herein.

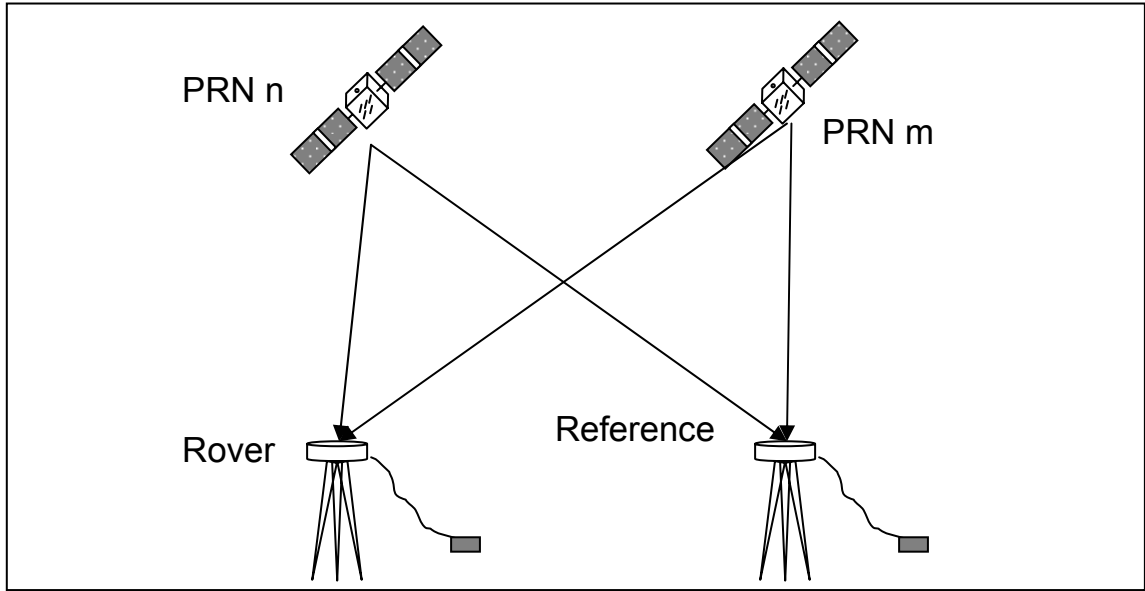


Figure 2.3 Double Differencing Concept

Figure 2.3 shows a typical DD set-up. In implementing DD, a single differenced (D) observation is derived first by subtracting measurements at a reference station from measurements at a user receiver for the same satellite. The corresponding code and phase observation equations can be constructed as follows (Misra and Enge, 2001):

$$\Delta P = \Delta \rho + \Delta d\rho + \Delta T + \Delta I + \Delta c(dT_u - dT^s) + \Delta \varepsilon_p \quad (2.3)$$

$$\Delta CP = [\Delta \rho + \Delta d\rho + \Delta T - \Delta I + \Delta c(dT_u - dT^s)] + \lambda \Delta N + \Delta \varepsilon_{CP} \quad (2.4)$$

By further taking the difference between measurements from the base satellite and measurements at other satellites, double-differenced observations can be obtained. The corresponding code and phase observation equations are formed as follows (Misra and Enge, 2001):

$$\nabla\Delta P = \nabla\Delta\rho + \nabla\Delta d\rho + \nabla\Delta T + \nabla\Delta I + \nabla\Delta c(dT_u - dT^s) + \nabla\Delta\varepsilon_p \quad (2.5)$$

$$\nabla\Delta CP = \nabla\Delta\rho + \nabla\Delta d\rho + \nabla\Delta T - \nabla\Delta I + \nabla\Delta c(dT_u - dT^s) + \lambda\nabla\Delta N + \nabla\Delta\varepsilon_{CP} \quad (2.6)$$

where Δ and $\nabla\Delta$ are single difference (D) and double-difference (DD) operators, respectively.

As such, many advantages can be achieved by DD. First, the receiver clock offset is removed. Second, since the satellite clocks are highly stable (Kaplan, 1996), the value of the double-differenced satellite clock error is reduced close to zero as long as the observations are differenced at approximately the same time at both the reference and rover stations. Third, the DD tropospheric error, DD satellite orbital error, and DD ionospheric error are much smaller than the un-differenced values. The DD observable has some disadvantage over the un-differenced observable, however. The most significant effect is that the noise and multipath level of the DD observable increases because of the non-spatially

correlated characteristics of noise and multipath error. Equations (2.5) and (2.6) can be further simplified as:

$$\nabla\Delta P = \nabla\Delta\rho + \nabla\Delta d\rho + \nabla\Delta T + \nabla\Delta I + \nabla\Delta\varepsilon_p \quad (2.7)$$

$$\nabla\Delta CP = \nabla\Delta\rho + \nabla\Delta d\rho + \nabla\Delta T - \nabla\Delta I + \lambda\nabla\Delta N + \nabla\Delta\varepsilon_{CP} \quad (2.8)$$

The DD phase observable represented by Equation (2.8) is generally used in applications requiring high positioning accuracy. However, the DD ambiguity $\nabla\Delta N$ must be resolved to its integer value to obtain such high levels of accuracy. For short baselines (less than 10 km), the main errors affecting ambiguity resolution are generally carrier phase multipath and receiver noise (assuming normal operating conditions). However ionospheric and tropospheric errors will become significant for long baselines (Lu, 1995; Raquet *et al.*, 1998). Detailed information about GPS error sources is presented in the following section.

2.1.3 GPS ERROR SOURCES

As mentioned in the above section, GPS DD observables are subject to many error sources, which will be briefly discussed in this section. DD errors can be classified into two categories based on the relation between the DD error and baseline length - namely the spatially correlated and non-spatially correlated

errors. Spatially correlated errors are those that tend to cancel between rover and reference receivers but which increase proportional to the baseline length. These errors include satellite orbital error, tropospheric error and ionospheric error. Non-spatially correlated errors are those that are not related to the baseline length and unique to each receiver or its environment. Therefore, non-spatially correlated errors cannot be cancelled through DD processing. The corresponding errors are multipath error and measurement noise. All of the above-mentioned error sources are discussed in detail later in this section.

GPS signals are affected by the medium through which they travel from the satellites to receiver. The traveling distance ranges from about 20,200 km when a satellite is overhead to about 26,000 km when it is rising or setting. All but the final 5% of the signal travel can be regarded as in a vacuum or free space, through which the electromagnetic signals travel with a constant speed, c . Closer to the surface of the Earth (Figure 2.4), at a height of about 1,000 km, the signals enter a layer of charged particles, called the ionosphere. Later in their earthward journey, at a height of about 40 km, the signals encounter an electrically neutral gaseous layer referred to as the troposphere. The refraction of the GPS signal in the Earth's atmosphere results in changes in both the signal's speed and direction. Accordingly, the ionospheric and tropospheric errors are referred to as signal propagation modeling errors.

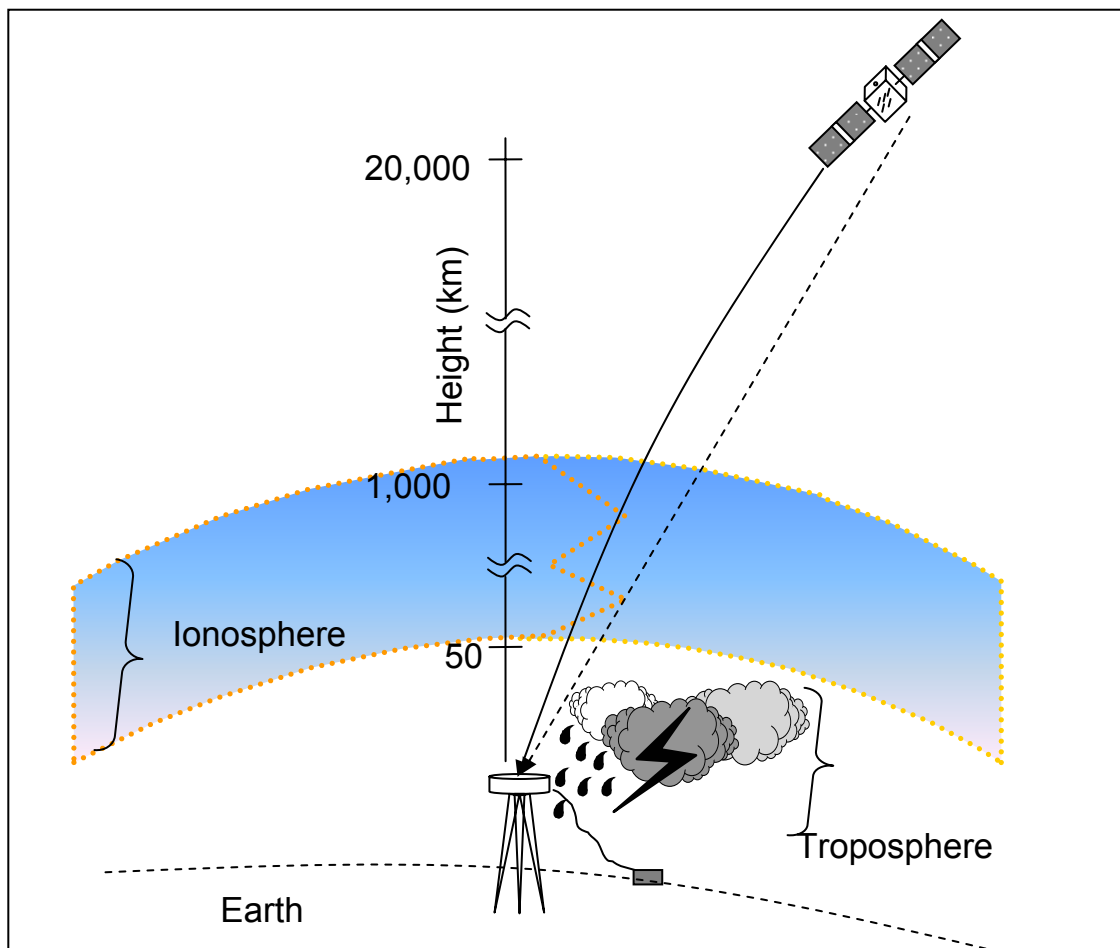


Figure 2.4 Refraction of GPS Signals in the Earth's atmosphere

An increase in path length due to bending of the signal ray, greatly exaggerated in Figure 2.4, is generally insignificant. The effect of the change in speed of propagation, however, is significant. With this in mind, the GPS signal propagation modeling errors are discussed as follows.

TROPOSPHERIC ERROR

The troposphere is the layer of the atmosphere closest to the Earth which reaches a height of about 50 km (Spiker, 1996). It has a nature of electrically neutral and non-dispersive for frequencies as high as 15 GHz. Because it is filled with water vapour, it refracts the GPS signals. The change of the refractivity from ionosphere space to the troposphere causes a reduction in the speed of the GPS signal, which produces a delay in the GPS signal. The tropospheric delay is composed of two parts, the dry and wet components, and is a function of temperature, pressure, and relative humidity. These weather parameters, however, have short spatial correlations, since the weather in one place might be very different from that in another location even only a few kilometres away. Thus, the DD technique can reduce this error only when the baseline is short and the weather conditions at the reference and rover are similar. Measurement of these weather parameters at widely spaced monitoring stations would be ineffective owing to their short spatial correlations (Kaplan, 1996). Unfortunately, no two frequency subtraction techniques will work in such situations due to its non-dispersive effect of the troposphere delay on two frequency GPS signals.

Generally, tropospheric delay can be modeled very well. Typically the

contribution of the troposphere to the differential positioning error budget varies from 0.2 to 0.4 parts per million (ppm), based on application of a model described in Lachapelle (2004). Consequently, the errors which are related to GPS receiver separations are typically quantified in terms of parts per million (ppm), where 1 ppm equals to 1 mm of error per kilometre of receiver separation. Assuming a nominal value of 0.4 ppm and a baseline of between 10 and 80 km, use the baseline length multiply 0.4 ppm, the residual tropospheric error is as high as 0.4 cm to 3.2 cm. This being said, for baselines less than 25 km, the residual tropospheric delay may be negligible, depending on local weather conditions and station height differences. For long baselines, say on the order of 80 km, in order to achieve a 2 to 3 cm level of positioning accuracy, either the residual tropospheric delay must be modelled explicitly or corrections have to be made to compensate for it.

There are quite a few of tropospheric delay models available for this purpose; e.g. as described in Hopfield (1970, 1972), Saastamoinen (1972), and Lanyi (1984). The Hopfield tropospheric delay model and Saastamoinen tropospheric model are the most frequently used to this end, and they give comparable results in most situations. The Hopfield tropospheric delay model was used herein.

The *Hopfield model* represents dry and wet tropospheric delay values for the

zenith direction using the equations $T_{z,d} = 77.6 \cdot 10^{-6} \frac{P_0 h_d}{T_0}$ and

$T_{z,w} = 0.373 \frac{e_0 h_w}{T_0^2}$, where T_0 is the temperature (Kelvin), P_0 is the total pressure

and e_0 is the partial pressure due to water vapour (both in millibars), all determined at the antenna location by measurements or on the basis of models of the standard atmosphere. h_d (≈ 43 km) is defined as the height above the antenna at which the dry refractivity is zero; and h_w ($= 12$ km) is defined as the height above the antenna at which the wet refractivity is zero.

IONOSPHERIC ERROR

The ionosphere is a region of ionized gases (free electrons and ions) which is caused by the Sun's radiation, and extends from a height of about 50 km to about 1,000 km above the Earth. The propagation speed of a radio signal in the ionosphere depends on the number of free electrons in its path, defined as the *total electron content* (TEC): the number of electrons in a tube of 1 m² cross-section extending from the receiver to the satellite (Misra and Enge, 2001). Ionized gas is a dispersive medium for radio waves, meaning that a GPS signal passing through the ionosphere is refracted, delaying the signal, and advancing the phase with equal magnitude but opposite sign. This effect is frequency-

dependent and highly dependent on the time of day, receiver latitude and solar cycles. The quantified ionospheric delay in terms of measurements of pseudorange (Equation 2.1) and carrier phase (Equation 2.2) is as follows:

$$I_p = -I_{CP} = \frac{40.3 \cdot TEC}{f^2} \quad (2.9)$$

where f is signal frequency. In simplified terms, the ionospheric group delay is represented as I and the phase delay as $-I$.

If a dual-frequency receiver is available (GPS broadcasts on two frequencies), the first order of ionospheric errors can be eliminated using a special linear combination observation of two frequencies. This is discussed further in Section 3.4.

The estimated contribution of the ionospheric error to the differential positioning error budget is about 1-2 ppm (Seeber, 1993) at the time of solar minimum. The contribution of the ionospheric error to the differential positioning error budget increases when solar activity increases and/or latitude decrease. The typical value of ionospheric error will be shown in Table 2.1. Say the ionospheric error contribution is 3 ppm, with a 10 to 80 km baseline; the differential positioning error budget is on the order of 3 cm to 24 cm. As a rule of thumb, the

instantaneous ambiguity resolution can be achieved when the line of sight error is less than half of wavelength. So the ambiguities might not be able to be resolved when baseline length longer than 30 km with 3 ppm ionospheric error contribution without considering the DOP values.

SATELLITE ORBITAL ERROR

Orbital error is a result of the discrepancies between the actual positions of the satellites and the predicted positions promulgated by the broadcast ephemeris. The influence of orbital error in computing position solution, according to Wells *et al.* (1986), can be represented as follows:

$$\frac{db}{b} = \frac{d\rho}{\rho} \quad (2.10)$$

where db is the total error in the length of the baseline b ; $d\rho$ is the total error in the coordinates of a satellite position; and ρ is the distance from the satellite to the respective stations. Equation (2.9) shows that the actual influence of the satellite orbital error on the baseline is limited. According to IGS (2005), the satellite orbital computed from the broadcast ephemeris has an root mean square (RMS) error of 2 m. Assuming an average satellite-receiver range of

20,200 km and a baseline of 10 to around 80 km, the contribution of the orbital error to the differential positioning error budget is on the order of about 0.2 to 1.6 cm. This being said, the contribution of the orbital error to the differential positioning error budget is less than 1 cm for baseline lengths under 50 km and thus can be negligible.

The errors listed above are spatially correlated, which means that they are correlated between stations as a function of their separation. With this in mind, a summary of the typical and extreme error magnitudes for spatially correlated errors is given in Table 2.1.

Table 2.1 Magnitudes of Spatially Correlated DD Error Sources (Petovello, 2003)

Error	Error Magnitude	
	Typical (RMS)	Extreme
Orbital	0.1 ppm	N/A
Troposphere ¹	< 1 ppm	1-3 ppm
Ionosphere	1-3 ppm ²	> 10 ppm ³

¹ After applying a tropospheric model

² Effects vary with geographic location and the solar activity

³ For Calgary region, effects near the equator can reach to 50 ppm

MULTIPATH

Multipath is exactly that - the propagation of the same signal along multiple

paths (Figure 2.5). Multipath is one of the largest GPS error sources. It is difficult to predict and to compensate for, since it is environmentally dependent and thus cannot be mitigated via the differential technique (Ray, 2000).

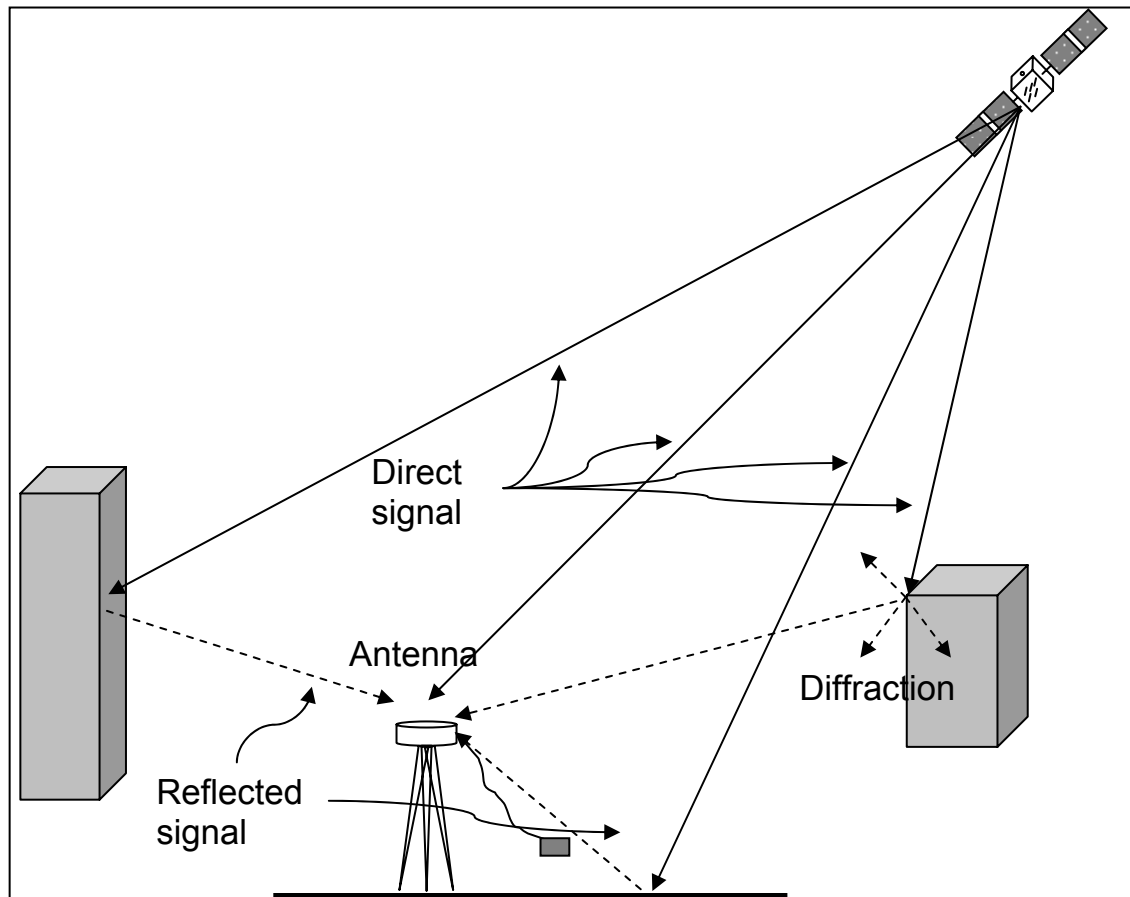


Figure 2.5 Multipath Sketch Map (Zhang, 2003)

As seen in Figure 2.5 a receiver may receive a signal from the satellite but is also receiving the same signal from the same satellite after it has bounced off the ground, buildings, etc., or diffracted upon encountering the edges of sharp objects. Receiving multiple signals from the same satellite in this way can add

additional error to the range to the satellite. There is currently no good way to prevent multipath completely. Some high-end receivers have choke-ring assemblies around the receiver element, which prevents most of the ground-reflected multipath, but not all.

MEASUREMENT NOISE

The code and carrier measurements are affected by random measurement noise, called receiver noise, which is a broad term covering the radio frequency radiation sensed by the antenna in the band of interest that is unrelated to the signal; noise introduced by the antenna, amplifiers, cables, and the receiver; interferences (i.e. interference from other GPS signal and GPS-like broadcasts from system augmentations); signal quantization noise, which are called by a joint name as thermal noise and the dynamic stresses effects on a receiver's tracking loop (Misra and Enge, 2001; Spilker, 1994). Measurement noise is usually considered as white noise as it is uncorrelated over time, channels and receivers, thus cannot be mitigated by DD. In fact, a rover receiver inherits the multipath and measurement noise errors incurred at the reference station. With differential corrections the receiver noise increases by $\sqrt{2}$, and two times with double-differencing due to the two differencing steps.

Multipath and measurement noise are non-spatially correlated error sources, which cannot be mitigated using the differential technique but are, rather, increased thereby. With this in mind, the typical magnitudes of multipath and measurement noise in un-differenced mode and their mitigation techniques are summarized in Table 2.2 (Misra and Enge, 2001).

Table 2.2 Magnitudes of Non-Spatially Correlated GPS Error Sources¹

Error	Error Magnitude	
	Un-differenced	Mitigation
Receiver Noise and Multipath ²	Code 0.5-1 m	Uncorrelated between antennas Mitigation through antenna design and siting, receiver design, and carrier-smoothing
	Phase 0.5-1 cm	
Noise	Code 0.05-0.1 m ³	Uncorrelated between receivers
	Phase 1-2 mm	Mitigation through receiver design

¹ using Narrow CorrelatorTM (0.1 chip) and in “clean” environments (open sky, obstacle-free)

² extremely the code and carrier multipath can reach up to 4 m and 2.5 cm respectively with 3 dB signal to multipath ratio in idea situation (only one reflected signal and unlimited bandwidth)

³ the code measurement precision of a NovAtel OEM4 DL receiver is 6 cm (RMS) (NovAtel, 2005)

As shown in Table 2.2, the multipath and measurement noise error, unlike the signal propagation error (ionospheric and tropospheric error) and GPS Control Segment-responsible error (satellite clock and orbit errors), are affected by receiver selection, antenna design and siting. Because it is difficult to completely correct for the multipath error, even in high precision GPS units, multipath is a serious concern to the GPS user. In fact, all error sources (satellite

clock and orbit error, ionospheric and tropospheric error, and receiver noise and multipath) can exist in a GPS measurement. The combined effect of these error sources on pseudorange measurements is referred to as the user range error (URE), also known as the user equivalent range error (UERE).

2.2 INS CONCEPTS

An inertial navigation system measures the position and attitude of a vehicle by measuring the accelerations and rotations applied to the system's inertial frame. It is widely used because it refers to no real-world item beyond itself. It is therefore immune to jamming and deception. An overview of INS principles, mechanization and error modeling, with a focus on the relevant equations, is presented in this section.

2.2.1 PRINCIPLES OF INS

An accelerometer is such an instrument that measures acceleration along its axis. Integrate the output once and velocity is computed. Integrate again, and the position is determined- or rather, the change in position - along the accelerometer's axis. The above concept is illustrated in following Figure 2.6.

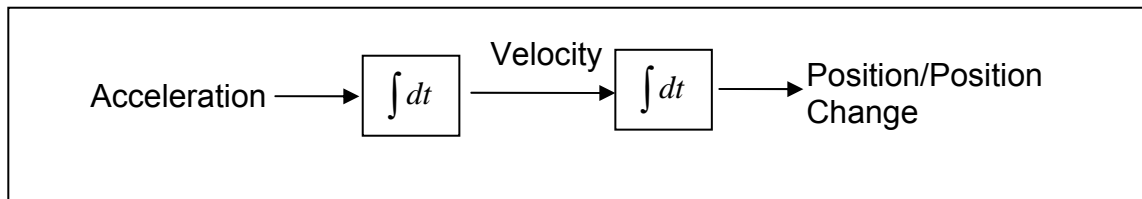


Figure 2.6 Inertial Navigation Concept Fundamental (Savage, 2000)

If the direction of travel is known, the current relative position can be deduced. In this sense, inertial navigation is simply a form of dead reckoning. In order to achieve the current coordinates referring to a particular frame, the starting point is needed. However, an inertial navigation device or system (INS) cannot find its initial position on the Earth; it can find latitude, with difficulty, but not longitude (Savage, 2000).

Three orthogonally arranged accelerometers, when maintaining alignment to the corresponding navigation frame (e.g. for local level frame maintaining alignment to north-south, east-west and vertical.), can measure the position and velocity changes relative to the navigation frame (Savage, 2000; Grewal *et al.*, 2001). First generation inertial navigation systems suspended the accelerometers in a set of three gimbals that were gyro-stabilized to maintain the direction (Savage, 2000; Grewal *et al.*, 2001; Greenspan, 1995). The gyros, similarly, are single axis devices, the integration of which gives an output proportional to the angle through which the gyros have been rotated (about their input axes) (Savage, 2000; Grewal *et al.*, 2001; Greenspan, 1995). The gyros in a first generation INS

are used as the sensing elements in null-seeking servos, with the output of each gyro connected to a servo-motor driving the appropriate gimbal, thus keeping the gimbal in a constant orientation in inertial space. The gimballed INS can be very reliable and accurate. However, its rather large size and mechanically complex gimbal arrangement make it an unwieldy piece of equipment. The modern ring laser gyro (RLG) inertial navigation measurement unit is about 7 x 11 x 11 inches (178 x 178 x 270 mm) in size, about 10 kg in weight, and costs some tens of thousands of dollars. This makes the RLG approximately two to three times better in every respect than the 'latest' gimballed inertial navigation measurement unit, while delivering about the same level of performance. Thus, since the 1970s, the INS industry began to contemplate an alternative, simpler arrangement (Savage, 2000; Grewal *et al.*, 2001; Greenspan, 1995). In the new concept, the gimbals were eliminated altogether and with the gyros and accelerometers simply 'strapped-down' onto the mounting frame. The gyros were not used as null-seekers, but as a means of measuring rotations in space. As such, the system senses the direction in which the accelerometer axis set is pointing at a given instant. In effect, it uses a 'mathematical gimbal' set to replace the mechanical gimbals. The equations used to convert the output of the IMU into useful position, velocity and attitude information are presented in the following section.

2.2.2 INS MECHANIZATION

In order to convert IMU output to useful spatial data, a series of equations have to be realized (Schmidt, 1978). The computation can be processed in different navigation frames based on the specific application and INS used (e.g. a strap-down, platform). In this thesis, the Earth-Centered Earth-Fixed (ECEF) frame was chosen as the computational frame. The algorithmic flowchart (EI-Sheimy, 2005) is shown in Figure 2.7.

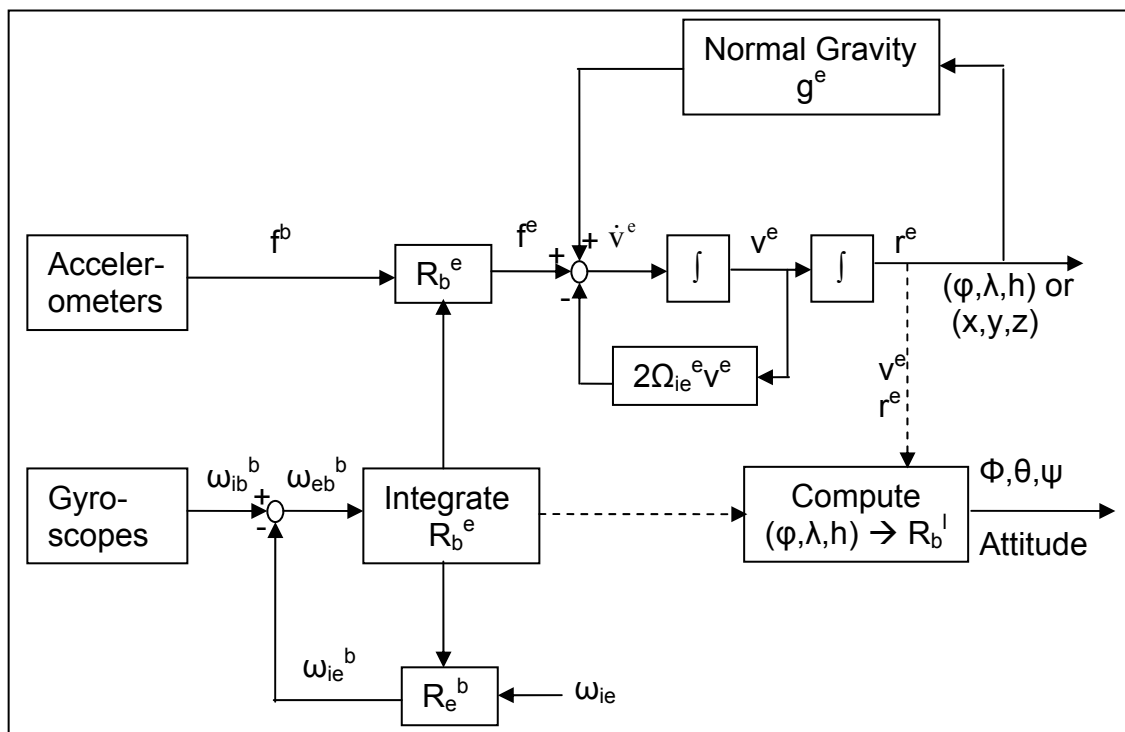


Figure 2.7 Mechanization in Earth-Centered Earth-Fixed Frame

In Figure 2.7, ϕ, λ, h represent latitude, longitude and altitude, respectively. Based on this functional process, the equation of motion can be summarized in

the ECEF frame as (Schwarz and Wei, 1999)

$$\begin{bmatrix} \dot{\mathbf{p}}^e \\ \dot{\mathbf{v}}^e \\ \dot{\mathbf{R}}_b^e \end{bmatrix} = \begin{bmatrix} \mathbf{v}^e \\ \mathbf{R}_b^e \mathbf{f}^b - 2\boldsymbol{\Omega}_{ie}^e \mathbf{v}^e + \mathbf{g}^e \\ \mathbf{R}_b^e (\boldsymbol{\Omega}_{ei}^b + \boldsymbol{\Omega}_{ib}^b) \end{bmatrix} \quad (2.11)$$

where a dot indicates a time derivative and \mathbf{g} represents the normal gravity; \mathbf{R}_b^e represents the rotation matrix from the body frame to ECEF frame; \mathbf{p} is the position vector; \mathbf{v} is the velocity vector; and $\boldsymbol{\Omega}$ is the skew-symmetric form of the rotation rate vector $\boldsymbol{\omega}$. As can be seen, the specific force, \mathbf{f}^b and the angular rate measurements, $\boldsymbol{\omega}_{ib}^b$, measured by the IMU act as inputs to the system (the inertial frame to body frame rotation as to measured in the body frame). The superscript indicates the frame from which states are measured. The mechanization equations process data received from the IMU to obtain updated navigation parameters without regard to the veracity of these parameters.

2.2.3 INERTIAL SENSOR ERROR EQUATIONS

Gyros and accelerometers, however, are subject to errors which limit the accuracy to which the observable can be measured. Due to these errors, the

solution of the above system of differential equations also contains errors, which can be systematic or stochastic in nature. Therefore, these two types of errors are determined first through error models and then compensated through Kalman filtering. The SINS systematic error models are defined by perturbing the above non-linear equations (Equation 2.11). On the other hand, the SINS stochastic error models, which represent the SINS sensor errors, should be modeled in a different way owing to the parameters of the sensor operation. The SINS accelerometer and gyro sensor errors consist of both deterministic and random components. The deterministic part includes biases and scale factors, which are determined by calibration and then removed from the raw measurements. The random part, however, is correlated over time, which is due essentially to variations in the SINS sensor bias terms and therefore is modeled stochastically. As such, these errors are included in the SINS error model. For most applications, a first-order Gauss-Markov model is usually used to describe the random errors associated with inertial sensors. Those error states are then estimated in an INS or INS/GPS filter.

Generally, the INS error states estimated in a navigation filter usually include three each of the following: position errors, velocity errors, attitude misalignments, gyro drifts and accelerometer biases. The dynamic models for the above parameters can be written as a series of first-order differential equations as follows:

$$\begin{aligned}
\delta \dot{\mathbf{p}}^n &= \delta \mathbf{v}^n \\
\delta \ddot{\mathbf{v}}^n &= -\mathbf{F}^n \boldsymbol{\varepsilon}^n + \mathbf{N}^n \delta \mathbf{p} - 2\boldsymbol{\Omega}_{in}^n \delta \mathbf{v}^n + \mathbf{R}_b^n (\mathbf{b}^b + \mathbf{w}_1) \\
\dot{\boldsymbol{\varepsilon}} &= -\boldsymbol{\Omega}_{in}^n \boldsymbol{\varepsilon}^n + \mathbf{R}_b^n (\mathbf{d}^b + \mathbf{w}_2) \\
\dot{\mathbf{b}}^b &= -\alpha \mathbf{b}^b + \mathbf{w}_3 \\
\dot{\mathbf{d}}^b &= -\beta \mathbf{d}^b + \mathbf{w}_4
\end{aligned} \tag{2.12}$$

Dots denote time derivatives and the superscripts “n” and “b” denote parameters in the navigation and body frame, respectively. Particularly if using an ECEF frame as the navigation frame, all superscripts “n” should be replaced by “e”.

The symbols in Equation (2.12) are interpreted as follows:

- $\delta \mathbf{p}$ is the vector containing the 3 position errors
- $\delta \mathbf{v}$ is the vector containing the 3 velocity errors
- \mathbf{F} is the skew-symmetric matrix of specific force
- $\boldsymbol{\varepsilon}$ is the vector containing the 3 attitude errors (misalignments)
- \mathbf{N} is the tensor of gravitational gradients
- $\boldsymbol{\Omega}_{in}^n$ is the skew-symmetric matrix of the rotation rate of the navigation frame relative to inertial space seen from the navigation frame
- \mathbf{R}_b^n is the rotation matrix from the body frame to the navigation frame
- \mathbf{d} is the vector containing the 3 gyro drifts
- \mathbf{b} is the vector containing the 3 accelerometer biases
- α, β are parameters for modeling the drift and bias terms as first-order

Gauss-Markov process, and

$\mathbf{w}_{i=1,2,3,4}$ is a noise term.

Appendix E gives the detailed dynamics matrix of the 15-state Kalman filter in both the local-level and ECEF frames corresponding to Equation (2.12).

2.3 GPS/INS INTEGRATION

Having reviewed major aspects of GPS and INS in the above sections, the integration of the two systems will be concentrated in following section. To this end, even if there is only one GPS and one possible INS, there will still be many ways to integrate them (e.g. loosely coupled, tightly coupled and deeply coupled integration). As an alternative, three of the four most commonly used approaches, according to Jekeli (2000) and Scherzinger (2000), are investigated in this section. The four most commonly used integration architectures are: uncoupled integration; loose integration; tight integration; and deep/ultra-tight integration. The loose and tight integration strategies along with the basic architecture – uncoupled integration are the most common in the literature and will be used herein. The following section describes the filter structures used in this research and in the software developed for its implementation.

The term tightly coupled usually uses a single Kalman filter to fuse all sensor

data. Loosely coupled, however, generally uses more than one Kalman filter with many possible coupling architectures (Carson, 1988; Wei and Schwarz, 1989).

2.3.1 GPS/INS INTEGRATION ARCHITECTURES

Two integration strategies, namely loose coupling with INS seeding and tight coupling, are employed herein (referred to herein for convenience simply as “loose coupling” and “tight coupling”, etc.). In the loose coupling with INS seeding strategy, separate GPS and INS filters are implemented and the position and velocity of the GPS filter are treated as observations in the INS filter. Position and velocity from the INS filter are further used to ‘seed’ the GPS filter when it needs to be initialized or reset following GPS data outages. In the tight coupling strategy, only one filter is used to estimate all relevant GPS and INS states. Figure 2.8 and Figure 2.9 show the two integration strategies (Petovello *et al.*, 2003; Zhang *et al.*, 2005). Note that, pursuant to the tight integration strategy, the shaded grey boxes correspond to their loose integration strategy counterparts and are included here solely for purposes of comparison.

Implied in the loose integration strategy is the fact that process noise is added to both the GPS and INS filters. This increased noise, relative to the noise added to the INS filters alone (as shown in the tight integration), will introduce some

discrepancies (Petovello *et al.*, 2003). This being said, the advantage of the loose integration strategy is that the dimension of the state vectors is reduced relative to the tight integration case, which allows for computationally more efficient programs due to a reduced number of floating point operations needed in the Kalman filtering algorithm. Furthermore, since the inputs to the INS filter in the loose integration case are position, velocity and the corresponding variance covariance output of a GPS filter, the output from a GPS receiver or existing software program can be directly used to update the INS filter, thus saving computational resources.

Since both integration strategies effectively deliver more information to the GPS data processing step, they should both positively affect the ambiguity resolution process, relative to the GPS-only case. More specifically, as more information is provided to the GPS data processing step, the resulting search space for GPS ambiguities should decrease. This, in turn, should yield shorter ambiguity resolution times. With this in mind, the increased process noise in the loose coupling approach, relative to the tight coupling approach, should increase the time to fix ambiguities after a complete GPS outage. Moreover, the direct correlation between ambiguity states and position states using the tight coupling strategy suggests more efficient ambiguity resolution as compared to the indirect correlation when the loose coupling strategy is used. Therefore, improvements in ambiguity resolution are expected to be lower for a loose integration strategy

compared to a tight integration strategy. Furthermore, for either integration strategy, the quality of the IMU will directly affect the quality of the data that is aiding the GPS.

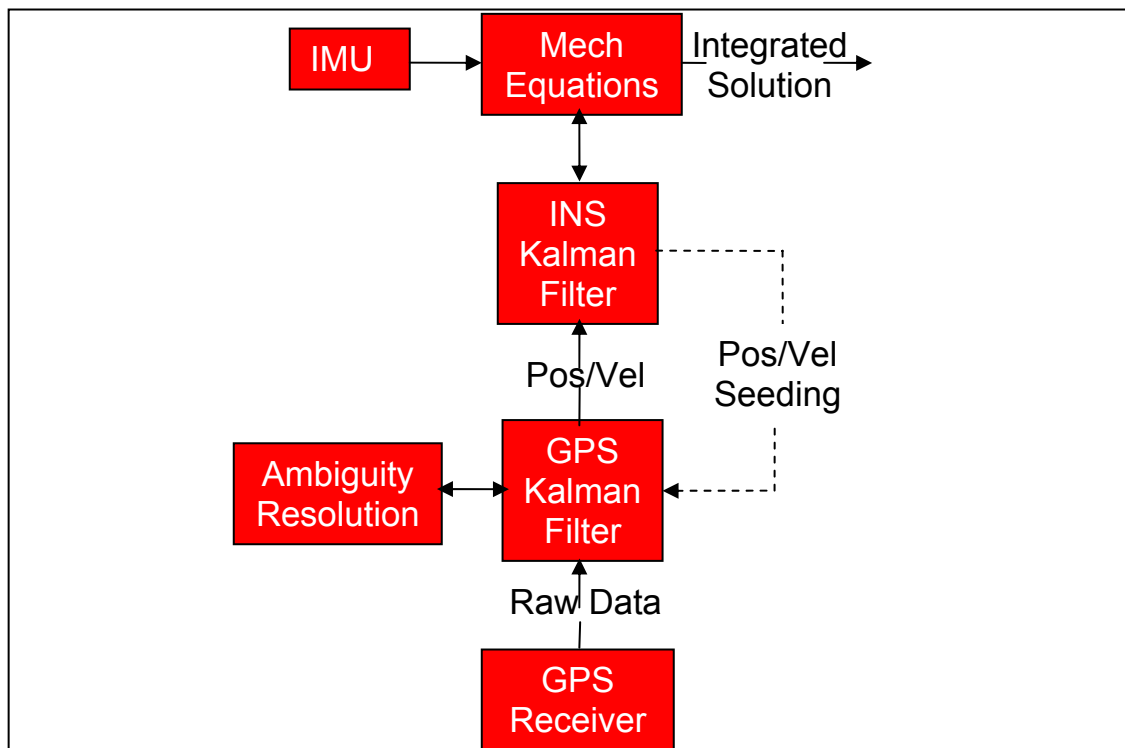


Figure 2.8 GPS/INS Information Flow Diagram Using the Loose Integration Strategy (Petovello *et al.*, 2003)

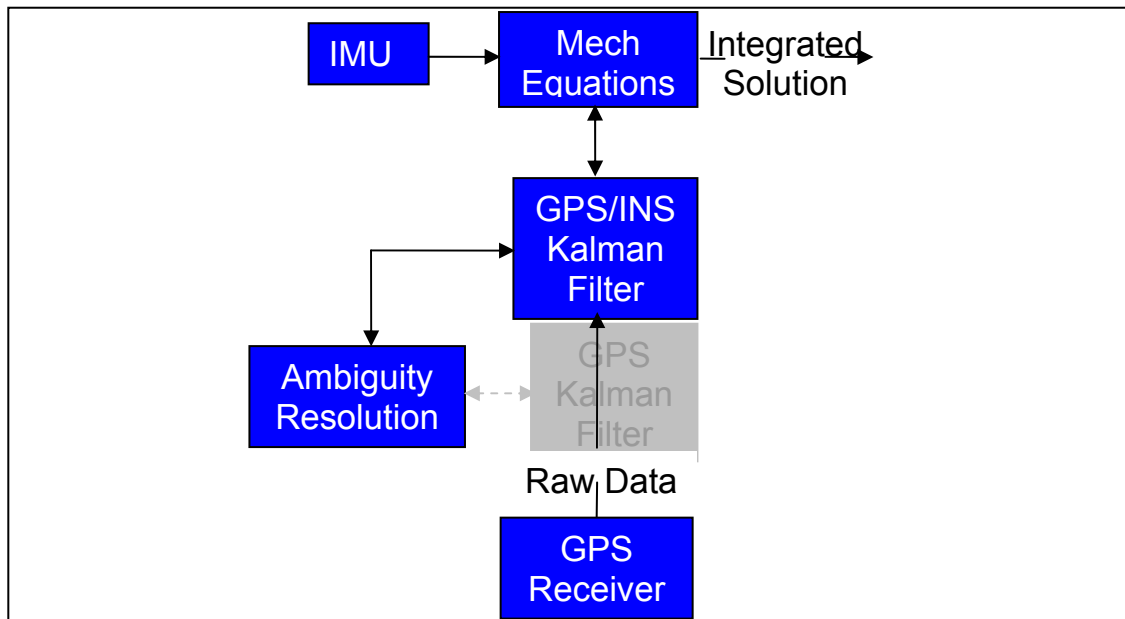


Figure 2.9 GPS/INS Information Flow Diagram Using the Tight Integration Strategy (Petovello *et al.*, 2003)

Detailed information about the GPS, INS and GPS/INS integration filters used herein is given in Petovello (2003).

It must be noted that the GPS/INS filter used in tightly coupled integration consists of a combination of GPS-only and INS-only filters. The GPS/INS case is simply the INS-only filter augmented with the double-difference ambiguities when they need to be estimated as real-valued quantities. This means that the GPS position and velocity error states coincide with the INS position and velocity errors in tightly coupled mode. In this way, the tightly coupled filter is identical to that of the INS filter discussed above, augmented by the necessary GPS ambiguity states. With this in mind, the tightly coupled GPS/INS filter and the

loosely coupled INS filter are essentially the same if all ambiguities have been resolved or during complete GPS outages. The processing noise incident to the loose coupling strategy, however, is higher. Furthermore, because of the indirect correlation between position and ambiguity states stemming from use of a loose coupling strategy, and higher processing noise, the loose coupling strategy is expected lower convergence speed compare to tight coupling with same initial position seeding.

CHAPTER THREE - OVERVIEW OF CARRIER PHASE

INTEGER AMBIGUITY RESOLUTION

GPS is a constellation of satellites, from which the broadcasts signals can be used to derive precise timing, location, and velocity information. Standard GPS position estimates can achieve metre to centimetre level accuracies (Lachapelle, 2003), depending on the measurements and methods employed. GPS position estimates can achieve centimetre level accuracy of by using carrier phase observables combined with differential GPS techniques involving two (or more) receivers. However, a navigation system based solely on GPS can achieve such a high accuracy only if the ambiguities have been resolved to their correct integer values. Consequently, several ambiguity resolution techniques have been investigated during the last decade. A brief review of the previous work on ambiguity resolution and validation that has been carried out by many research groups from all over the world will be presented in this chapter.

3.1 OVERVIEW OF AMBIGUITY RESOLUTION

As shown in Table 3.1, the desired GPS carrier phase observable is the number of full carrier cycles, plus the fractional cycle, between the satellites and receiver.

However, a GPS receiver cannot distinguish one carrier cycle from another. The best it can do is measure the instantaneous fractional phase and keep track of whole-cycle changes to the phase; hence, the initial phase value when a receiver starts tracking a satellite contains an arbitrary integer number of cycles. The initially unknown number of cycles between the receiver and a satellite is called the ambiguity.

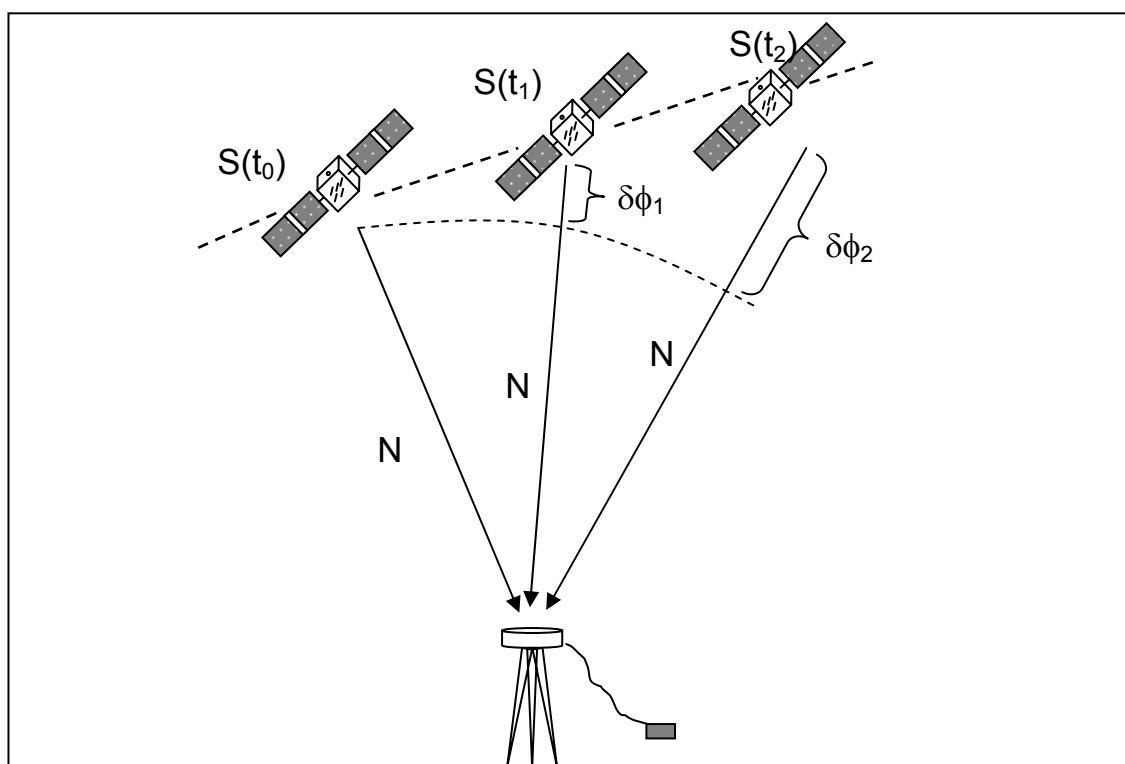


Figure 3.1 - Geometrical Interpretation of Ambiguity (Cannon and Lachapelle, 2003)

As shown in Table 3.1, only after these ambiguities are resolved to be their *integer* values is centimetre level positioning possible (Kaplan, 1996; Lachapelle, 2003). Much research has therefore been focused on resolving the integer

ambiguities in as short a time as possible.

Table 3.1 Achievable Accuracy vs. Different Positioning Choice (Kaplan, 1996; Lachapelle, 2003)

Mode	Achievable Accuracy (m)			
	0.01	0.10	1.0	10.0
Point Positioning (Narrow Correlator™)			←→	
Differential (Standard C/A Code)			←→	
Differential (Narrow Correlator™)			↔	
Differential (Carrier Smoothed, Standard C/A code)			←→	
Differential (Narrow Correlator™ carrier smoothed)			←→	
Differential (Carrier phase)	Fixed	Floating	←→	

The data-processing procedure to determine the integer ambiguity value is called ambiguity resolution (AR).

Since it is simply the exploitation of the integer nature of ambiguities that allows for high-accuracy position estimates in a reasonable time period, the ambiguity resolution procedure is of great consequence in research geared towards the development of high precision GPS applications. Accordingly, three major steps described in foundational studies by Liu (2002) and Lachapelle (2003) to resolve integer ambiguity are adhered to; these are:

- (1) Search space definition (generate the potential integer ambiguity combinations, that should be considered by the algorithm; each combination is comprised of an integer ambiguity for each of the double-difference satellite pairs.);
- (2) Ambiguity resolution (Identify the correct integer ambiguity combination);
and
- (3) Ambiguity validation (Verify the ambiguities resolved in step 2 previously).

Some of the concepts indicated in the above procedures are investigated in further detail below.

SEARCH SPACE

The search space is the volume of uncertainty that surrounds the approximate coordinates of the unknown GPS receiver antenna location. Furthermore, the size of the search space will affect the efficiency - i.e., the computational speed, of ambiguity resolution. Because a larger search space yields a higher number of potential integer ambiguity combinations to assess, this consequently increases the computational burden. It is necessary to balance computational load with a conservative search space size. Much research has been dedicated on this aspect, for example by Teunissen (1997) and Teunissen *et al.* (1996) to

name a couple.

AMBIGUITY RESOLUTION

The criterion used by many ambiguity resolution techniques in identifying the correct integer ambiguity combination is the selection of the integer combination which minimizes the sum-of-squared residuals (SSR) in the least squares adjustment. This introduces the argument that the combination that best fits the data indicates the correct result and, if this combination is correct, the amount of confidence to be accorded. Since only the correct integer ambiguity combination can provide centimetre-level position accuracy, the quality of a GPS ambiguity resolution strategy is closely related to its reliability. More specifically, if a non-optimal ambiguity set is selected, the resulting position error will far exceed the estimated accuracy of that position, resulting in an integrity threat. As such, the ability of the ambiguity resolution process to correctly identify the proper ambiguity resolution set is paramount, especially for safety-critical applications.

AMBIGUITY VALIDATION

Following selection of an integer ambiguity combination, a test (namely the integrity test or a validation procedure) to check the correctness of this solution

must be implemented. Some investigations for verifying the ambiguity resolution have been done. Traditionally, ambiguity validation test procedures are based on the so-called *F-ratio* of the second minimum quadratic form of the least-squares residuals and the minimum quadratic form of the least-squares residuals (Counselman and Abbot, 1989). In this particular method, the F-ratio is approximately treated as a Fisher statistic for comparison. Wang *et al.* (1998) proposed another ambiguity validation test procedure, namely the discrimination function test. This approach is based on the so called W-ratio, the ratio of the difference between the minimum and second minimum quadratic forms of the least-squares residuals and its standard deviation. In this method the W-ratio has a Student's *t* distribution. Furthermore, Teunissen (1998, 1999), proposed a measure of the probability success of the ambiguity resolution approach, particularly for the integer bootstrapping technique adopted by the LAMBDA method.

To this end, Euler and Ziegler (2000) and Kotthoff *et al.* (2003) described the strategy of increasing ambiguity resolution reliability through a repeated search process. In the repeated search process method, the integer ambiguities are continuously recomputed at certain intervals as part of a background process. The presence of different integer ambiguity results will lead to an alarm state, which is a particular value of the ratio, in percentage terms, of one integer ambiguity solution to all possible integer ambiguity solutions of one satellite;

once the previous solution has been proven as incorrect, the process continues with the newly found ambiguity set and monitoring courtesy of the background repeated search process.

3.2 OVERVIEW OF AMBIGUITY SEARCH TECHNIQUES

As the previous sections have described, once the initial ambiguities, along with their respective error covariance values, construct a search space, the search algorithm basically finds appropriate combinations of integer candidates in this search space. The search can be implemented in either the measurement, coordinate or ambiguity domains. Hatch and Euler (1994) presented a comprehensive study of the classification of the ambiguity resolution techniques based on the domain in which the search can be implemented. Some techniques for ambiguity resolution presented during the last decade will be introduced in this section according to this classification. Consistent with the work of Hatch and Euler (1994), the classification of ambiguity search techniques is three-fold.

The first class, which is the simplest ambiguity resolution technique, is in the measurement domain which uses C/A or P-code pseudoranges directly to determine the ambiguities of the corresponding carrier phase observations. This

method is also referred to as geometry-free ambiguity resolution technique (Misra and Enge, 2001). However, because of the relatively poor precision of raw C/A or even P-code pseudoranges for determination of the integer ambiguities, inter-frequency linear combinations of L1 and L2 observations are commonly used with a smoothing process for the estimated ambiguities. Comprehensive studies of the inter-frequency combination can be found in papers of Cocard and Geiger (1992), Liu *et al.* (2002), Liu (2003) and Collins (1999) to name a few of which an investigation follows.

The search algorithms in the coordinate (position) domain (the second class) include the very first ambiguity resolution technique, namely the *Ambiguity Function Method* (AFM) (Counselman and Gourevitch, 1981). Pursuant to the fact that only the fractional value of the instantaneous carrier phase measurement is used in this technique, the ambiguity function values are not affected by the whole-cycle change of the carrier phase or by cycle slips. However, this technique provides poor computational efficiency and consequently it has garnered little interest in recent years, even though significant improvements on the original algorithm have been made by Han and Rizos (1996).

Nowadays, most investigations on ambiguity resolution techniques are focused on techniques based on the theory of integer least-squares estimation

(Teunissen, 1993) in the ambiguity domain, which is the third class. In this theory, ambiguity estimation can be carried out in three steps: (1) the float solution; (2) the integer ambiguity estimation and validation; and (3) the fixed solution (Liu, 2002). Each ambiguity resolution technique makes use of the variance-covariance matrix of the ambiguities obtained at the float solution step, which forms the ambiguity search space mentioned in the previous section; it employs different ambiguity search processes at the integer ambiguity estimation step, then validates the estimated integer ambiguity. According to the nature of the ambiguity search process, different ambiguity resolution techniques have been developed during the last decade, such as the *Least-Squares Ambiguity Search Technique* (LSAST) (Hatch, 1990), the *Fast Ambiguity Resolution Approach* (FARA) (Frei and Beutler, 1990), the *Least-Squares AMBiguity Decorrelation Adjustment* (LAMBDA) (Teunissen, 1994), the *Fast Ambiguity Search Filter* (FASF) (Chen and Lachapelle, 1995), the modified Cholesky decomposition method (Euler and Landau, 1992), the null space method (Martin-Neira *et al.*, 1995) and the *Optimal Method for Estimating GPS Ambiguities* (OMEGA) (Kim and Langley, 1999) to name a few. Further investigation into some of the ambiguity resolution techniques in ambiguity domain mentioned above will be presented in the following section.

3.3 AMBIGUITY SEARCH TECHNIQUES

The ambiguity search techniques which belong to the first two classes delineated in the previous section are so straightforward and thus will not be further discussed. As for the third class, however, only the well-known and often-used search methods are introduced herein. A brief comparison and investigation of all search techniques belonging to the third class is given first in this section to achieve a general appreciation of these techniques.

3.3.1 CLASSIFICATION OF AMBIGUITY SEARCH TECHNIQUES

In comparing and investigating the search techniques, we kept in mind two questions:

- 1) How do the techniques describe or limit the ambiguity search space? and
- 2) How do the techniques deal with the ambiguity parameters?

As mentioned in Section 3.1, reducing the search space that comprises the ambiguity candidate sets is a general approach to improve the computational efficiency. In this case, the correct ambiguity set should be retained in the reduced search space included in the original search space. To date, two approaches have been developed for reliable search space reduction. One

method is the search domain transformation method which transforms the original ambiguity sets into corresponding forms in a transformed space. The reduction effect in this approach is usually achieved through a “many-to-one” relationship between the original and transformed sets, and/or through redefining a more efficient search space than the original (Abidin, 1993; Martin-Neria *et al.*, 1995). The other method for reducing the search space is to define the conditional search ranges in multi-level searches (e.g., FARA and FASF). The basic idea of this approach is based on the fact that the ambiguity parameters of lower search levels are conditioned by those of higher search levels. Naturally, some techniques endeavour to use both transformation and conditional methods simultaneously (e.g., LAMBDA and OMEGA).

To improve the clarity of the above discussion, the following observation is offered: in sum, ambiguity resolution techniques have been classified into three categories as seen in Figure 3.2 by answering “How do the techniques describe or limit the ambiguity search space?”. Figure 3.2 graphically sets out the relationship between the three types of techniques.

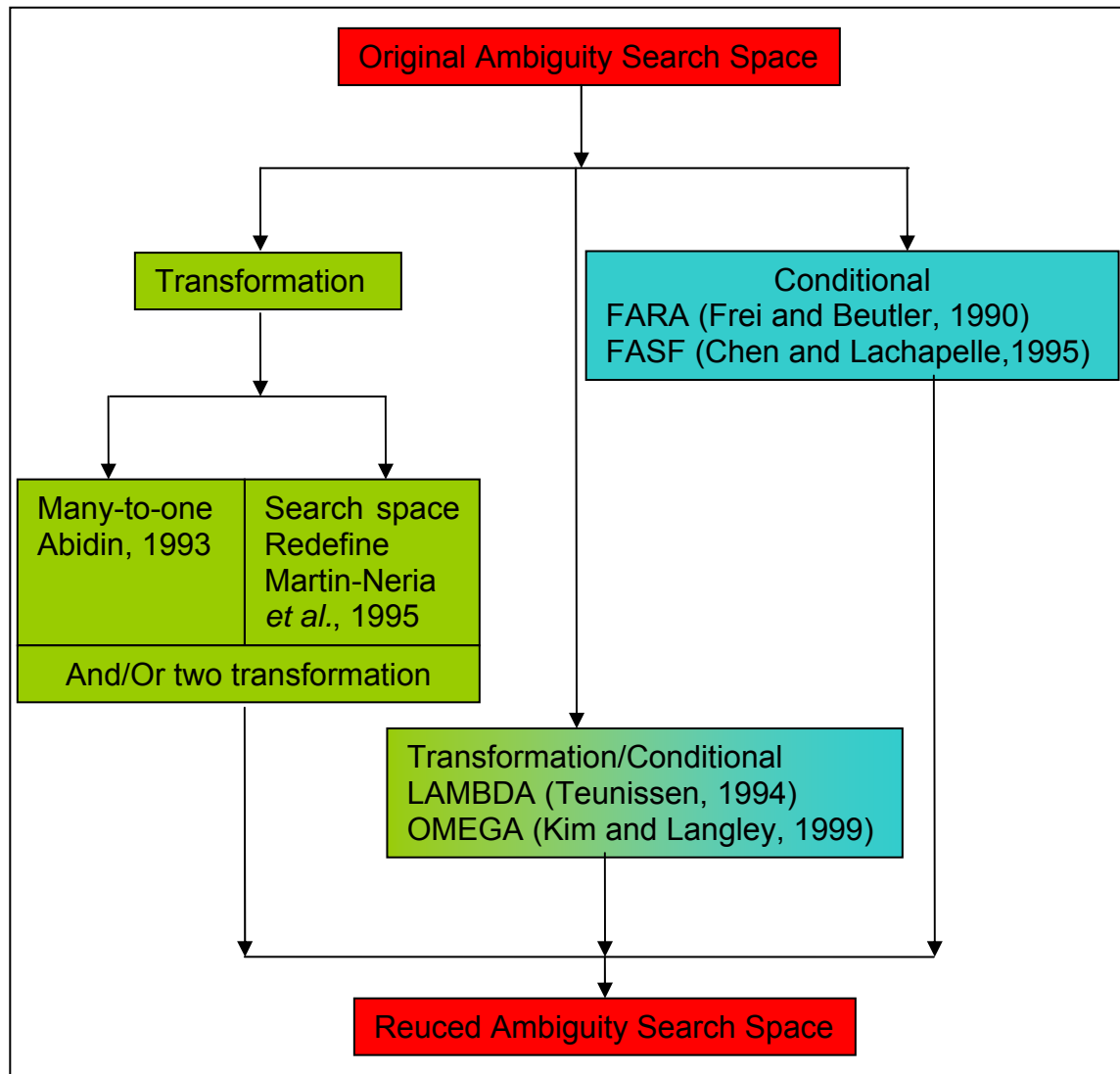


Figure 3.2 Ambiguity Search Techniques Classification

To answer the second question, “How do the techniques deal with the ambiguity parameters?”, the ambiguity search techniques can be grouped into two classes: (1) the “*all-ambiguity-search*” method (e.g., FARA, LAMBDA, FASF and modified Cholesky decomposition method); and (2) the “*independent-ambiguity-search*” (Kim and Langley, 2000) method (e.g., LSAST and OMEGA). The first

method uses all of the ambiguity parameters to generate the ambiguity search space. The second one uses only independent ambiguity parameters which provide a unique solution for the system (or observation equations). The second one enables the determination of dependent ambiguity parameters once their independent homologues are given (Hatch, 1990). One well-known search method that is performed on a transformation/conditional basis (namely LAMBDA) is further described in the following section since it is the search method chosen for use herein.

3.3.2 LAMBDA METHOD

The LAMBDA (Least-square AMBiguity Decorrelation Adjustment) method was investigated by Teunissen in 1993 and 1994. It applies the normal least-squares techniques to obtain the float ambiguities, $\nabla\Delta\hat{N}$, and its variance-covariance (VCV) matrix, $\mathbf{Q}_{\nabla\Delta\hat{N}}$. However, nowadays, the initial float ambiguities and the VCV matrix are usually arrived at through GPS Kalman filtering. Nevertheless, the LAMBDA search technique is still essentially the same in terms of its use of the same candidate ambiguities and VCV information. The search process consists basically of a procedure to find the appropriate $\nabla\Delta N$ satisfying the following condition

$$\left(\nabla\Delta\hat{N} - \nabla\Delta N\right)^T \mathbf{Q}_{\nabla\Delta\hat{N}}^{-1} \left(\nabla\Delta\hat{N} - \nabla\Delta N\right) = \text{minumum} \quad (3.1)$$

Unfortunately, the standard techniques, which are commonly available for solving ordinary least-squares problems, generally cannot be used for solving Equation (3.1) due to the integer property of the ambiguity candidates. Consequently, methods that in one way or another make use of a discrete search strategy to find the minimization of Equation (3.1) must be used. The idea is to use the objective function of Equation (3.1) to introduce an ellipsoidal region in \mathbb{R}^n . A search is then performed on the basis of that ellipsoidal region for the minimization of Equation (3.1). The ellipsoidal search space, or search region, is given by (Teunissen, 1993)

$$\left(\nabla\Delta\hat{N} - \nabla\Delta N\right)^T \mathbf{Q}_{\nabla\Delta\hat{N}}^{-1} \left(\nabla\Delta\hat{N} - \nabla\Delta N\right) \leq \chi^2 \quad (3.2)$$

where χ^2 is a positive constant and the selection of which can control the size of ellipsoidal search region. The search region is centred at the float solution, $\nabla\Delta\hat{N}$, with its shape being determined by the variance-covariance matrix, $\mathbf{Q}_{\nabla\Delta\hat{N}}$. However, the quadratic form of Inequality Equation (3.2) cannot be used as a criterion to identify the set of candidate grid-points. So the ellipsoidal planes of support are introduced to replace the inequality in Equation (3.2) with an equivalent description, and the search region bounded by the planes of support

represented by Inequality Equation (3.2) becomes (Teunissen, 1993)

$$\left(\nabla\Delta\hat{N}_i - \nabla\Delta N_i\right)^2 \leq \sigma_{\nabla\Delta\hat{N}_i}^2 \chi^2, i = 1, 2, \dots, n \quad (3.3)$$

Where $\sigma_{\nabla\Delta\hat{N}_i}^2$ is the variance of the estimator of $\nabla\Delta\hat{N}_i$. Inequality Equation (3.3) can be used to select candidate grid-points from which the minimization of (3.1) can then be chosen. Although Inequality Equation (3.3) is promising in its simplicity, the search can be very time consuming when the search region defined by Inequality Equation (3.3) is significantly larger than the original ellipsoidal region. Furthermore, this will definitely occur when the ellipsoid is both elongated and rotated with respect to the grid axes. To address this situation, adjustable bounds are introduced. Bounds are made dependent on the stage of progress of the search process. These bounds were obtained through a sequential conditional least-squares adjustment, which resulted in the introduction of the conditional estimated float ambiguities. The bounds can be represented as follows (Teunissen, 1993)

$$\left(\nabla\Delta\hat{N}_{i|N, N=1, 2, \dots, n} - \nabla\Delta N_i\right)^2 \leq \lambda_{\nabla\Delta\hat{N}_i} \sigma_{\nabla\Delta\hat{N}_{i|N, N=1, 2, \dots, n}}^2 \chi^2, i = 1, 2, \dots, n \quad (3.4)$$

$$\lambda_{\nabla\Delta\hat{N}_i} = \left[1 - \sum_{j=i+1}^n \frac{\left(\nabla\Delta N_j - \nabla\Delta\hat{N}_{j|M, M=1, 2, \dots, n}\right)^2}{\sigma_{\nabla\Delta\hat{N}_{j|M, M=1, 2, \dots, n}}^2 \chi^2} \right] \quad (3.5)$$

These bounds, as represented by Inequality Equation (3.4) and Equation (3.5), are indeed much less conservative than Inequality Equation (3.3). The search space given by Inequality Equation (3.2), makes it difficult to implement the search due to the non-diagonal of the variance-covariance matrix $\mathbf{Q}_{\nabla\Delta\hat{N}}$. To facilitate the search and achieve better efficiency, a LAMBDA decorrelation is applied to $\mathbf{Q}_{\nabla\Delta\hat{N}}$. The LAMBDA decorrelation basically performs a Z-transformation which makes $\mathbf{Q}_{\nabla\Delta\hat{N}}$ nearly diagonal (which means that the ambiguities become almost fully decorrelated). After the LAMBDA decorrelation is applied, the ambiguities as well as the variance-covariance matrix are transformed into the Z domain. The search problem is then converted into the transformed search space. Denoting the transformed float ambiguities and its variance-covariance matrix as \hat{z} and $\mathbf{Q}_{\hat{z}}$, the quadratic form of Equation (3.1) can then be written in the following form (Teunissen, 1993; Teunissen, 1994)

$$\left(\nabla\Delta\hat{N} - \nabla\Delta N\right)^T \mathbf{Q}_{\nabla\Delta\hat{N}}^{-1} \left(\nabla\Delta\hat{N} - \nabla\Delta N\right) = \left(\hat{z} - z\right)^T \mathbf{Q}_{\hat{z}}^{-1} \left(\hat{z} - z\right) \quad (3.6)$$

Based on the triangular decomposition of the variance-covariance matrix $\mathbf{Q}_{\hat{z}}$, the quadratic form of Equation (3.3) can be further expressed as a sum of independent squares in the individual ambiguities (Teunissen, 1993)

$$(\hat{z} - z)^T \mathbf{Q}_{\hat{z}}^{-1} (\hat{z} - z) = \sum_{i=1}^n (\hat{z}_{i|N, N=1,2,\dots,i-1} - z_i)^2 / \sigma_{\hat{z}_{i|N, N=1,2,\dots,i-1}}^2 \quad (3.7)$$

Where $\sigma_{\hat{z}_{i|N, N=1,2,\dots,i-1}}^2$ is the i^{th} diagonal element of matrix $\mathbf{Q}_{\hat{z}}$, which represents the conditional variance of ambiguity z_i conditioned on all previous ones ($N = 1, 2, \dots, i-1$). The term $\hat{z}_{i|N, N=1,2,\dots,i-1}$ denotes the conditional ambiguities, also conditioned on all previous values. Inequality Equation (3.4) and Equation (3.5) can be further represented as

$$(\hat{z}_{i|N, N=1,2,\dots,n} - z_i)^2 \leq \lambda_{z_i} \sigma_{\hat{z}_{i|N, N=1,2,\dots,n}}^2 \chi^2, i = 1, 2, \dots, n \quad (3.8)$$

$$\lambda_{z_i} = \left[1 - \sum_{j=i+1}^n \frac{(z_j - \hat{z}_{j|M, M=1,2,\dots,n})}{\sigma_{\hat{z}_{j|M, M=1,2,\dots,n}}^2 \chi^2} \right] \quad (3.9)$$

Inequality Equation (3.8) and Equation (3.9) allow performance of the search for the transformed integer least-squares ambiguities in a highly efficient manner.

A search performed within all ranges defined by Inequality Equation (3.8) and Equation (3.9) attempts to find two integer candidate sets with the smallest and the second-smallest sum-of-squared (SOS) residuals. The discrimination test will use the ratio of the smallest and the second-smallest SOS residuals by comparing each with a predefined threshold to decide if the candidate set

ambiguities with the smallest SOS is deemed to be the correct integer solution. The fixed integers are then transformed back from Z domain by applying an inverse Z-transformation.

3.3.3 AMBIGUITY RESOLUTION IMPROVEMENTS WITH AIDING OF INERTIAL DATA

The foregoing investigation on GPS, INS, GPS/INS integration and GPS ambiguity search techniques leads naturally to the question of how GPS ambiguity resolution can be improved with the aid of inertial data. To this end, many researchers, such as Farrell *et al.* (2000), Sennott and Senffner (1997), and Grejner-Brzezinska *et al.* (1998) to name a few, have conducted studies only on the aspect of accuracy improvements realized through aiding by inertial data. In recent years, researchers such as Škaloud (1998), Petovello *et al.* (2001), Petovello (2003a), Petovello *et al.* (2003), and Scherzinger (2000) explored the improvements in ambiguity resolution search space and time to fix based inertial data aiding; however, an investigation of the magnitude of improvement in ambiguity resolution with inertial data aiding is still desired. Zhang *et al.* (2005) first proposed an analytical equation to quantify the ambiguity resolution improvements with respect to the INS free-inertial solution after GPS outages. To better accommodate the uniqueness of each type of coupling strategy, this section focuses on analyzing the quantity of improvement.

Generally, the time to fix ambiguities after a GPS outage depends on three factors: (1) The float ambiguity estimate from the GPS or GPS/INS filter after the first phase measurement following a GPS outage; (2) The filter's convergence speed; and (3) GPS measurement noise and the level of tropospheric, ionospheric and multipath errors. The first factor, the float ambiguity candidates from the GPS or GPS/INS filter after the first phase measurement following a GPS outage, will definitely decide the initial states and corresponding variance-covariance (VCV) matrix. The second factor, the convergence speed of filters used, will decide how rapidly the VCV decreases to a reasonable value leading to a successful search. The third factor, measurement noise and the level of tropospheric, ionospheric and multipath errors, usually affects the overall success of the search process in terms of time to fix and correctness of fix. The desired quantity improvements will be investigated as follows through an analysis of the three factors identified above. The fact that loosely and tightly coupled integration strategies have different abilities to affect the second factor (convergence speed of filters) mentioned above must be kept in mind before further investigation.

The *a priori* and *a posteriori* VCV matrices are partitioned as $\mathbf{P} = \begin{bmatrix} \mathbf{P}_s & \mathbf{P}_{sa} \\ \mathbf{P}_{sa}^T & \mathbf{P}_a \end{bmatrix}$ with

$\mathbf{P}_s = \begin{bmatrix} \mathbf{P}_{\hat{\delta p}} & \mathbf{P}_{12} \\ \mathbf{P}_{12}^T & \mathbf{P}_2 \end{bmatrix}$ where $\mathbf{P}_{\hat{\delta p}}$ is the estimation error VCV matrix for inertial position

error states. \mathbf{P}_2 is the VCV of remaining velocity error, misalignment and inertial error states when using a tight coupling strategy, and is the VCV of velocity error states when a loose coupling strategy is used. \mathbf{P}_a is the VCV of estimated float ambiguity states.

The float ambiguity states are re-initialized following a GPS outage to reflect complete loss of phase information so that, consistent with theory in (Scherzinger, 2002), $\mathbf{P}_a^- = \sigma_{a_0}^2 \mathbf{D}^T \mathbf{D}$ and $\mathbf{P}_{sa}^- = \mathbf{0}$. This means that the \mathbf{P}_a^- is essentially the same using either integration strategy (GPS only, loose coupling or tight coupling).

To this end, the equation representing the updated ambiguity covariance matrix after a resetting of the ambiguity states can be written as (Scherzinger, 2002)

$$\mathbf{P}_a^+ = \mathbf{P}_a^- - \lambda^2 \mathbf{P}_a^- \left[\mathbf{D}^T \mathbf{A} \mathbf{P}_{\phi}^- \mathbf{A}^T \mathbf{D} + \lambda^2 \mathbf{P}_a^- + \mathbf{R}_\phi \right]^{-1} \mathbf{P}_a^- \quad (3.10)$$

In the above equation, the superscript minus (“-”) denotes a quantity before update and the superscript plus (“+”) denotes a quantity after update, and

\mathbf{P}_a is the covariance matrix of the ambiguity states,

\mathbf{D} is the double-difference operator,

\mathbf{A} is the single-difference design matrix of the observations,

λ is the phase wavelength

$\mathbf{P}_{\delta p}$ is the covariance matrix of the position errors prior to incorporating the carrier phase data, and

\mathbf{R}_{ϕ} is the covariance matrix of the phase observation noise.

$\mathbf{P}_{\delta p}$ in the GPS only case is simply the double-differenced code solution position error VCV. In the integrated case, however, it can be computed as following Equation (3.11).

In the current context, the significance of Equation (3.10) is that it shows that the covariance of the ambiguities decreases with a smaller *a priori* covariance matrix of the position errors (prior to incorporating the carrier phase data), thus reducing the time required to fix ambiguities. To this end, the *a priori* covariance matrix of the position errors after resetting of the ambiguity states (i.e., after a data outage) can be thought of as the weighted average of the differential GPS code solution at that time and the INS solution, as shown in the following equation

$$\mathbf{P}_{\delta p}^{-1} = \mathbf{P}_{INS}^{-1} + \mathbf{P}_{Code}^{-1} \quad (3.11)$$

where \mathbf{P}_{Code} is the covariance matrix of the differential code position solution and

\mathbf{P}_{INS} is the covariance matrix of the INS position solution. To better understand Equation (3.11), the 3-by-3 covariance matrices, $\mathbf{P}_{(\cdot)}$, is replaced with the corresponding 3-D position variance, $\sigma_{(\cdot)}^2$. In this way, Equation (3.11) can be written as

$$\sigma_{\delta p} = \frac{1}{\sqrt{\frac{1}{\sigma_{Code}^2} + \frac{1}{\sigma_{INS}^2}}} = \frac{\sigma_{Code}\sigma_{INS}}{\sqrt{\sigma_{Code}^2 + \sigma_{INS}^2}} \quad (3.12)$$

Now consider that for the GPS-only case, the initial position accuracy before adding the carrier phase data after a data outage will be given by the differential code accuracy (i.e., $\sigma_{\delta p} = \sigma_{Code}$). However, for the integrated case, the initial position accuracy before adding the carrier phase data will be given by Equation (3.12). The percentage improvement in $\sigma_{\delta p}$ relative to the GPS-only case, $I_{\%}$, can therefore be written as

$$\begin{aligned} I_{\%} &= \frac{\sigma_{GPS} - \sigma_{GPS/INS}}{\sigma_{GPS}} \times 100 \\ &= \left(1 - \frac{\sigma_{INS}}{\sqrt{\sigma_{Code}^2 + \sigma_{INS}^2}} \right) \times 100 \end{aligned} \quad (3.13)$$

Returning to Equation (3.10), with a different *a priori* covariance $\mathbf{P}_{\hat{p}1}^-$ and $\mathbf{P}_{\hat{p}2}^-$,

which represents *a priori* covariance using the GPS-only and integrated strategies, respectively, the updated ambiguity states' covariances are different. According to the property of Equation (3.11), $\mathbf{P}_{\hat{p}1}^- - \mathbf{P}_{\hat{p}2}^-$ is positive semi-definite.

As such

$$\mathbf{P}_{a1}^+ - \mathbf{P}_{a2}^+ = \lambda^2 \sigma_{a_0}^4 \mathbf{D}^T \mathbf{D} \mathbf{R}_{a_2}^{-1} \mathbf{D}^T \mathbf{A} (\mathbf{P}_{\hat{p}1}^- - \mathbf{P}_{\hat{p}2}^-) \mathbf{A}^T \mathbf{D} \mathbf{R}_{a_1}^{-1} \mathbf{D}^T \mathbf{D} \quad (3.14)$$

Thus, improvements in $\sigma_{\hat{p}}$ should translate directly into improvements in ambiguity resolution time following a data outage. Equation (3.13) can be considered as an analytical estimate of the ambiguity resolution improvement (relative to GPS-only), as a function of σ_{Code} and σ_{INS} . Note that the translation from Equation (3.11) to Equation (3.12) does not take the cross-correlation values into account, so that this relation is simply an analytical estimation under ideal conditions. Furthermore, Equation (3.13) does not account for phase measurement noise and assumes that the cross-correlation between position states and ambiguity states is very small. As discussed in the first paragraph of Section 3.3.3, this equation might be different since distinct integration strategies have different abilities to affect the other two factors which, in turn, affect the time to fix ambiguities after GPS outages. This will be further shown in Chapter Six.

It is important to note at this point that the above analysis is based on a simplification of the equations to accommodate ideal conditions, which can be better represented by a tight coupling strategy as mentioned in Section 2.3.1. Tightly coupled integration provides for enhanced observability of the floated ambiguities when the inertial position error is sufficiently small via the cross-correlation between the roving position error and floated ambiguities generated by the phase DD measurement (Scherzinger, 2002). As such, compared to loosely coupled integration, it has a faster converging filter. That implies that the analytical equation represented by Equation (3.13) is more suitable for tightly coupled integration, and the improvements gained through the use of loosely coupled integration is expected to be lower than the values computed using Equation (3.13). It is important to note that Equation (3.13) is capable of simply predicting the GPS-only ambiguity resolution improvements, and cannot be used directly to improve the ambiguity resolution in the GPS-only case. Thus, with a given system and data set, the ambiguity resolution performance of GPS-only has already been determined. The significance of Equation (3.13) is solely to predict how much improvement can ideally be expected compared to GPS-only with inertial aiding in terms of the free-inertial accuracy at the end of a GPS data outage. It should also be noted that in Equation 3.10, the covariance of the phase measurement noise is assumed to be negligible as compared to other factors inside the brackets. However, under certain conditions, the effects of phase measurement noise are not negligible; e.g., a weak signal is typically

characterized by a very low GPS signal to noise ratio. Equation 3.13 might not be applicable in such a situation.

3.4 OVERVIEW OF GPS OBSERVABLES – GPS INTER-FREQUENCY CARRIER PHASE COMBINATION

Following the above investigation of ambiguity resolution techniques, an overview of GPS inter-frequency carrier phase combinations available from dual frequency GPS carrier phase observations and relative errors is given in this section. According to the general rule of thumb that instantaneous ambiguity resolution is possible if the position accuracy (along the line-of-sight to the satellite) is known to better than half of the wavelength of the ambiguities being resolved (de Jong *et al.*, 2002), the inter-frequency carrier phase combinations and relative errors will be evaluated with two different scales: cycles and metres.

L1, L2 OBSERVATION:

The simplified versions of the GPS L1 and L2 carrier phase observations can be presented as:

$$CP_1[\text{cycle}] = \frac{\rho + \lambda_1 N_1 - I + \varepsilon_{CP1}}{\lambda_1} \quad (3.14)$$

$$CP_2[\text{cycle}] = \frac{\rho + \lambda_2 N_2 - q^2 I + \varepsilon_{CP2}}{\lambda_2} \quad (3.15)$$

where ρ represents the geometric range plus troposphere, clocks and orbit error; $\lambda_{1/2}$ represents the wavelength associated with each frequency; $N_{1/2}$ is the corresponding cycle ambiguity; $\varepsilon_{CP1/CP2}$ is the carrier phase noise and multipath error associated with each frequency; I is the ionospheric propagation delay on the L1 frequency; and q is the ratio of L1 frequency to L2 frequency which is $f_1/f_2 = 77/60$. Thus, the general expression for a linearly combined carrier phase observation is

$$CP_{i,j} = iCP_1 + jCP_2 \quad (3.16)$$

The wavelength of $CP_{i,j}$ can be expressed as $\lambda_{i,j} = \left(\frac{i}{\lambda_1} + \frac{j}{\lambda_2} \right)^{-1}$ with ambiguity

$$N_{i,j} = iN_1 + jN_2.$$

The observation for a linearly combined carrier phase observation can be presented as

$$CP_{i,j} = \frac{\rho}{\lambda_{i,j}} + N_{i,j} - (i + jq) \frac{I}{\lambda_1} + e(CP_{i,j}) \quad (3.17)$$

where e is the un-modeled error (multipath, noise, residual tropospheric error) combined of two frequencies, and ρ is the double-differenced satellite to receiver range. When the measurement noise (including of carrier phase noise and multipath) of the phase linear combination exceeds a certain threshold, correct ambiguity resolution becomes difficult or highly unlikely. So the measurement noise of the linear combined observation is investigated in a generic manner as following.

Assuming that the measurement noise of a L1 and L2 phase observation has the same portion of its wavelength in cycle (e.g. $\alpha\%$ un-differenced), the corresponding double-differenced measurement noise of L1 and L2 is:

$$\begin{aligned} e(CPi) &= 2\alpha\% \quad (\text{cycles}) \\ &= 2\alpha\% \times \lambda_i \quad (\text{metres}) \end{aligned}$$

Then the linear combined measurement noise will be:

$$\begin{aligned}
e(CP_{i,j}) &= \sqrt{i^2 + j^2} 2\alpha\% && \text{(cycles)} \\
&= \sqrt{i^2 + j^2} 2\alpha\% \lambda_{i,j} && \text{(metres)}
\end{aligned}$$

The most commonly used linear combinations such as widelane (WL), ionosphere free (IF) and narrowlane (NL) consequently can be achieved according to previous equations and will be presented in detail as follows.

WIDELANE COMBINATION ($CP_{WL}, i = 1, j = -1$):

$$\begin{aligned}
CP_{WL} &= \frac{\rho}{\lambda_{WL}} + N_{WL} - \frac{17}{60} \frac{I}{\lambda_1} + e(CP_{WL}) \\
N_{WL} &= N_1 - N_2 \\
\lambda_{WL} &= \left(\frac{1}{\lambda_1} - \frac{1}{\lambda_2} \right)^{-1} \\
&= 0.862 \text{ m} \\
e(CP_{WL}) &= \sqrt{2} \times 2\alpha\% && \text{(cycles)} \\
&= \sqrt{2} \times 2\alpha\% \lambda_{WL} && \text{(metres)}
\end{aligned} \tag{3.18}$$

With a very small ionospheric effect (in cycles) which is reduced to 17/60 of an L1 wavelength – meaning that, if the ionospheric bias on the L1 observable is one L1 cycle, the corresponding ionosphere error on the WL observable is only 17/60 of a cycle. Consequently, the widelane combination is more resistant to ionospheric errors (in cycles) than either L1 or L2 and is more reliable for

ambiguity resolution under adverse ionospheric conditions. Despite the reduction in the impact of the ionospheric error in terms of the number of cycles, the widelane approach amplifies the ionospheric effect in metres

($\frac{17}{60} \frac{I}{\lambda_1} \lambda_{WL} = \frac{77}{60} I$) and noise in the widelane observable. The result is a noisier

position estimate, compared to the corresponding L1 or L2 case.

NARROWLANE COMBINATION ($CP_{NL}, i = 1, j = 1$):

$$\begin{aligned}
 CP_{NL} &= \frac{\rho}{\lambda_{NL}} - N_{NL} - \frac{137}{60} \frac{I}{\lambda_1} + e(CP_{NL}) \\
 N_{NL} &= N_1 + N_2 \\
 \lambda_{NL} &= \left(\frac{1}{\lambda_1} + \frac{1}{\lambda_2} \right)^{-1} \\
 &= 0.107 \text{ m} \\
 e(CP_{NL}) &= \sqrt{2} \times 2\alpha\% \quad (\text{cycles}) \\
 &= \sqrt{2} \times 2\alpha\% \lambda_{NL} \quad (\text{metres})
 \end{aligned} \tag{3.19}$$

The narrowlane combination (NL) has the unusual property of reducing the noise (in terms of metre units). This means that, after resolving NL ambiguities, the position accuracy will be increased. As a result, the narrowlane should give better positioning results than L1, WL and IF, if the ionospheric error is negligible. However, the decreasing of NL wavelength makes resolution of NL ambiguities very difficult. Further more, the narrowlane combination amplifies the

measurement noise in cycle and the ionospheric effect which is equal to what wideband has. In this research, the narrowband is not investigated further since its integer ambiguity is difficult to resolve.

IONOSPHERE-FREE (IF) COMBINATION ($CP_{IF}, i=1, j=-\frac{\lambda_1}{\lambda_2}$):

$$\begin{aligned}
 CP_{IF} &= \frac{\rho}{\lambda_{IF}} - N_{IF} + e(CP_{IF}) \\
 N_{IF} &= N_1 - \frac{\lambda_1}{\lambda_2} N_2 \\
 \lambda_{IF} &= \left(\frac{1}{\lambda_1} - \frac{\lambda_1}{\lambda_2^2} \right)^{-1} && (3.20) \\
 &= 0.483 \text{ m} \\
 e(CP_{IF}) &= 0.9\sqrt{2} \times 2\alpha\% \quad (\text{cycles}) \\
 &= 0.9\sqrt{2} \times 2\alpha\% \lambda_{IF} \quad (\text{metres})
 \end{aligned}$$

Obviously, the removal of the first-order effects of the ionosphere is the main advantage of the ionosphere-free (IF) combination; however, the IF ambiguities are no longer integer in nature and must therefore be estimated as real-valued parameters.

A detailed comparison of inter-frequency carrier phase combination is presented in Table 3.2 (Liu, 2002; Collins, 1999; Lachapelle, 2003).

Table 3.2 Inter-frequency carrier phase combination characteristics

$CP_{i,j}$	i	j	$\lambda_{i,j}$	$\lambda_1/\lambda_{i,j}$	Amplification (cycles)			Amplification (length)		
					noise	ion	mp	noise	ion	mp
CP_1	1	0	19.0	1	1	1	1	1	1	1
CP_2	0	1	24.4	0.78	1	1.28	1	1.28	1.63	1.28
CP_{WL}	1	-1	86.2	0.22	1.41	-0.28	1.41	6.42	-1.28	6.42
CP_{NL}	1	1	10.7	1.78	1.41	2.28	1.41	0.80	1.28	0.80
CP_{IF}	1	-77/60	48.3	0.39	1.26	0	1.26	3.23	0	3.23

3.5 AMBIGUITY ESTIMATION PROCESSING STRATEGIES

With the various combinations of observables discussed in the previous section, many ambiguity estimation processing strategies arise, as detailed in Liu *et al.* (2003) and Liu (2002).

Table 3.3 given by Liu *et al.* (2003) presents eight different strategies in terms of ambiguities estimated and observables used. The pseudorange observable P is used in every strategy and $CP_{1/2}$ represents the corresponding L1 or L2 carrier phase observable, while $N_{1/2/WL}$ represents L1, L2 or widelane ambiguities

Table 3.3 Processing Strategy Summary¹

Strategy	Ambiguities estimated	Observables used	Ionosphere
1	N_1	$CP_1 P$	Not Parameterized
2	N_{WL}	$CP_1 CP_2 P$	
3	$N_1 N_2$	$CP_1 CP_2 P$	
4	$N_1 N_{WL}$	$CP_1 CP_2 P$	
5	$N_1 N_{WL}$ (IF fixed)	$CP_1 CP_2 P$	Ionosphere-Free Combinations
6	N_{IF} (IF float)	$CP_1 CP_2 P$	
7	$N_1 N_2$	$CP_1 CP_2 P$	Stochastic Ionosphere Modeling
8	$N_1 N_{WL}$	$CP_1 CP_2 P$	

¹ Refer to Section 3.4, "Overview of GPS Observables", for details on the advantages and disadvantages of each inter-frequency combination.

The eight strategies shown in Table 3.3, can be separated into three categories. Strategies 1 to 4 belong to the first class, which does not take ionosphere bias into account. The second class consists of strategies 5 and 6. By using the IF observable, the second class can remove the first-order ionosphere bias and, by estimating ionosphere bias through stochastic ionospheric modeling, the third class, which contains strategies 7 and 8, can significantly eliminate the ionosphere bias.

Based on the test results given by Liu *et al.* (2003) a further investigation into the advantages and disadvantages of different processing strategies is given as follows.

1. WL ambiguity resolution is reliable as well as easier to resolve than both the L1 and L2 ambiguities. However, WL combinations cannot guarantee the

optimal position results in terms of accuracy under conditions of high ionospheric activity because of the amplification of ionospheric bias in the WL observable in units of metres.

2. The IF combination observable or the stochastic ionosphere modeling processing strategies are more suitable for high ionospheric activity conditions for achievement of optimal position results.
3. Because the WL ambiguity is easier to resolve than both the L1 and L2 ambiguity, better position results can be achieved after the WL ambiguities are correctly fixed while L1 ambiguities are not fixed if L1 and WL ambiguities are estimated in the same filter, instead of L1 and L2 ambiguities. And since resolution of WL ambiguities can speed up the convergence speed of filters, this strategy is expected faster time to fix L1 ambiguities compared to Strategy 1 when the filter start from the same initial condition. This being said, start from same condition (same initial position, velocity, VCV and so on) the Kalman filter using strategy 1 and strategy 4 has different convergence speed with the filter of using strategy 4 faster. For instance, GPS-only Kalman filter using strategy 1 needs more time than that of using strategy 4 when the Kalman filters initialized with the same initial values (which is the case after GPS outage) to converge to same level.
4. For Strategy 5, the reduced wavelength results in a longer time to fix the L1 ambiguities, thus limiting the real-time use of this case. Furthermore, because of the slow convergence, Strategy 5 can obtain only an ionospheric-free solution if the L1 ambiguities are not fixed. This effectively makes Strategy 5 unsuitable for practical purposes. So this strategy will not be implemented in the software used herein, and not be investigated in this thesis either.

5. By comparison, Strategy 1 can provide the accurate solution and typically used in most applications, but its success is dependent on several factors, such as measurement noise, residual tropospheric error, multipath and the ionospheric level.

So, the strategy 1 will be investigated in Chapter Six with emphasize on short baseline results. Strategy 1, 2, 3, 4, 6, 7, 8 will be investigated in Chapter Seven to compare the performance of each strategy with presence large differential errors (long baseline).

CHAPTER FOUR - OPTIMAL BACKWARD SMOOTHING FOR BRIDGING POSITION ERROR DURING GPS OUTAGES

GPS generally provides high quality carrier phase measurements (via tight coupling), and accurate position and velocity information (via loose coupling). However, in many cases, the GPS signal might be blocked or lost, which means that no update is available. If accurate positions are required during such outages, some bridging algorithms must be used for estimating improved positions for these periods (Nassar, 2002). One of the bridging methods, namely optimal backward smoothing, is profiled in this chapter.

4.1 INS/GPS EXTENDED KALMAN FILTER

As discussed in Chapter Two, more detailed information about the system and measurement model can be found in Wu (2003). The discrete error model and measurement model can be written as

$$\begin{aligned}\delta\mathbf{X}_k &= \Phi_{k,k-1}\delta\mathbf{X}_{k-1} + \mathbf{W}_{k-1} \\ \delta\mathbf{Z}_k &= \mathbf{H}_k\delta\mathbf{X}_k + \mathbf{V}_k\end{aligned}\tag{4.1}$$

$\delta\mathbf{X} = [\delta\mathbf{p} \ \delta\mathbf{v} \ \boldsymbol{\varepsilon} \ \mathbf{b} \ \mathbf{d}]^T$ represents the Kalman filter error states. Double-differenced ambiguity correction states should be added in tightly coupled mode. The parameters in Equation (4.1) are interpreted as follows for the purposes of convenience:

$\delta\mathbf{X}_k$ is the system error state vector to be estimated at time t_k ,

$\Phi_{k,k-1}$ is the system state transition matrix,

\mathbf{W}_{k-1} is the vector of the system input random noise, and

$E[\mathbf{W}_k \mathbf{W}_j^T] = \mathbf{Q}_k \delta_{kj}$ where $\delta_{kj} = \begin{cases} 1, & j = k \\ 0, & j \neq k \end{cases}$, \mathbf{Q}_k is system noise covariance matrix,

$\delta\mathbf{Z}_k$ is the vector of the system observations (measurement update) at time t_k ,

\mathbf{H}_k is the design matrix relating the system measurements to the system error states, and

\mathbf{V}_k is the vector of measurements random noise. And $E[\mathbf{V}_k \mathbf{V}_j^T] = \mathbf{R}_k \delta_{kj}$

where $\delta_{kj} = \begin{cases} 1, & j = k \\ 0, & j \neq k \end{cases}$, \mathbf{R}_k is the measurement noise covariance matrix.

It should be noted that the measurement model depends on whether a loosely or tightly coupled strategy is used.

For optimal estimation of the SINS error state vector components, an Extended Kalman Filter (EKF) is used herein; the discrete EKF algorithm can be summarized as

$$\begin{aligned}
 \delta \hat{\mathbf{X}}_{k,k-1} &= \Phi_{k,k-1} \delta \hat{\mathbf{X}}_{k-1} \\
 \mathbf{P}_{k,k-1} &= \Phi_{k,k-1} \mathbf{P}_{k-1} \Phi_{k,k-1}^T + \mathbf{Q}_{k-1} \\
 \mathbf{K}_k &= \mathbf{P}_{k,k-1} \mathbf{H}_k^T [\mathbf{H}_k \mathbf{P}_{k,k-1} \mathbf{H}_k^T + \mathbf{R}_k]^{-1} \\
 \delta \hat{\mathbf{X}}_k &= \delta \hat{\mathbf{X}}_{k,k-1} + \mathbf{K}_k [\delta \mathbf{Z}_k - \mathbf{H}_k \delta \hat{\mathbf{X}}_{k,k-1}] \\
 \mathbf{P}_k &= (\mathbf{I} - \mathbf{K}_k \mathbf{H}_k) \mathbf{P}_{k,k-1}
 \end{aligned} \tag{4.2}$$

Equation (4.1) is the result of the perturbed system represented by Equation (2.15). After achieving the optimal estimation $\delta \hat{\mathbf{X}}_{k-1}$, $\delta \hat{\mathbf{X}}_{k-1}$ is used to correct the mechanization results. Thus, $\delta \hat{\mathbf{X}}_{k-1}$ is always zero, which means that the first step in such prediction is always zero.

$$\delta \hat{\mathbf{X}}_{k,k-1} \equiv \mathbf{0} \tag{4.3}$$

As seen in Equations (4.2) and (4.3), in the case of SINS/GPS integration, the state vector can be estimated with GPS measurement updates. In case of a GPS outage, no GPS measurement updates are available. Therefore, the measurement noise covariance matrix \mathbf{R}_k in Equation (4.2) can be considered

to equal infinity ∞ and, hence, the Kalman gain matrix \mathbf{K}_k in the same equation will be zero. Consequently, during GPS outage intervals, the updated Equation (4.2) will take the following forms:

$$\begin{aligned}\hat{\delta\mathbf{X}}_k &= \hat{\delta\mathbf{X}}_{k,k-1} \equiv \mathbf{0} \\ \mathbf{P}_k &= \mathbf{P}_{k,k-1} = \Phi_{k,k-1} \mathbf{P}_{k-1} \Phi_{k,k-1}^T + \mathbf{Q}_{k-1}\end{aligned}\tag{4.4}$$

This being said, the mechanization solution error continually grows and the error correction cannot be estimated until GPS updates become available again.

4.2 BACKWARD SMOOTHING ALGORITHMS

In the previous section, optimal estimation of the error states vector at epoch k , provided by EKF, is obtained using measurements that are available only up to epoch k . Optimal Backward Smoothing (BS), however, allows an optimally smoothed estimation of the state vector at epoch k using all or some of the measurements that are available before and after epoch k . Basically, the BS algorithm could be considered as a means of optimally combining forward estimation and backward estimations. With this in mind, the development of an optimal smoother algorithm is presented in this section. For simplicity's sake, $\delta\mathbf{X}$ and $\delta\mathbf{Z}$ will be referred to as \mathbf{X} and \mathbf{Z} , respectively, in the following

discussion.

4.2.1 SMOOTHER BASIC

In late 1950s, many needs in applications such space navigation, statistical communication theory, made Wiener filter (Wiener, 1949) comes into reality. Kalman in 1961 introduced Kalman filter which can be mechanized easily on the present-day digital computer. These two filters were very closely bonded to navigation application since they were introduced, major reason of that is both filters can predict and estimate optimal solution. However, Kalman did not consider the important problem of smoothing, which obviously has very good potential ability to be used in navigation application too. Before Wiener filter, Kalman filter and smoother applied in GPS/INS integration, they are mainly applied in control application.

In practice, all measurements are achieved in finite time duration. Thus, the most effective and reasonable smoothing method will take advantage of all measurements in this duration and to estimate all states in this duration – this is referred as *Fixed Interval Smoothing*. A basic BS method which uses variance weight forward and backward solution as optimal solution is investigated in this section. As mentioned above, the forward Kalman filter generates the optimal estimate at any time based on all past measurements and it does not use any

information in future measurements. A Kalman filter running backward in time (referred to as a backward Kalman filter) from some end time T will exhibit a similar optimality with respect to future measurements, which is shown in Figure 4.1.

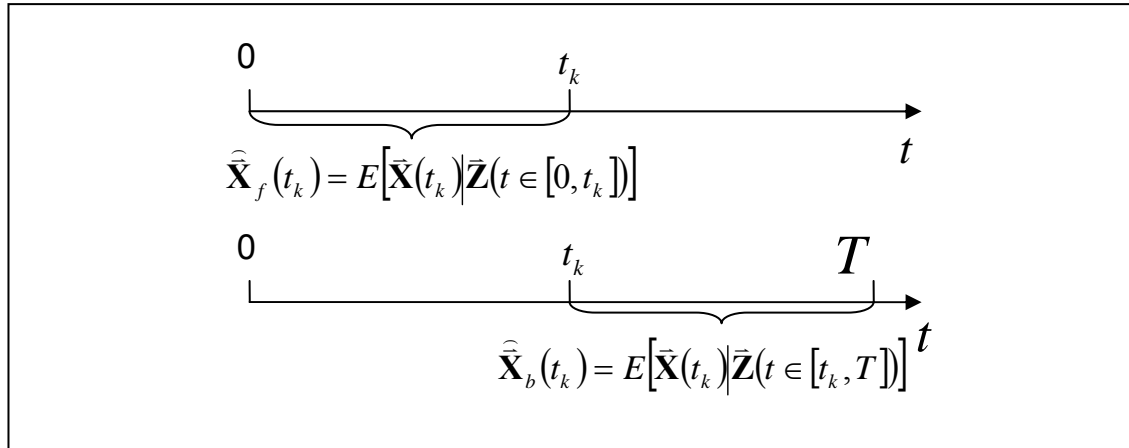


Figure 4.1 Forward and Backward Kalman Filter

Figure 4.1 shows the basic principle on which both forward and backward Kalman filtering is based. The subscripts, f and b , represent forward and backward operations, respectively.

By definition, the smoothing is seeking a combination of these two estimates that optimally uses all measurements in the fixed interval $[0, T]$. The combination, which has to be linear in this case, can be defined as

$$\begin{aligned} \hat{\tilde{\mathbf{X}}}_s(t) &= A\hat{\tilde{\mathbf{X}}}_f(t) + B\hat{\tilde{\mathbf{X}}}_b(t) \\ \tilde{\tilde{\mathbf{X}}}_s(t) &= \hat{\tilde{\mathbf{X}}}_s(t) - \bar{\mathbf{X}}(t) = A\tilde{\tilde{\mathbf{X}}}_f(t) + B\tilde{\tilde{\mathbf{X}}}_b(t) + [A + B - I]\bar{\mathbf{X}}(t) \end{aligned} \quad (4.5)$$

where subscripts “s”, “f”, “b” represent smoothed estimation, forward estimation and backward estimation, respectively; and “^” and “~” represent estimated solution and estimation error, respectively. The smoothed estimation should be unbiased; hence $B = I - A$ and $A + B - I = 0$. Then the estimation error in Equation (4.5) above can be rewritten as

$$\tilde{\mathbf{X}}_s(t) = A\tilde{\mathbf{X}}_f(t) + (I - A)\tilde{\mathbf{X}}_b(t) \quad (4.6)$$

The coefficients A and $I - A$ were given as follows by Scherzinger (2004):

$$\begin{aligned} A &= \mathbf{P}_b(t)(\mathbf{P}_f(t) + \mathbf{P}_b(t))^{-1} \\ I - A &= \mathbf{P}_f(t)(\mathbf{P}_f(t) + \mathbf{P}_b(t))^{-1} \end{aligned} \quad (4.7)$$

the corresponding VCV matrix of smoothed solution were given as (Scherzinger, 2004):

$$\begin{aligned} \mathbf{P}_s(t) &= \mathbf{P}_b(t)(\mathbf{P}_f(t) + \mathbf{P}_b(t))^{-1} \mathbf{P}_f(t)(\mathbf{P}_f(t) + \mathbf{P}_b(t))^{-1} \mathbf{P}_b(t) \\ &\quad + \mathbf{P}_f(t)(\mathbf{P}_f(t) + \mathbf{P}_b(t))^{-1} \mathbf{P}_b(t)(\mathbf{P}_f(t) + \mathbf{P}_b(t))^{-1} \mathbf{P}_f(t) \\ &= \mathbf{P}_b(t)(\mathbf{P}_f(t) + \mathbf{P}_b(t))^{-1} (\mathbf{P}_b^{-1}(t) + \mathbf{P}_f^{-1}(t))^{-1} \\ &\quad + \mathbf{P}_f(t)(\mathbf{P}_f(t) + \mathbf{P}_b(t))^{-1} (\mathbf{P}_f^{-1}(t) + \mathbf{P}_b^{-1}(t))^{-1} \\ &= (\mathbf{P}_f^{-1}(t) + \mathbf{P}_b^{-1}(t))^{-1} \end{aligned} \quad (4.8)$$

or

$$\mathbf{P}_s^{-1}(t) = \mathbf{P}_f^{-1}(t) + \mathbf{P}_b^{-1}(t) \quad (4.9)$$

The above implies that the optimal smoothed information is always better than the information in either the forward or backward filter. Hence optimal smoothing will always improve the estimation error. However, smoothing is performed after the filtering stage. Hence all smoothing algorithms will be dependent on the filtered solution obtained. Thus, accurate filtering is required for accurate smoothing. As mentioned in Section 2.3.1, the tightly coupled GPS/INS filter and loosely coupled INS filter perform essentially the same during complete GPS outages. Hence, backward smoothing is applied only with the tightly coupled strategy in this research. The result based on use of a loosely coupled strategy is expected to be the same as that obtained through use of a tightly coupled strategy.

4.3 RAUCH-TUNG-STRIEBEL (RTS) SMOOTHER

Based on the theory mentioned in Section 4.2, Rauch *et al.* (1965) introduced the Rauch-Tung-Striebel (RTS) smoother. The RTS smoother consists of algorithms taking advantages of both forward sweep information and backward

sweep information. The forward sweep is the common Kalman filter represented as

$$\begin{aligned}
 \hat{\mathbf{X}}_{k,k-1} &= \mathbf{\Phi}_{k,k-1} \hat{\mathbf{X}}_{k-1} \\
 \mathbf{P}_{k,k-1} &= \mathbf{\Phi}_{k,k-1} \mathbf{P}_{k-1} \mathbf{\Phi}_{k,k-1}^T + \mathbf{Q}_{k-1} \\
 \mathbf{K}_k &= \mathbf{P}_{k,k-1} \mathbf{H}_k^T \left[\mathbf{H}_k \mathbf{P}_{k,k-1} \mathbf{H}_k^T + \mathbf{R}_k \right]^{-1} \\
 \hat{\mathbf{X}}_k &= \hat{\mathbf{X}}_{k,k-1} + \mathbf{K}_k \left[\mathbf{Z}_k - \mathbf{H}_k \hat{\mathbf{X}}_{k,k-1} \right] \\
 \mathbf{P}_k &= (\mathbf{I} - \mathbf{K}_k \mathbf{H}_k) \mathbf{P}_{k,k-1}
 \end{aligned} \tag{4.10}$$

Store information from Equation (4.2) during forward Kalman filtering the new measurements $\tilde{\mathbf{Z}}_k = \mathbf{Z}_k - \mathbf{H}_k \hat{\mathbf{X}}_{k,k-1}$; gain matrix $\mathbf{K}_k^* = \mathbf{P}_{k,k-1} \mathbf{H}_k^T \left[\mathbf{H}_k \mathbf{P}_{k,k-1} \mathbf{H}_k^T + \mathbf{R}_k \right]^{-1}$.

The backward sweep begins at the end of the forward filter (i.e. at epoch N) with the initial conditions of $\hat{\mathbf{X}}_N^s = \hat{\mathbf{X}}_N^f$ and $\mathbf{P}_N^s = \mathbf{P}_N^f$, Where superscript “s” and “f” represent forward Kalman filter and backward smoother, respectively. The RTS algorithm equations are developed as follows:

The smoothed results will take advantage of all measurements after epoch k to generate optimal estimate of epoch k, which can be represented as:

$$\hat{\mathbf{X}}_{k,N} = \hat{\mathbf{X}}_{k,k-1} + \sum_{l=k}^N \mathbf{K}_l^* \tilde{\mathbf{Z}}_l \tag{4.11}$$

$$\mathbf{P}_{k,k-1}^* = \mathbf{P}_{k,k-1} \prod_{l=k}^{N-1} (\Phi_{l+1,l} - \mathbf{K}_l^* \mathbf{H}_l) \quad (4.12)$$

By definition the Equation (4.12) can be re-written as:

$$\mathbf{P}_{k,k-1}^* = \mathbf{P}_{k,k-1} \Phi_{N,k}^T \quad (4.13)$$

where $\Phi_{N,k}^T = \prod_{l=k}^{N-1} (\Phi_{l+1,l} - \mathbf{K}_l^* \mathbf{H}_l)$ and $\Phi_{k,k} = \mathbf{I}$.

Then,

$$\hat{\mathbf{X}}_{k,N} = \hat{\mathbf{X}}_{k,k-1} + \sum_{l=k}^N \mathbf{P}_{k,k-1} \Phi_{l,k}^T \mathbf{H}_l^T [\mathbf{H}_l \mathbf{P}_{l,l-1} \mathbf{H}_l^T + \mathbf{R}_l]^{-1} \tilde{\mathbf{Z}}_l \quad (4.14)$$

or

$$\hat{\mathbf{X}}_{k,N} = \hat{\mathbf{X}}_k + \sum_{l=k+1}^N \mathbf{P}_{k,k-1} \Phi_{l,k}^T \mathbf{H}_l^T [\mathbf{H}_l \mathbf{P}_{l,l-1} \mathbf{H}_l^T + \mathbf{R}_l]^{-1} \tilde{\mathbf{Z}}_l \quad (4.15)$$

thus

$$\hat{\mathbf{X}}_{k,N} = \hat{\mathbf{X}}_k + \mathbf{P}_k \Phi_{k+1,k}^T \mathbf{P}_{k+1,k}^T \left(\hat{\mathbf{X}}_{k+1,N} - \hat{\mathbf{X}}_{k+1,k} \right) \quad (4.16)$$

Equation (4.16) subtract $\hat{\mathbf{X}}_k$ on both side then we get:

$$\tilde{\hat{\mathbf{X}}}_{k,N} - \mathbf{P}_k \mathbf{\Phi}_{k+1,k}^T \mathbf{P}_{k+1,k}^T \hat{\mathbf{X}}_{k+1,N} = \tilde{\hat{\mathbf{X}}}_k - \mathbf{P}_k \mathbf{\Phi}_{k+1,k}^T \mathbf{P}_{k+1,k}^T \mathbf{\Phi}_{k+1,k}^T \hat{\mathbf{X}}_k \quad (4.17)$$

By definition: $\text{Cov}[\tilde{\hat{\mathbf{X}}}_{k,N}, \hat{\mathbf{X}}_{k+1,N}] = 0$ and $\text{Cov}[\tilde{\hat{\mathbf{X}}}_k, \hat{\mathbf{X}}_k] = 0$ where Cov represents

covariance matrix operator. And, $\text{Cov}[\hat{\mathbf{X}}_k, \hat{\mathbf{X}}_k] = \text{Cov}(\hat{\mathbf{X}}_k) - \text{Cov}(\tilde{\hat{\mathbf{X}}}_k)$ similarly,

$\text{Cov}[\hat{\mathbf{X}}_{k,N}, \hat{\mathbf{X}}_{k,N}] = \text{Cov}(\hat{\mathbf{X}}_k) - \text{Cov}(\tilde{\hat{\mathbf{X}}}_{k/N})$. Furthermore,

$\text{Cov}(\hat{\mathbf{X}}_k) = \mathbf{\Phi}_{k,k-1} \text{Cov}(\hat{\mathbf{X}}_{k-1}) \mathbf{\Phi}_{k,k-1}^T + \mathbf{Q}_{k-1}$. Compute covariance matrix both side of

Equation (4.17), then the smoothed covariance matrix is as following:

$$\mathbf{P}_{k,N} = \mathbf{P}_k + \mathbf{P}_k \mathbf{\Phi}_{k+1,k}^T \mathbf{P}_{k+1,k}^T (\mathbf{P}_{k+1,N} - \mathbf{P}_{k+1,k}) \mathbf{P}_k \mathbf{\Phi}_{k+1,k}^T \mathbf{P}_{k+1,k}^T \quad (4.18)$$

Summarized from above the RTS smoother can be written as following:

$$\begin{aligned} \hat{\mathbf{X}}_k^s &= \hat{\mathbf{X}}_k^f + \mathbf{G}_k (\hat{\mathbf{X}}_{k+1}^s - \hat{\mathbf{X}}_{k+1,k}^f) \\ \mathbf{G}_k &= \mathbf{P}_k^f \mathbf{\Phi}_{k+1,k}^T (\mathbf{P}_{k+1,k}^f)^{-1} \\ \mathbf{P}_k^s &= \mathbf{P}_k^f + \mathbf{G}_k (\mathbf{P}_{k+1}^s - \mathbf{P}_{k+1,k}^f) \mathbf{G}_k^T \end{aligned} \quad (4.19)$$

It should be noted that, in this particular research, since the extended Kalman

filter is used, the predicted states vector $\hat{\mathbf{X}}_{k+1,k}^f$ in forward Kalman filtering is always zero.

In general, the RTS smoother propagates the smoothed solution directly, using the forward Kalman filter states, covariance and model parameters as inputs.

CHAPTER FIVE - FIELD TESTING DESCRIPTION AND DATA PROCESSING

One field test conducted in a modified passenger van is discussed in this chapter. Two base stations were set up during the data collection run, one of which provides a short baseline (about 8 km), and the other a long baseline of about 80 km. The corresponding tests are denoted as the Short Baseline Test and Long Baseline Test, and the results using corresponding data are denoted as Short Baseline Results and Long Baseline Results. Results from the modified software under distinct integration scenarios using short baseline data are presented in this chapter to verify the quality of the GPS-only and INS/GPS integrated solutions. Results of the long baseline test are presented in Chapter Seven to illustrate how different ambiguity processing strategies perform in the presence of large differential errors. The discussion begins with the use of short baseline data to achieve a reference trajectory.

5.1 SYSTEMS OVERVIEW

5.1.1 EQUIPMENT AND FIELD TESTING

A field test was performed by the Mobile Multi-Sensor Research Group of the Department of Geomatics Engineering at the University of Calgary in conjunction with NovAtel Inc. This test was conducted on July 18, 2003 near Balzac, which is north of Calgary in an area which provided good satellite visibility. The remote GPS reference station data collection, which provided long baseline results, was conducted using the Three Hills station of the Southern Alberta GPS Network (SAN). SAN is a network of 14 dual-frequency GPS receivers covering part of southern Alberta which collects GPS data on a continuous basis (Dao, *et. al.* 2004, Dao, 2005). The data from four stations is available in real-time and can be used for a variety of purposes, including real-time kinematic (RTK) testing in single and multiple reference station modes as well as for atmospheric studies (Dao, 2005; Dao, *et. al.* 2004; Alves, 2004; Skone and Hoyle). The stations filled with blue color in Figure 5.1 shows the position of the SAN reference station used in this particular test, the local reference station and the test area as well. The distance between remote and local reference stations is about 80 km.



Figure 5.1 Southern Alberta Network, Local and Remote Base

The remote and local GPS reference stations are as shown in Figure 5.1 and Figure 5.2. The baseline length to the local reference station during the test was a maximum of eight kilometres, while the baseline length to the remote reference during the test was about eighty kilometres. Figure 5.3 shows the K_p index for the day of the test as well as for two days on either side of the test day. As shown, the K_p index for the period of the test is relatively low considering that the K_p index has a range from zero to nine (GFZ-Potsdam, 2004).

The coordinates of the local base station were computed using Bernese

software (Hugentobler *et al.*, 2005) with more than 5 hours carrier-phase measurements respect to Three Hill base station which is used as the other base station in this test. The accuracy given by Bernese is at milli-metre level, thus the relative accuracy of two base stations used herein is expected very high.

The HG1700 rover GPS antenna and an LN200 IMU were mounted on the roof of the test van as shown in Figure 5.4. The short baseline results can provide an accurate CDGPS/INS integration solution which could be used as a reference for evaluating the integrated system (the next two chapters contain details of their implementation). Ionospheric conditions during the test are not considered to be significant for the short baseline data, taking into consideration the baseline length and the Kp index value. Appendix D gives the estimated ionospheric delay for the short and long baseline conditions, respectively. The estimated ionospheric delay was about 1 ppm during the data collection.



Figure 5.2 GPS Reference Remote (left) and Local (right) Station Setup

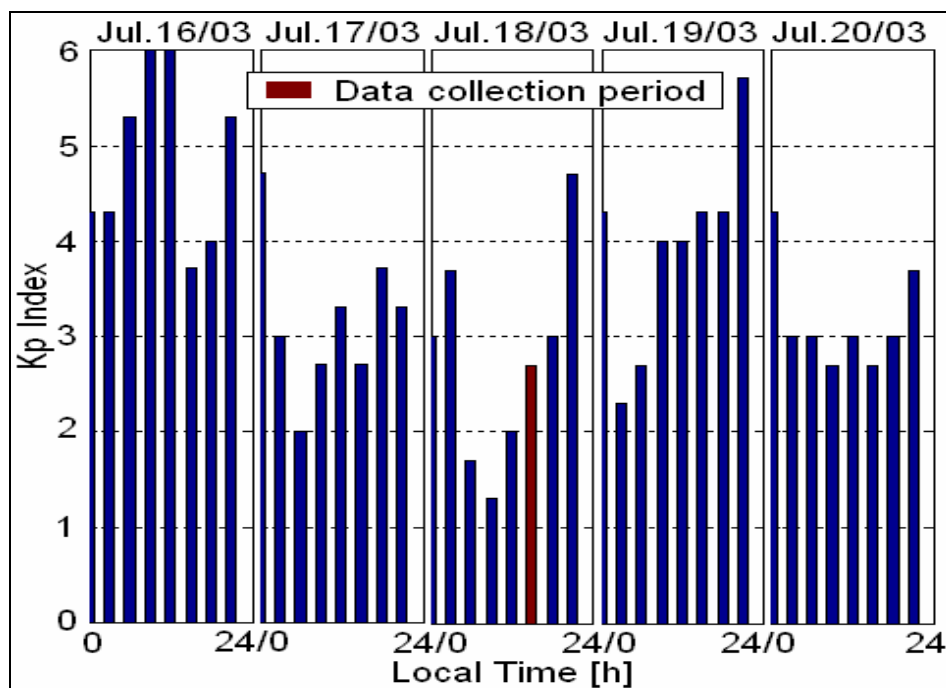


Figure 5.3 Kp Index Before and After Data Collection Period

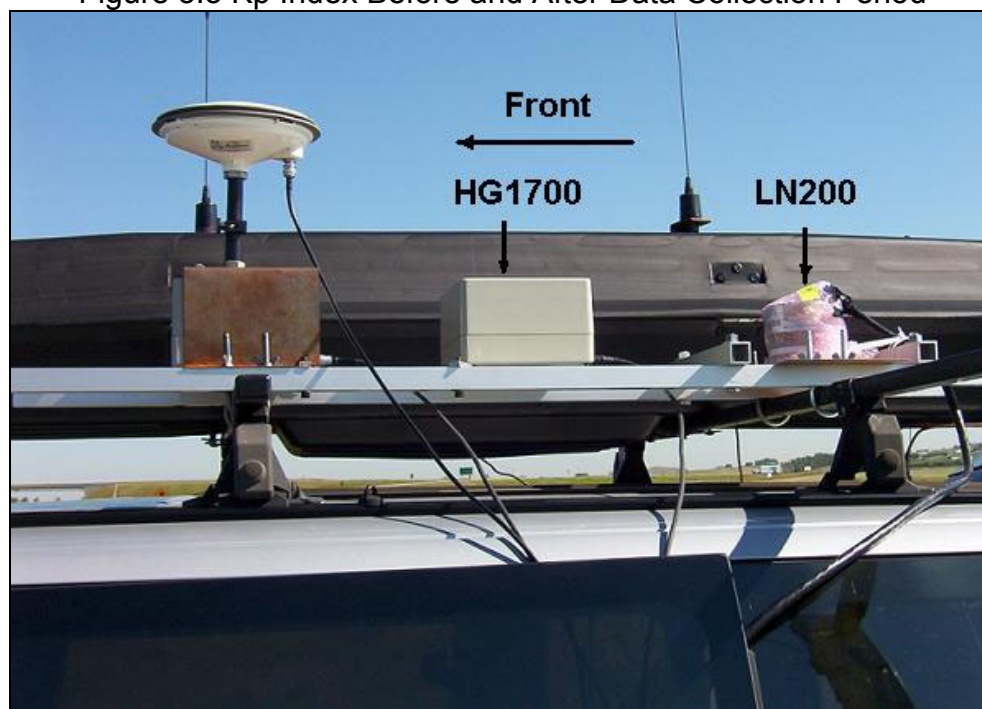


Figure 5.4 Test Hardware Setup Showing the Rover GPS Antenna, the HG1700 IMU and the LN200 IMU

One data collection run was performed, which began with a static initialization period of about 5 minutes followed by about 40 minutes of driving. The vehicle trajectory during the test, relative to the local reference station, is shown in Figure 5.5 (the trajectory was traversed twice) in which black arrows denote the direction of travel. Vehicle speeds varied from 0 to 110 km/h (30 m/s) as shown in Figure 5.6, which plots the estimated vehicle velocity versus time for the complete run after the initial alignment period.

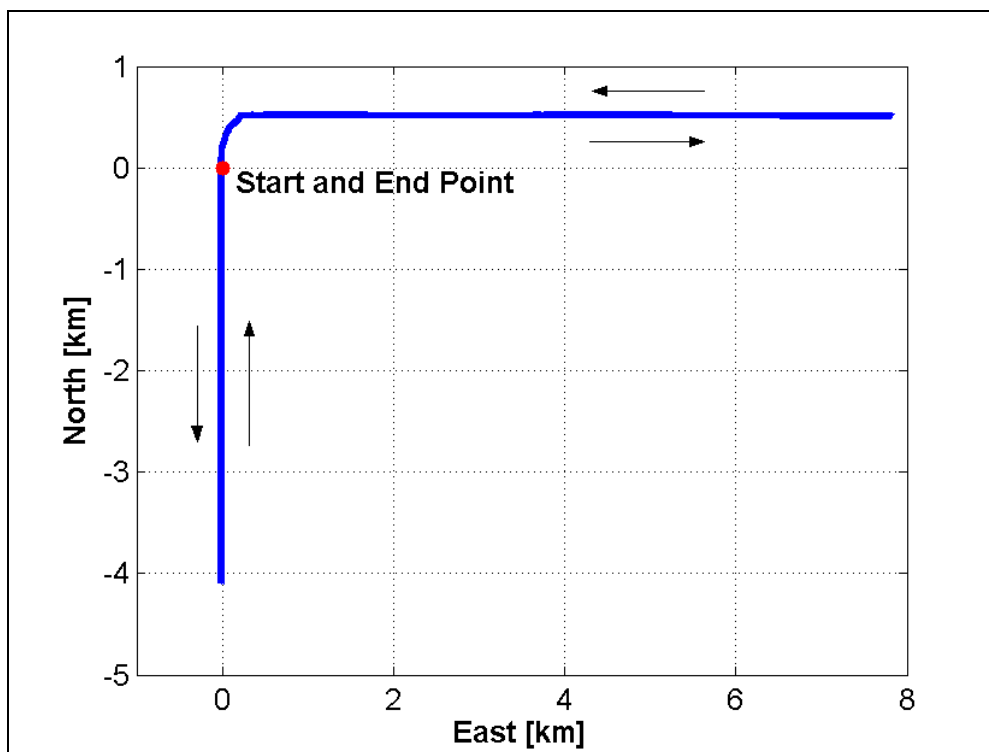


Figure 5.5 Test Trajectory with respect to Local Reference Station

The local reference station was overlapped with the start and end points in Figure 5.5 above. As can be seen, the longest baseline length is about 8 km.

The reason for setting the end point very near the start point in the test is to verify the correctness of ambiguities. The trajectory comprised most dynamics typical of vehicle motion such as left, right and U-turns, acceleration and deceleration; the trajectory included no sudden stops or large changes in elevation or grade.

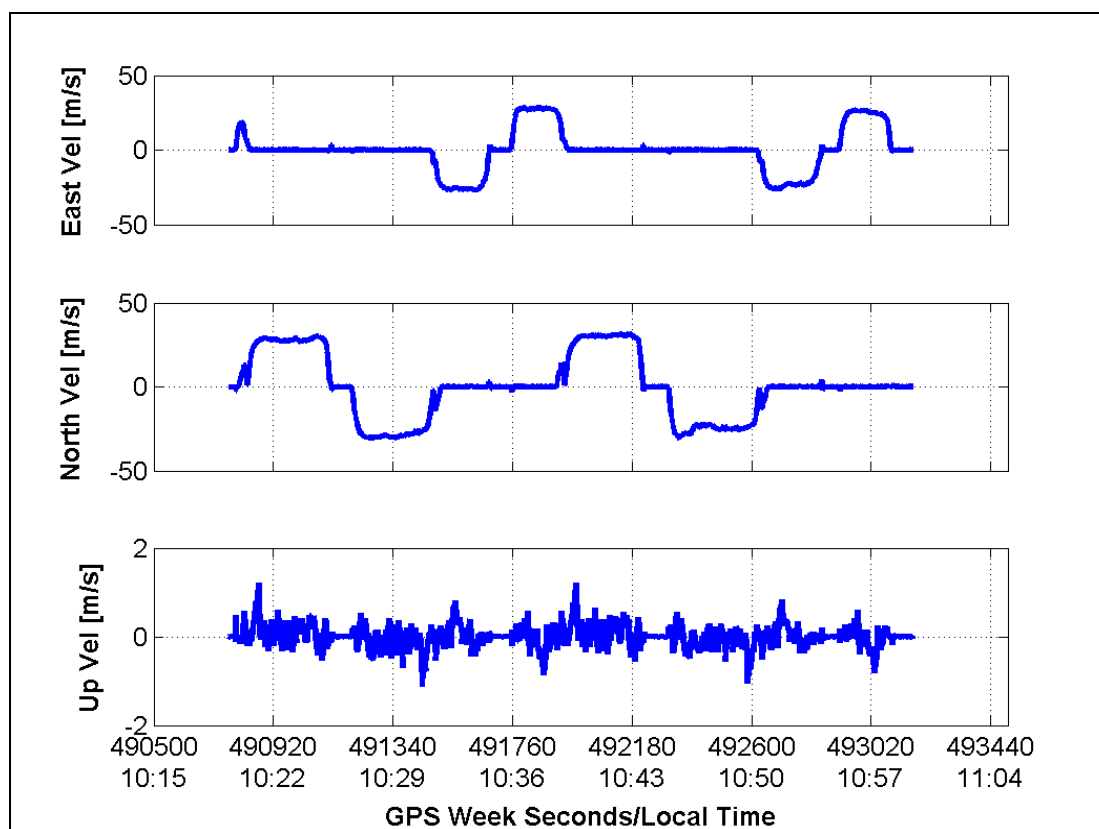


Figure 5.6 Estimated Vehicle Velocities Using Tight Coupling Short Baseline Solution

The NovAtel OEM4, which is high quality dual-frequency GPS receiver capable of generating low noise code, Doppler and carrier phase measurements, was used at each of the GPS reference stations (Novatel, 2005a). Two rover GPS

OEM4 receivers were mounted in the test vehicle and integrated with each of the HG1700 and LN200 IMUs. The IMU data from both systems was received and time-tagged by the corresponding GPS receiver before being output through one of the receiver's serial ports. This process eliminates any significant timing discrepancies between the GPS and IMU data. When processing the data, the GPS data used was from only one of the receivers in the test vehicle, thus allowing for a fair comparison. All GPS receivers (at the reference and remote stations and the rover receivers) used NovAtel 600 series antennas (Novatel, 2005b). Some of the more relevant performance specifications for the IMUs tested are as shown in Table 5.1.

Table 5.1 IMU Specifications

Parameter	HG-1700¹	LN-200²
Gyro Bias (deg/h)	1~10	1~10
Angular Random Walk (deg/\sqrt{h}) (max)	0.152	0.04~0.1
Accel Bias (m/s²)	9.8e-3	2e-3~9.8e-3
Velocity Random Walk (m/s/\sqrt{h}) (max)	0.0013	0.001

¹ Honeywell (1997)

² Litton Inc. (2004)

The coordinates of the local GPS reference stations were computed using differential carrier phase positioning techniques and are considered accurate to within several centimetres.

5.1.2 PROCESSING SOFTWARE

Data was processed using the University of Calgary's Satellite And Inertial Navigation Technology (SAINT™) software (Petovello *et al.*, 2004). With different combinations of inter-frequency observables (Liu, 2002; Collins, 1999), many ambiguity estimation processing strategies are possible (Liu *et al.*, 2003; Liu, 2002) after the software being modified (the original version SAINT™ only process L1 only and WL only strategies shown in Table 5.2 as Strategies 1 and 2). A summary of ambiguity processing strategies is presented in Table 5.2. The modified SAINT™ software can process carrier phase observables using any of the strategies shown in the table. Compared to those strategies in Table 3.3, only Strategy 5 in Table 3.3 is not implemented in SAINT™, since it was not suitable for practical purposes as mentioned in Chapter Three.

It should be noticed that in strategy 6 and 7, Ionospheric error is modeled as first order Gauss-Markov process and treated as error states in GPS or GPS/INS Kalman filter (Liu, 2002).

Table 5.2 SAINT™ Ambiguity Processing Strategy Summary

Strategy	Ambiguities estimated	Observables used	Ionosphere
1	N_1	$CP_1 P$	Not Parameterized
2	N_{WL}	$CP_1 CP_2 P$	
3	$N_1 N_2$	$CP_1 CP_2 P$	
4	$N_1 N_{WL}$	$CP_1 CP_2 P$	
5	N_{IF} (IF float)	$CP_1 CP_2 P$	Ionosphere-Free Combinations
6	$N_1 N_2$	$CP_1 CP_2 P$	Stochastic Ionosphere Modeling
7	$N_1 N_{WL}$	$CP_1 CP_2 P$	

Since the Short Baseline Test provided baseline lengths of less than 10 km, and considering that the Kp index is about 3 which means ionospheric error is at a low level, the ionospheric error was assumed to be about 3 ppm (parts per million). The maximum position error caused by the ionosphere is about 3 cm. This conjecture is supported by the residual analysis included in Section 5.2. In light of this, for the Short Baseline case the L1 carrier phase ambiguities were amenable to direct resolution. As such, the reference trajectory was therefore processed using the Strategy 1 which incorporated L1 carrier phase data, as well as L1 C/A code and Doppler measurements, using the double-difference technique. The GPS integer ambiguities are resolved using the LAMBDA method (Teunissen, 1994). In the long baseline case, the ionospheric error becomes the dominant error source. There is a very good chance to not be able to resolve the L1 and L2 ambiguities. The position error performance using different ambiguity resolution strategies in the long baseline case will be further

investigated in Chapter Seven.

5.2 REFERENCE TRAJECTORY GENERATION

In order to assess the performance of the two systems and the long baseline solution, a reference trajectory is needed. To determine a reference trajectory, all of the GPS and INS raw measurements of short baseline data were processed together using the tightly coupled integration strategy. The tightly coupled solution was favoured over a GPS-only solution because the GPS-only solution is output only at 1 Hz, while the tightly coupled solution is output at 10 Hz. Moreover, the trajectory was computed using all available information and should thus be of the highest quality. Thereafter, the RTS optimal smoothing technique was used to improve the accuracy. The accuracy of this solution is dependent on two factors. One is the GPS kinematic carrier phase differential solution accuracy which will define the absolute accuracy of the system. The other is the relative accuracy of the INS which will then determine how this initial GPS error is propagated forward in time between GPS data updates. Since the accuracy of the GPS solution is fairly well known - floating ambiguity solutions can provide decimetre accuracy while fixed integer solutions are capable of centimetre accuracy over short baselines (Cannon, 1997) - the reference trajectory is considered to be centimetre-level since almost all of the

ambiguities were fixed and maintained throughout the run. The only exceptions were a few instances when at most three ambiguities (of nine) were temporarily lost but were recovered no more than 5 seconds later. An analysis of the residuals during the run (see Section 5.2.1 below), and the static position at the start and end of the run (shown in Figure 5.5), indicate that the ambiguities were indeed resolved correctly. The following subsections analyze the quality of the truth trajectory after initial fixing of the ambiguity. First, the quality of the GPS-only solutions is investigated followed by an analysis of the integration solutions. A comparison of different integration approaches is also included to illustrate their differences. All investigations in this section focus only on the short baseline solution.

5.2.1 SHORT BASELINE GPS-ONLY SOLUTION

The GPS-only solution is investigated in this section in order to assess the GPS data quality and ionospheric error effects.

This section provides the carrier phase differential solution from the software using the short baseline data. For the short baseline case, as mentioned above, the L1 ambiguity can be easily resolved. Since the L1-only strategy provides the highest accuracy, the GPS data was processed using L1 carrier phase and the majority of ambiguities were resolved to their integer value and maintained

through the run in this particular case (as shown in Figure 5.7). The only exceptions were a few instances when at most three ambiguities (of nine) were temporarily lost but were recovered at most 85 seconds later. Thus, the GPS-only solution is considered to be at the centimetre-level. To help confirm this, the upper plot in Figure 5.7 shows the absolute L1 carrier phase residuals as a function of time for the satellites whose ambiguities are fixed, as computed using the GPS-only strategy. Also shown on the plot is the distance of the vehicle from the reference station. The number of satellites available above a cut-off angle of 10 degrees and the number of satellites whose ambiguities are fixed are shown in the lower graph. Baseline lengths of approximately zero occur when the vehicle is stationary next to the reference station.

Throughout the data set, the L1 carrier phase residuals are about 2 to 3 cm, and do not change with baseline length. This being said, the ionospheric effect is considered negligible in this short baseline case and the only remaining errors using double differencing are those due to multipath and noise. Although the residuals are typically 2 to 3 cm, there are some cases when they are larger than 3 cm and even up to 4.8 cm at one epoch. It was found that in all cases when the phase residual was larger than 3 cm occurred with low elevation satellites; typically less than 15 degrees (see Appendix A which shows the DOP values and satellite elevation angles during the test for more details). The larger ambiguity residuals are therefore most likely caused by multipath errors since

the GDOP values shown in Figure A.1 changes very little (from 2 to 1.8) after local time 10:20. Also, as shown in Figure A.2, it can be concluded that from GPS time 490400 s to 492100 s (10:13 AM to 10:42 AM local time) there were several GPS satellites at very low elevation angles (around 10 to 15 degrees, 3 satellites are dropping in and 3 satellites are dropping out), that potentially gave noisier GPS measurements during that time.

Finally, it can be also seen in the lower plot of Figure 5.7 that the majority of L1 carrier phase ambiguities were fixed and maintained throughout the test run. As mentioned above, at some epochs some of the ambiguities were lost and then recovered very quickly. However, given the number of visible satellites, if ambiguities from only a few satellites are lost the influence on the ultimate positioning accuracy is negligible. Given the above, the GPS-only solution can be assumed to be accurate to the 2 to 4 cm level at all times.

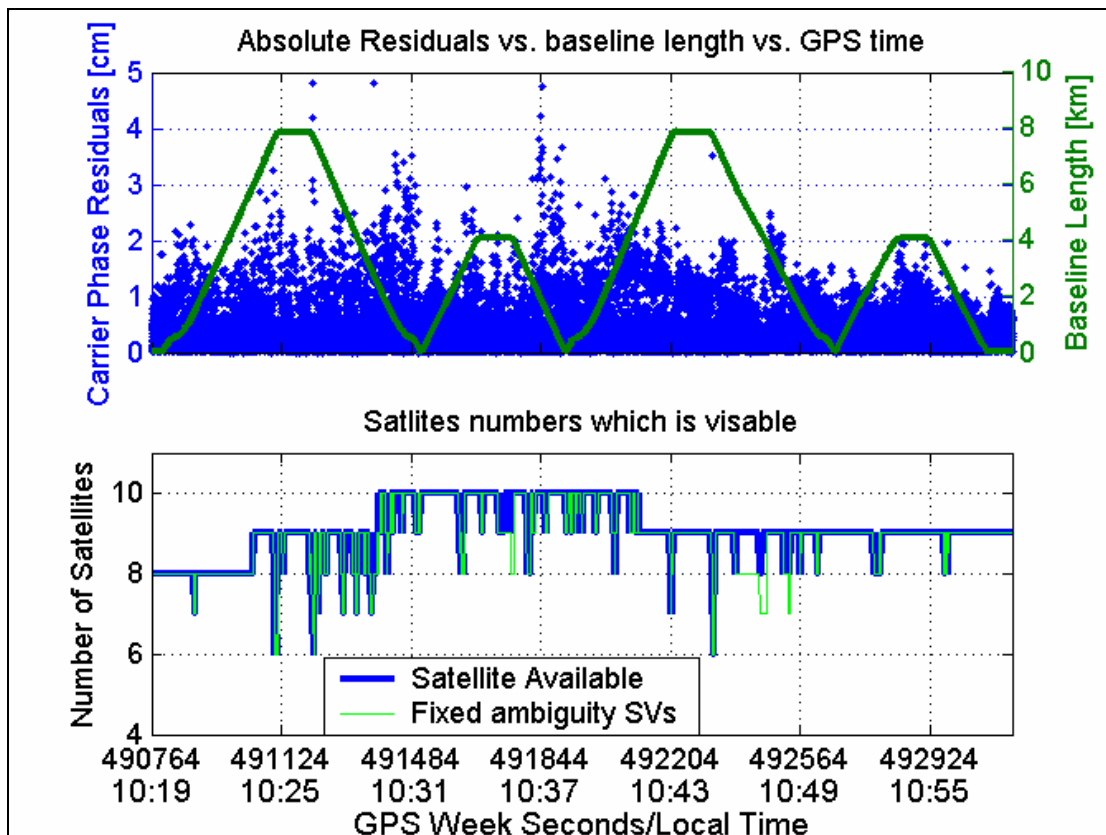


Figure 5.7 Absolute Value of GPS-Only Solution Fixed Ambiguity L1 Carrier Phase Residuals vs. Baseline Length without Data Outages (upper plot); Number of Satellites Visible, and Number of Satellites with Ambiguities Fixed (lower plot)

5.2.2 SHORT BASELINE INS/CDGPS INTEGRATION SOLUTION

The above analysis focused on the GPS-only solutions, since this will ultimately determine the absolute accuracy of the integrated system. However, an assessment of the integrated system performance is also important. Moreover, the GPS-only solution can only provide a 1 Hz output. A good indication of the quality of the integrated solution is the magnitude of the corrections applied to

INS position and velocity states, as well as the fixed ambiguity L1 residuals.

Table 5.3 shows the RMS three-dimensional corrections to the position and velocity error states for each run. Since the corrections are an indicator of the smoothness of the trajectory over time, it can be seen that the trajectories are smooth to about the centimetre level in position. Furthermore, since the GPS solutions analyzed above will determine the absolute accuracy of the system, the truth trajectories are assumed to be accurate to within 2 to 4 cm at all times. In addition, the required correction to INS using the HG1700 is 3 mm higher than that using the LN200. This implies that the LN200 has lower inherent noise than the HG1700.

Table 5.3 RMS of Corrections to INS Position and Velocity Errors States Using a Tight Integration Without Data Outages

Corrections	HG1700/CDGPS	LN200/CDGPS
Position	9 mm	6 mm
Velocity	5 mm/s	2 mm/s

COMPARISON OF LOOSE AND TIGHT INTEGRATED SOLUTIONS

As mentioned in Section 2.3.1, the loose and tight integration approaches can be assumed to be almost equivalent under ideal situations. This section

investigated different integration approaches' differences in practical situations by comparing the solution of each integration approach. Table 5.4 shows the difference between the loosely and tightly coupled solutions. As can be seen, the difference between the two solutions is at the millimetre level. These differences are most likely because the tight integration approach has better ability to smooth the GPS noise than loose integration does (Petovello, 2003). For greater clarity, the implications of this concept are revisited below.

Table 5.4 RMS Difference Between Positions Computed Using Loose and Tight Integration Strategies without Data Outage

Axis	HG1700/CDGPS	LN200/CDGPS
East	2 mm	1 mm
North	1 mm	1 mm
Up	2 mm	1 mm

Table 5.5 shows the RMS statistics of the fixed L1 carrier phase residuals for the GPS-only, loose and tight integration solutions respectively. The RMS of the fixed L1 carrier phase residuals using the tightly coupled strategy is larger than that of using either the loosely coupled, or GPS-only, strategies. This helps to confirm that the position differences in Table 5.4 are caused by high-frequency errors in the measurements. Furthermore, it implies that the tight integration approach is better able to filter the GPS measurements. Specifically, since the ambiguity has been fixed, more high-frequency measurement noise is forced

into the residuals, and not into the position estimates as in the case of loose integration. Although it can filter the GPS noise using INS position and velocity seeding - the ability of the loosely coupled strategy to filter GPS noise is weak. This can be confirmed by reference to Table 5.5 that the RMS of the fixed L1 carrier phase residuals are the same using either the GPS-only or loosely coupled strategies. Overall, the two integration approaches can be assumed to be equivalent under ideal conditions (e.g. with no measurement noise), with the tight integration approach providing the smoother trajectory. This being said, although the loosely coupled strategy and tight coupling have very similar performances in the position domain, they have different abilities to filter GPS measurement noise. As can be seen in Table 5.5, the mean of the absolute fixed L1 residuals using either the loosely coupled or GPS-only strategy are at a level of 7 mm for both the HG1700 and LN200 systems. However, that of the tightly coupled strategy is 1 mm and 2 mm higher for the HG1700 and LN200 systems, respectively. This implies the ability to filter GPS measurement noise is related to the quality of the IMU.

Table 5.5 Mean of Absolute Fixed L1 Carrier Phase Residuals Computed Using Different Integration Strategies

Mean Absolute Residuals	HG1700/CDGPS	LN200/CDGPS
GPS-only	7 mm	7 mm
Loosely Coupled	7 mm	7 mm
Tightly Coupled	8 mm	9 mm

Given the above, the tightly coupled short baseline solution as a reference trajectory is considered to be accurate to the 2 to 4 centimetre level.

5.2.3 GPS DATA OUTAGE SIMULATION

To assess the GPS/INS performance in terms of (i) position accuracy, and (ii) integer ambiguity resolution during and after GPS data outages, nine complete data outages were simulated during post-mission processing. The GPS data outages were selected to encompass a wide range of vehicle dynamics, from (approximately) constant velocity to relatively large along-track and lateral accelerations. In this way, the evaluation of the GPS/INS integrated systems is done over a wide range of operational conditions. To help clarify this, Figure 5.8 shows the baseline length as a function of time (i.e., same as the top plot in Figure 5.7) along with the starting points of each of the simulated data outages.

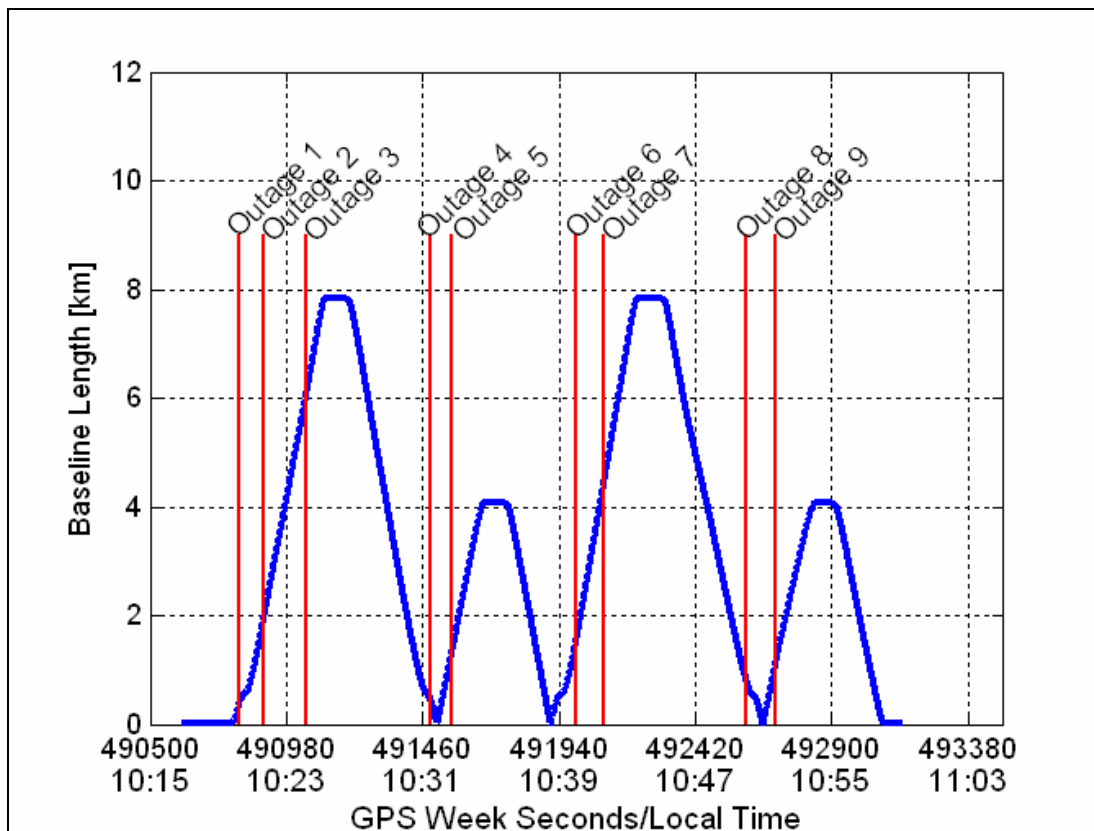


Figure 5.8 Baseline Length and the Starting Points of each of the Simulated GPS Outages

The duration of the simulated GPS data outages was varied from 2 to 100 seconds to help determine:

- 1 The length of time over which the different INS's can provide instantaneous ambiguity resolution compared to the GPS-only solution; and
- 2 The length of time over which the different INS's are able to assist in the integer ambiguity resolution process, even if instantaneous ambiguity

resolution is not possible.

It is noted that only one data outage was simulated per processing run. In this way, the best available position is available prior to each outage. By way of contrast, if multiple outages were simulated over each processing run, then the effect of any one outage may influence the performance subsequently obtained. Although this approach will yield fairly optimal results, it represents a fair method with which to compare the two systems tested. It is also should be noted that complete GPS outages are simulated simply by setting the elevation cut off angle to 90 degrees at some epochs. However, in reality GPS outages are generally precluded by a deterioration of the measurements. Thus these results based on simulated GPS outages are not necessarily representative of real GPS outages in the strictest sense.

5.2.4 DATA ANALYSIS STRATEGY

The results obtained during the simulated GPS outages are compared with the reference solution. The position accuracy during the data outages (i.e., the free-inertial solution) is assessed by means of a comparison with the reference trajectory. Since the reference trajectory is accurate to the centimetre-level, the resulting position difference is almost entirely due to errors in the INS in the absence of GPS updates (i.e., to the free-inertial error). The free-inertial solution

accuracies are a reliable indicator of system functioning when comparing two integrated systems in the position domain since they are affected only by the performance of the IMU's.

When the GPS data is re-introduced at the end of the data outage, the necessary GPS ambiguities must be re-resolved. Once these are resolved to their integer values, they are compared with the reference ambiguity values to ensure their veracity. Also of interest in this regard is the time required for the ambiguities to be resolved to their integer values, relative to the GPS-only case, with shorter times indicating greater relative improvement. Since the exploitation of the integer nature of the GPS carrier phase ambiguities is what allows for high-accuracy position estimates in a reasonable time period, the ambiguity resolution procedure is critical. The ambiguity resolution process is highly affected by the size of the ambiguity search space, which is related to the covariance matrix of the estimated ambiguities (Teunissen *et al.*, 1996).

To assess the above performance parameters, complete GPS data outages were simulated during post-processing by artificially rejecting all satellites in view. In many cases, kinematic applications which would benefit from the inclusion of inertial measurements the most are those requiring an instantaneous or nearly instantaneous ambiguity resolution to become successful (Skaloud, 1998). With this in mind, the time taken to fix ambiguities

after different durations of complete GPS data outages is investigated to evaluate the improvements in ambiguity resolution resulting from the addition of inertial data.

The above data processing routine was repeated for each of the different GPS/INS integration systems – namely, the GPS/HG1700 and GPS/LN200 – and repeated for each of the different integration strategies, namely loose coupling and tight coupling. The corresponding results are presented in Chapter Six.

In many cases, the use of a short baseline such as would be found on shipboard navigation applications, is not practical. Thus the performance under the different ambiguity resolution processing strategies under long baseline conditions (in the presence of large differential errors) is also investigated. Since, in the long baseline case, only the WL ambiguities can be resolved, the results achieved using long baseline data are compared with the reference trajectory only in position domain. The corresponding results are presented in Chapter Seven.

CHAPTER SIX - PERFORMANCE COMPARISON OF TWO INTEGRATED SYSTEMS

The short baseline data results are presented in this chapter to compare the performance of the two integrated systems in position and ambiguity domain. Furthermore, the ambiguity resolution improvements with the aiding of inertial data have also been investigated. In doing so, an analytical relation mentioned in section 2.3.2 between ambiguity resolution improvements with aiding of inertial data and INS system performance in position domain is verified using two different INS. The RTS smoother's ability to bridge the position error during and after GPS outage is presented as the final step in this analysis. The performance of the two systems is assessed in terms of position accuracy and ambiguity resolution, as discussed in the following sections.

6.1 COMPARISON IN POSITION DOMAIN

To compare the free-inertial positioning capability of the two integrated systems during data outages, the 3-D position errors were computed as a function of the time elapsed since the most recent GPS update for each simulated outage. The RMS position error across all nine simulated data outages was computed and is

assumed to be a good indicator of the ability of the two systems to bridge data outages. The top plots in Figure 6.1 and Figure 6.2 show the RMS position error of the tight coupling solution obtained from L1 data, during complete GPS outages. Also shown is the average estimate of the filters' 3-D standard deviation (STD) (across all nine outages) of each integrated system. As can be seen, the estimate of the filter's 3-D STD agrees reasonably well with the RMS of the position error, although the estimated error appears to be slightly pessimistic. The agreement between the actual and estimated errors suggests that appropriate model parameters were used for modeling the system error states. More detailed analyses for the selection of the IMU sensor error model parameters can be found in Appendix C. Since the errors appear to be well modeled in both systems, and all other processing parameters were the same (Appendix C), the primary explanation for the different performance between the systems is the quality of the IMU sensor. Finally, it is noted that, although the results in Figure 6.1 and Figure 6.2 are for the tight integration approach only, the results obtained using loose integration are nearly identical, and were therefore omitted for clarity.

It is noted that the middle and bottom plots in Figure 6.1 and Figure 6.2 zoom the upper plot in y-axis with the same scale on x-axis, in doing so, clearer relation between RMS position error and time into GPS data outage can be seen.

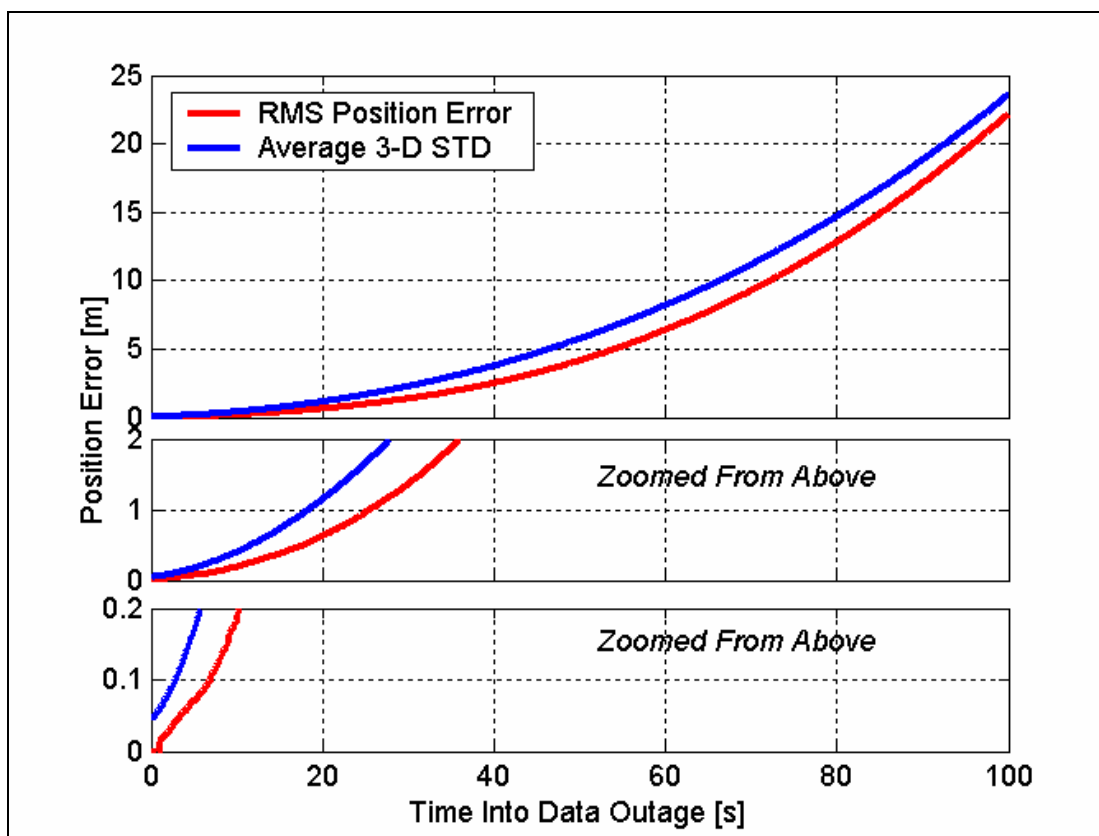


Figure 6.1 GPS/HG1700 Integrated System 3-D RMS Errors and Average Estimated Standard Deviations during All Complete Data Outages Using L1 Carrier Phase Updates and a Tight Integration

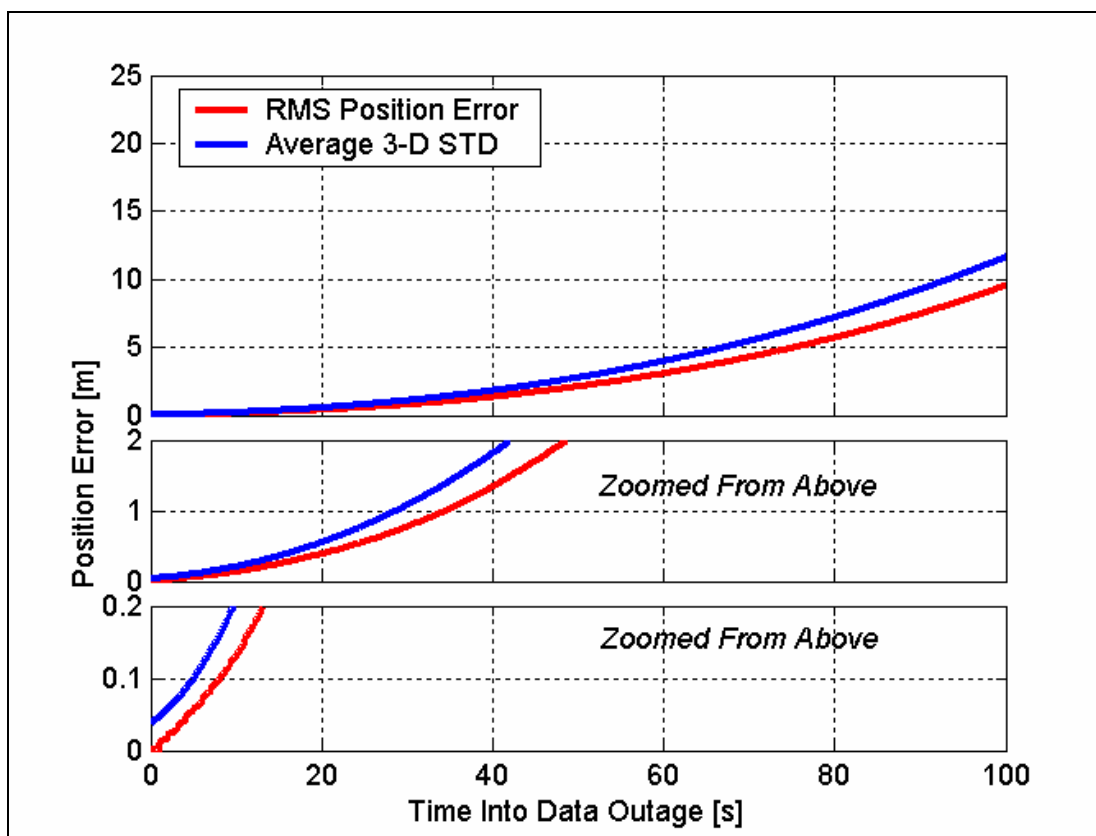


Figure 6.2 GPS/LN200 Integrated System 3-D RMS Errors and Average Estimated Standard Deviations During All Complete Data Outages Using L1 Carrier Phase Updates and a Tight Integration

To begin the analysis, let us consider the RMS position error as a function of time. As seen in Figure 6.1 and Figure 6.2, the errors grow quadratically, as expected. Upon closer inspection, the HG1700 and LN200 systems are seen to provide 10 cm accuracy for approximately 6 and 8 seconds, respectively. Furthermore, the errors grow to 2 m after about 36 and 49 seconds, respectively. For longer data outages, the position errors grow quite rapidly to a maximum of 20 and 10 m after 100 seconds, respectively. Overall, this type of performance

compares well with previous investigations. Specifically, for purposes of comparison, in Petovello (2003a) the 3-D positioning error reached 10 cm and 2 m after approximately 6 and 40 seconds, respectively, using the HG1700 unit. Similarly, Scherzinger (2000) obtained 3-D errors of 10 cm and 1.8 m after 10 and 60 seconds, respectively, using an LN200 combined with other sensors (hence the slightly better performance than observed herein).

Now, recall that one of the objectives of this chapter is to correlate free-inertial positioning accuracy and ambiguity resolution improvements after data outages (relative to GPS alone). As a first step in accomplishing this, a correlation between the free-inertial positioning accuracy and the GPS-only positioning accuracy should be obtained. More specifically, a relationship between the estimated free-inertial position accuracy and the estimated GPS-only code accuracy is desired (i.e., relate the free-inertial and GPS 3-D STD values). The reason for this is threefold. First, from a system design and analysis standpoint, being able to use estimated position accuracies (e.g., from covariance simulations) is very pragmatic. Second, after a GPS data outage, the estimated GPS-only position accuracy will be determined almost exclusively by the differential code measurements (while the carrier phase data will be used primarily to estimate the ambiguity states). As such, the differential code accuracy directly defines the size of the GPS-only ambiguity search space. Third, the estimated differential code accuracy is easily computed and is thus

available for potential use in the processing software (whereas the actual positioning error is not available). In light of this, the GPS-only 3-D STD was computed for all epochs for the data set under consideration. The average value across the data set was then computed to be 1.8 m (1σ). This value is used in the subsequent analysis. It should be noted that the average GPS-only 3-D STD of 1.8 m is computed on the basis of the data used herein. This is not a universal value and should not be expected to occur when using a different GPS data set.

With the above analysis in mind, the subsequent analysis (in this section) focuses on the estimated free-inertial accuracy relative to the GPS-only case. The middle graphs of Figure 6.1 and Figure 6.2 (which are zoomed versions of the top graphs) show that the estimated 3-D STD of the free-inertial solution is as good or better than 1.8 m (i.e., the GPS-only 3-D STD) for data outages lasting up to about 26 s and 40 s for the HG1700 and LN200 systems, respectively. In turn, this should relate to improvements in ambiguity resolution times after GPS outages (see Section 6.2 for an in-depth treatment of this issue). Finally, the estimated accuracy of the free-inertial solution is as good or better than 10 cm for data outages lasting up to 2 s and 4 s for the HG1700 and LN200 systems, respectively.

Having correlated the free-inertial and GPS-only accuracies, the following section attempts to further correlate free-inertial performance with ambiguity resolution performance.

6.2 COMPARISON IN THE AMBIGUITY RESOLUTION DOMAIN

As a first step in assessing the ambiguity resolution performance of the integrated systems, Figure 6.3 and Figure 6.4 show the average time needed to resolve the L1 carrier phase ambiguities after each data outage for the HG1700 and LN200 systems, respectively. Specifically, the average is taken across all nine simulated GPS outages of the same duration. The results show four important characteristics.

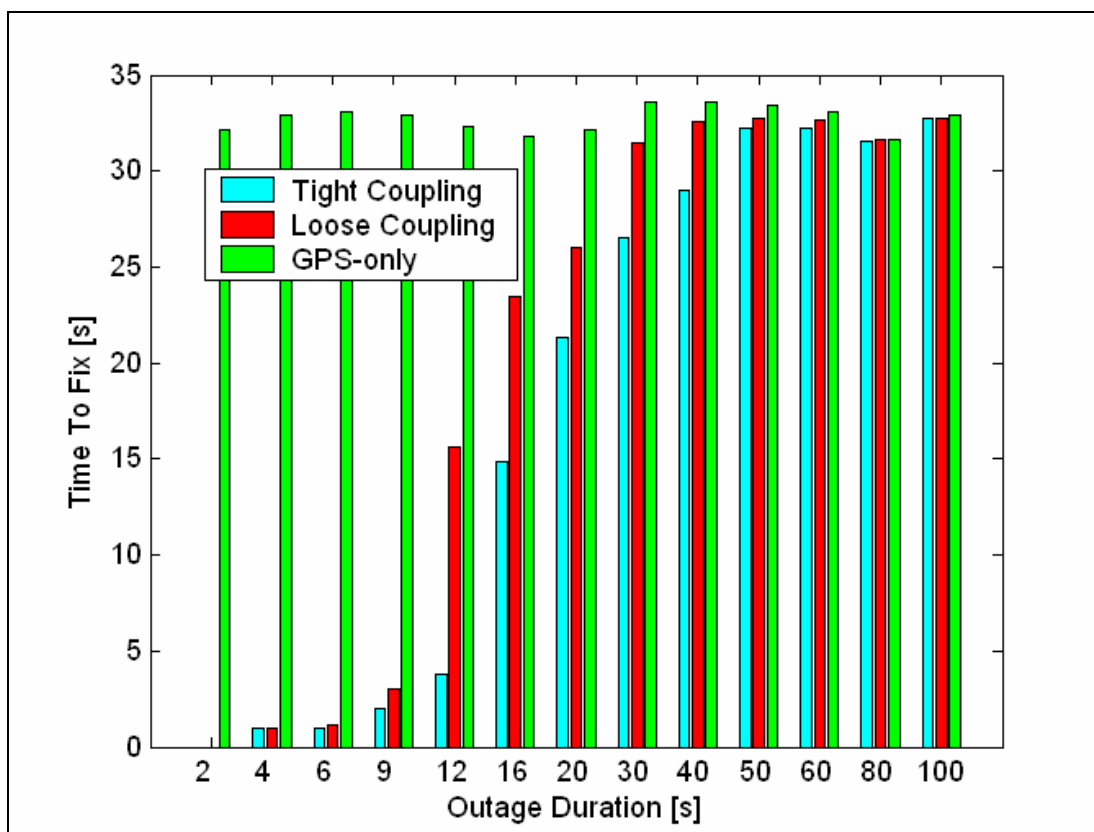


Figure 6.3 Average Time to Fix L1 Carrier Phase Ambiguities after Complete Data Outages for CDGPS/HG1700

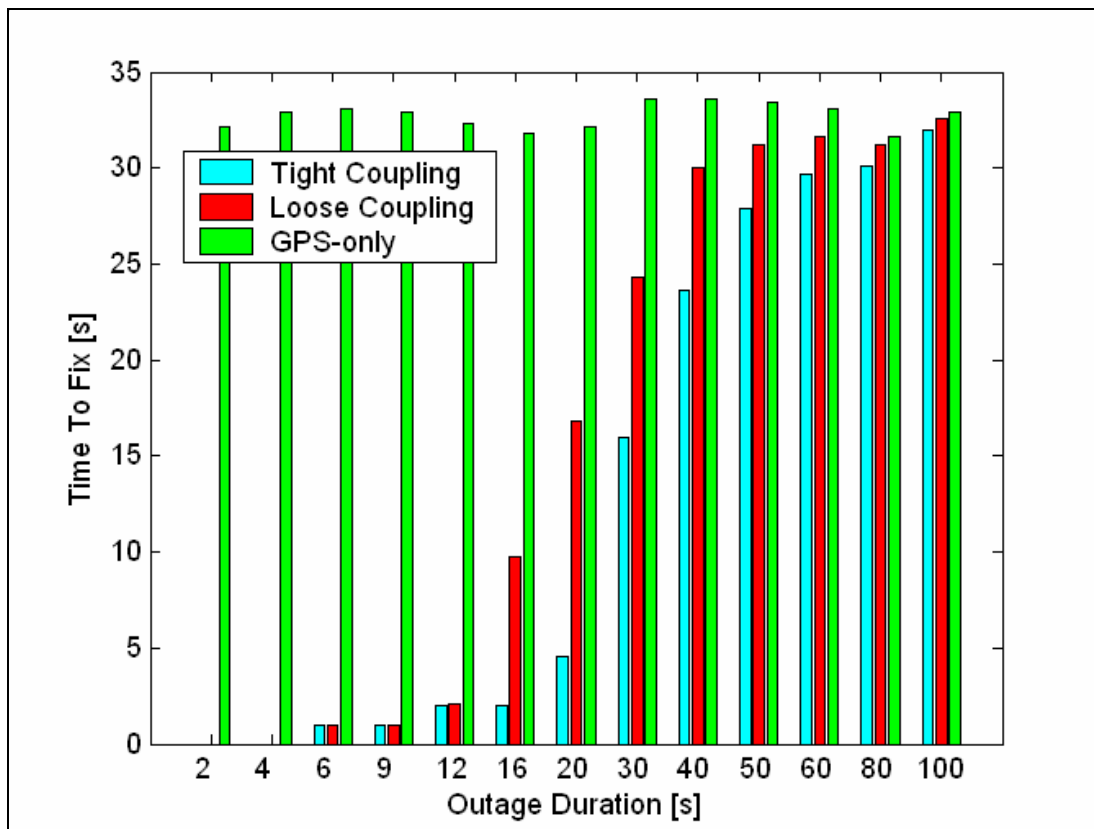


Figure 6.4 Average Time to Fix L1 Carrier Phase Ambiguities after Complete Data Outages for CDGPS/LN200

First, regardless of how long the GPS outage lasts, the GPS-only filter needs, on average, approximately the same amount of time to resolve the ambiguities. This is because the time needed to resolve ambiguities using GPS alone is based primarily on measurement noise, multipath effects and satellite geometry, all of which are expected to be approximately constant throughout the data set. Although Figure 6.3 and Figure 6.4 represent average values, Figure 6.5 and Figure 6.6 show each of the individual cases. Note that because the average time to fix the ambiguities using either integration strategy is approximately the

same as for the GPS-only case after the 40 s mark, for the sake of clarity, only durations shorter than 40 seconds are shown.

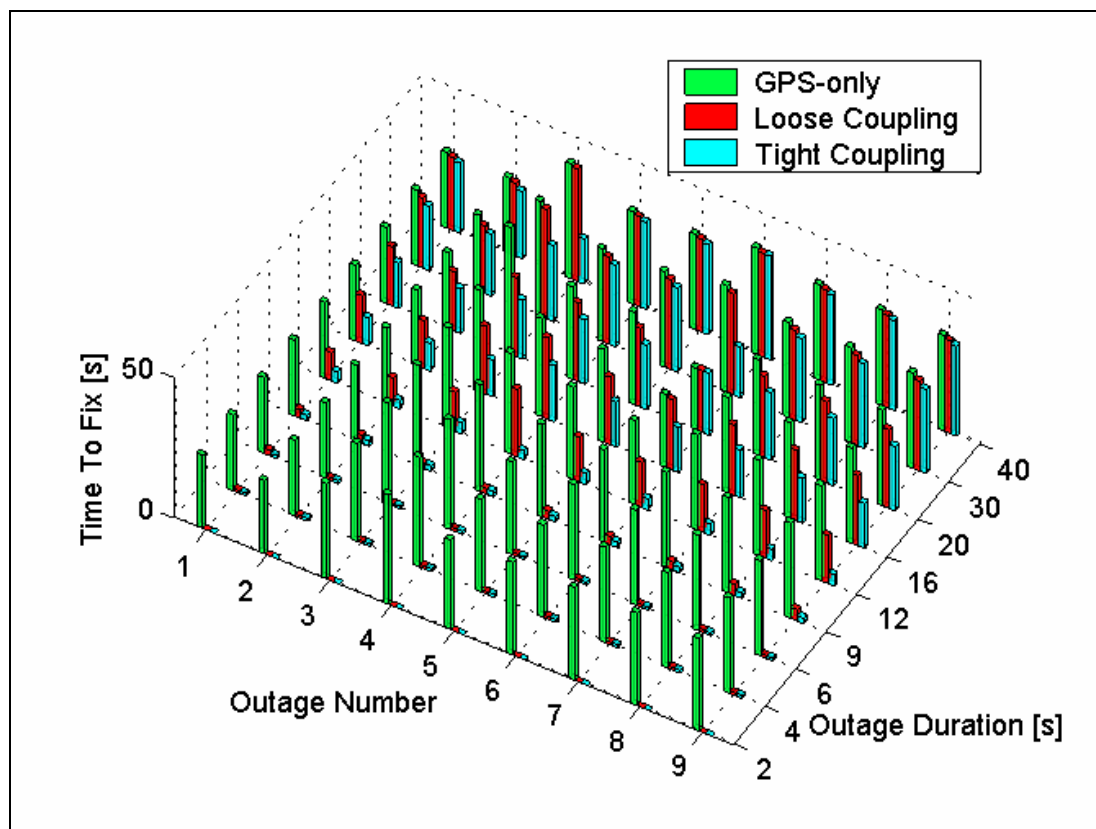


Figure 6.5 Time to Fix L1 Ambiguities After Each Complete GPS Data Outages (CDGPS/HG1700)

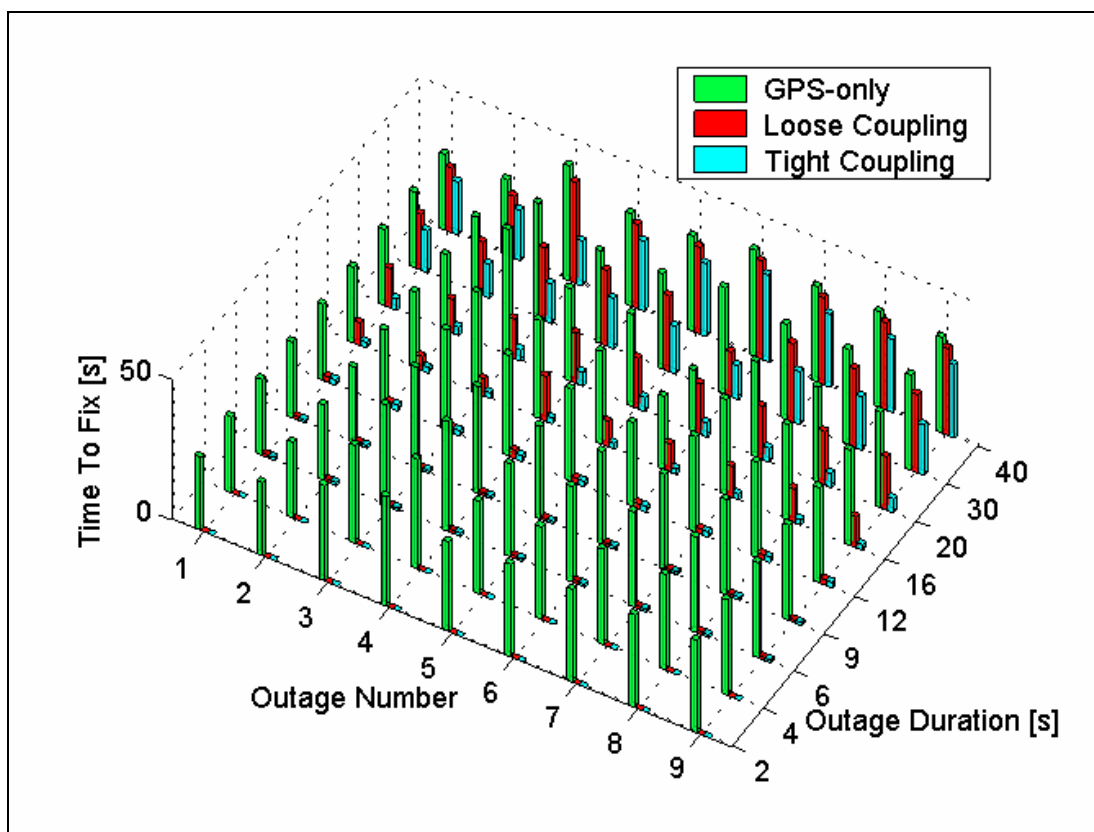


Figure 6.6 Time to Fix L1 Ambiguities After Each Complete GPS Data Outages (CDGPS/LN200)

Second, the GPS-only solution performs the poorest, relative to either integrated solution. In some of the cases, a 100% improvement over GPS-only can be achieved using the integrated systems, meaning that instantaneous ambiguity resolution is possible. Specifically, for data outages up to 2 and 4 seconds for the HG1700 and LN200 systems, respectively, instantaneous ambiguity resolution is possible using either integration strategy.

Third, for outage durations lasting approximately 12 to 40 s (depending on the

IMU), there is also a noticeable improvement when using tight integration over loose integration with GPS seeding. This improvement is suspected to be due to the reduced level of process noise in the tight integration approach and the stronger cross-correlation between position and ambiguity states using tight coupling than that of using a loose coupling strategy, which makes the ambiguity states converge faster after GPS outage.

Fourth, as the inertial position covariance increases over time during a data outage, the benefit to the ambiguity resolution process decreases accordingly, with the limit being the GPS-only case. To see this more clearly, Table 6.1 gives the average percentage improvement in L1 ambiguity resolution times after complete data outages using different approaches for both systems. The improvement of each outage can be computed as

$$Im\% = \frac{(\text{Time To Fix}_{\text{GPS-only}} - \text{Time To Fix}_{\text{Tight/Loose}})}{\text{Time To Fix}_{\text{GPS-only}}} \times 100\% \quad (6.1)$$

The subscripts represent the corresponding integration strategies used herein. It should be noted that the average improvements, in percentage terms, after a 16-second outage attenuates rapidly (shown as an improvement gap) compared to that observed following 12-second outages for the HG1700, with similar

performance observed for the LN200 system after a 30-second outage. A fuller discussion of this is given in the following section.

Table 6.1 Average Percent Improvement in L1 Ambiguity Resolution Times After Complete Data Outages Using Different Approaches

Outage Duration [s]	Average Percent Improvement %			
	HG1700		LN200	
	T/G ¹	L/G ²	T/G	L/G
2	100 ³	100	100	100
4	96.9	96.9	100	100
6	96.9	96.5	96.9	96.9
9	93.8	90.7	96.9	96.9
12	88.2	52.1	93.7	93.4
16	53.3	26.1	93.6	69.3
20	31.8	17.7	85.3	46.0
30	19.9	6.5	51.7	26.9
40	12.4	3.0	29.0	10.9
50	3.7	2.0	17.0	6.7
60	2.7	1.3	10.5	4.5
80	0.4	0.0	5.1	1.5
100	0.3	0.2	2.8	1.1

¹ improvements realized through use of tight coupling over GPS-only strategy

² improvements realized using loose coupling with seeding strategy over GPS-only strategy

³ denotes instantaneous ambiguity resolution achieved

6.3 AMBIGUITY RESOLUTION IMPROVEMENTS WITH AIDING OF INERTIAL DATA

In the previous section, a correlation between the free-inertial position accuracy and the differential code position accuracy was explored. Now, a correlation

between the differential code accuracy and the improvements in the time to fix the ambiguities is desired.

To begin, the results in Table 6.1 are cross-referenced with those from the positioning accuracy assessment in the previous section. Specifically, instantaneous ambiguity resolution is possible as long as the estimated INS 3-D STD after the data outage is below 10 cm. This corresponds to 2 or 4 seconds, depending on the IMU. Second, once the estimated INS 3-D STD degrades to approximately the same level as that of the GPS-only case (i.e., 1.8 m), the improvement in the ambiguity domain is less than approximately 30%, on average. While these conclusions are important, it is still desirable to identify a more rigorous analytical relationship. However, recall from the previous mentioned that the accuracy of the differential code solution (σ_{Code}) is 1.8 m. When this value is substituted into equation (3.13), an approximate estimate of the percentage improvement in the ambiguity resolution performance as a function of the INS 3-D STD at the end of a data outage is obtained. To evaluate this equation, Figure 6.9 and Figure 6.10 show the actual improvement in ambiguity resolution times as a function of the INS position accuracy at the end of the data outage along with the estimated value from Equation (3.13).

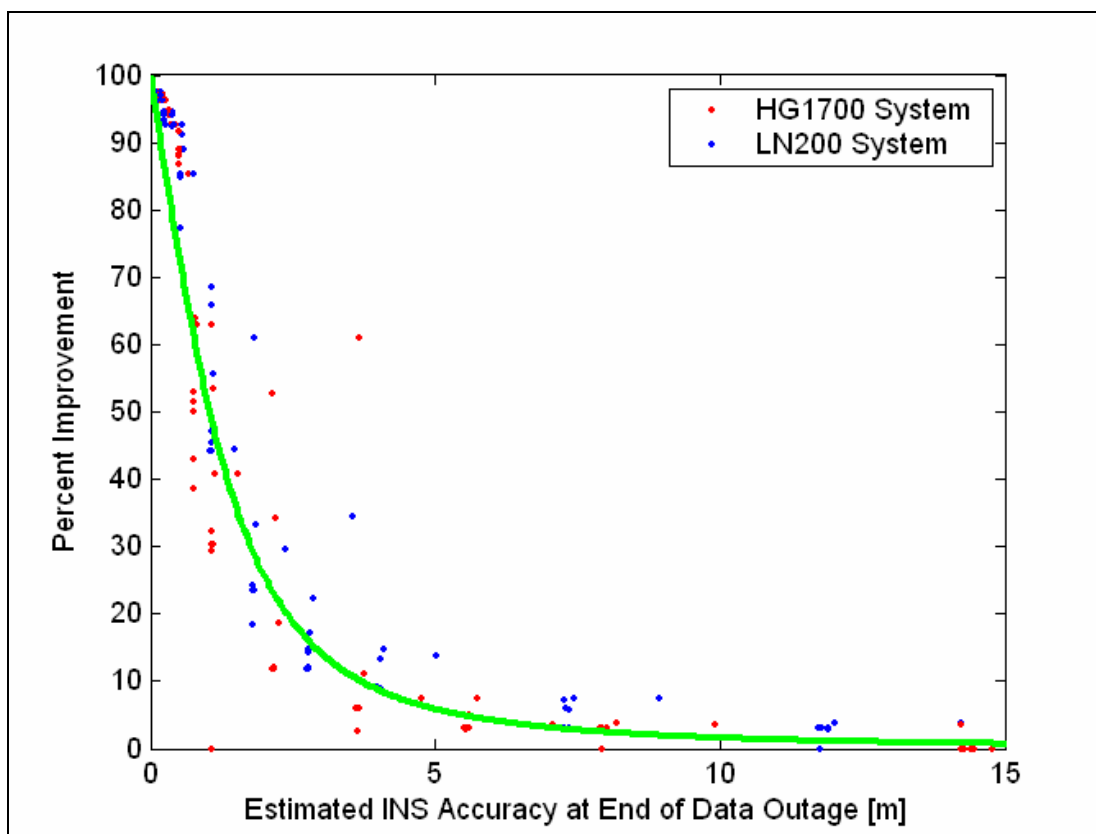


Figure 6.7 Time to Fix L1 Ambiguity Improvements after Each Complete GPS Outage and Each Duration vs. Corresponding Estimated STD of Filter using Tight Coupling

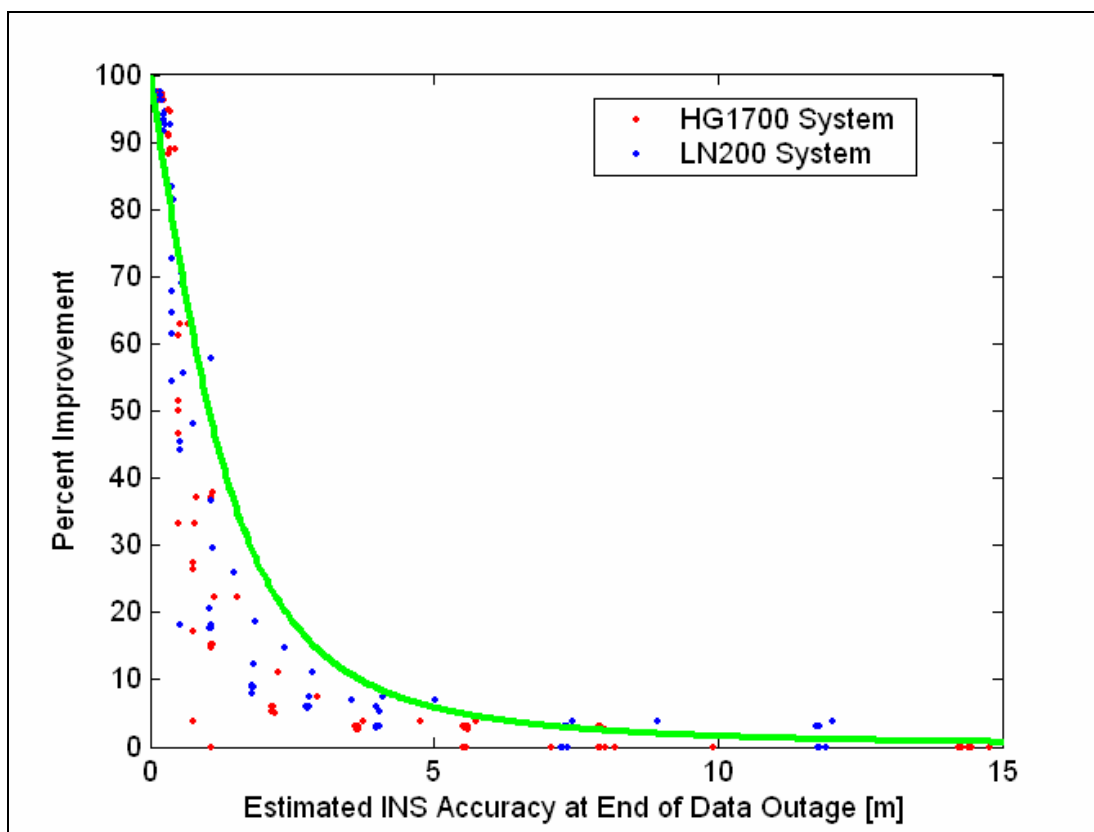


Figure 6.8 Time to Fix L1 Ambiguity Improvements after Each Complete GPS Outage and Each Duration vs. Corresponding Estimated STD of Filter using Loose Coupling

As can be seen in Figure 6.8, the values predicted from equation (3.13) agree reasonably well with actual improvements in the ambiguity resolution times overall. However, a couple of points should be noted. First, the analytical estimate appears to be better suited to predicting the performance of the tight integration strategy. The reason for this is, as mentioned in Chapter Three, that the analytical relation is more suitable for the tightly coupled strategy. The improvements in the loosely coupled case are expected to be lower than that of

the tightly coupled strategy, since loose coupling has indirect correlation between position states and ambiguity states, a lower convergence speed filter and a higher level of processing noise. Second, there appear to be some “outliers” along the x-axis where there is almost no improvement. Upon closer inspection, nearly all such data points were found to correspond to GPS data outages lasting on the order of 30 s. In this case, the free-inertial solution accuracy is already at the metre level and thus does not always yield the desired improvements. Specifically, the improvement will not only be a function of the estimated position accuracy (which is the inherent assumption in the current analysis), but also of the true position (velocity, and attitude) errors, phase measurement noise and possibly the cross-correlation between the various INS and/or GPS error states. Thirdly when the estimated INS position error is smaller than 0.1 metres, a 100 percent improvement can always be achieved using either a loosely or tightly coupled integration strategy. The points showing 100 percent improvement are overlapping and thus cannot be seen clearly in the above figures.

Although the above results are very promising, the solid curves shown in Figure 6.9 and Figure 6.10 are derived assuming an estimated differential code accuracy of 1.8 m. Although this is valid for the data processed herein, more investigation is necessary to ascertain whether Equation 3.13 provides similar performance under real situations. To make it clear, Figure 6.9 and Figure 6.10

were plotted again as Figure 6.9 and Figure 6.10. The actual improvements in ambiguity resolution using different systems are the same as that depicted in Figure 6.9 and Figure 6.10. The predicted improvements, however, which are represented by the green dots, are computed with estimated double differential code accuracy and estimated INS position accuracy at end of data outages using Equation (3.13). Figure 6.9 and Figure 6.10 give more clear and detailed views of Figure 6.7 and Figure 6.8.

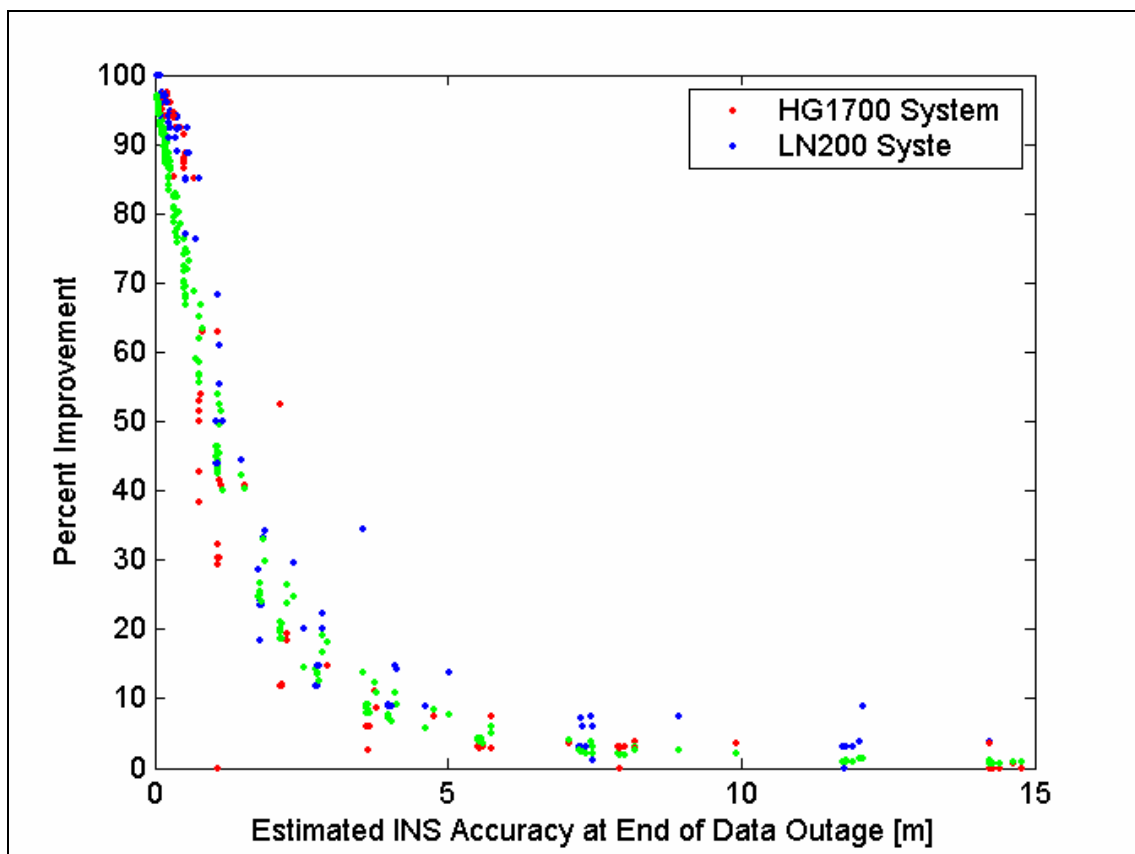


Figure 6.9 Time to Fix L1 Ambiguity Improvements after Each Complete GPS Outages and Each Duration vs. Corresponding Estimated STD of Filter using Tight Coupling

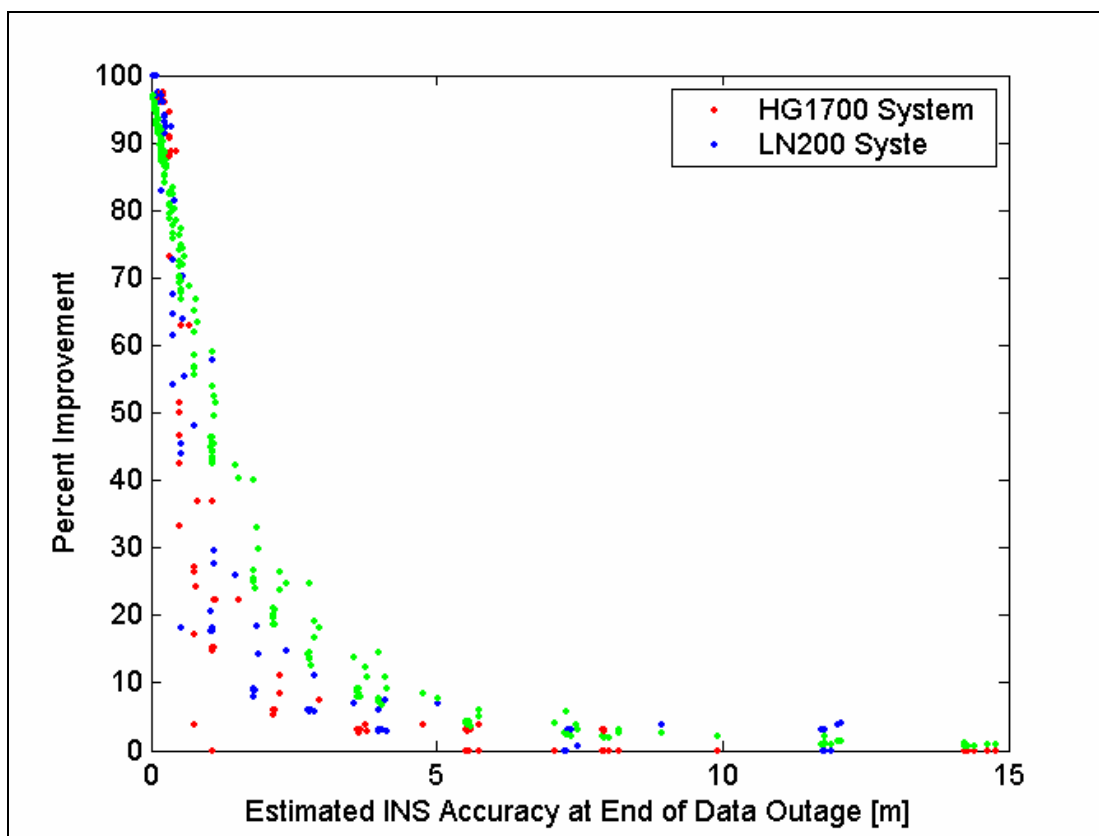


Figure 6.10 Time to Fix L1 Ambiguity Improvements after Each Complete GPS Outages and Each Duration vs. Corresponding Estimated STD of Filter using Loose Coupling

As can be seen in Figure 6.9 and Figure 6.10, the ambiguity resolution improvements realized using a loosely coupled strategy are slightly worse than in the case of tight coupling. As mentioned in the above section, Equation (3.13) is more accurate when using a tightly coupled strategy. However, the improvements produced with the use of a loosely coupled strategy are still very promising. Figure 6.10 above shows that the highest improvement can hardly be larger than the improvement computed using Equation (3.13) when position

covariance is bigger than about 20 cm after GPS outages using a loosely coupled strategy, which can still provide insight into the level of improvement that can be expected, in terms of ambiguity resolution, when using either a loose or tight coupling strategy. This conclusion is expected to be emulated by any chosen grade of IMU. From the above analysis, the “improvement gap” observed after 12 and 20-second outages for the HG1700 and LN200 systems, respectively, is actually reasonable and can be predicted using Equation 3.13. Essentially, this “improvement gap” can be viewed as the result of the position error attenuating in a non-linear fashion.

6.4 RTS BACKWARD SMOOTHING TEST RESULTS

The data used in the above analysis is used to test the performance of the Backward Smoothing (BS) algorithm in bridging GPS outages as well. Although different outage durations are simulated, only one of 100 s outages of the HG1700/GPS system has been selected as an example to illustrate the actual behaviour of the INS positioning error during and after GPS outage periods (before smoothing) as well as the effect of BS on these errors.

The averaged absolute position differences between the free-inertial solution and the reference solution, for the chosen outage period across all nine

simulated data outages are given in Figure 6.11 and Figure 6.12. Average absolute residual position errors for the same outage interval after RTS smoothing are also shown in the same figures.

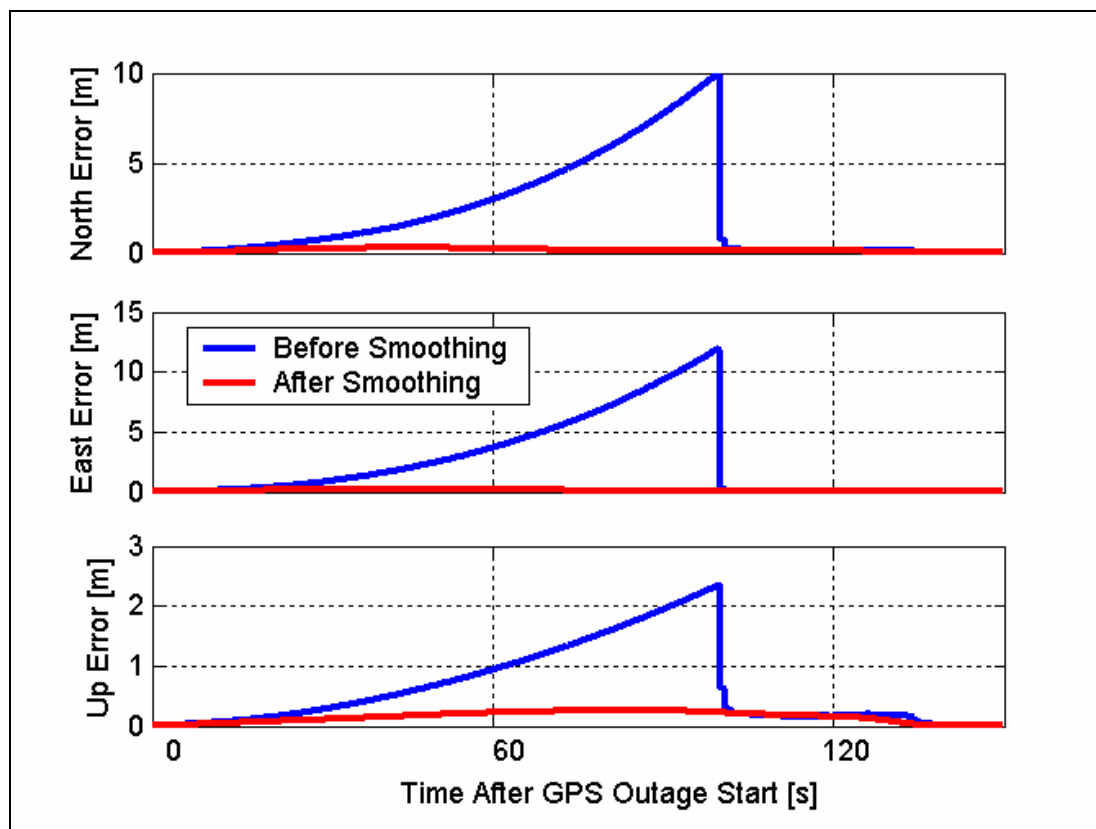


Figure 6.11 Average Absolute Position Error Across All 9 Simulated GPS Outages Before and After RTS Smoothing (HG1700/GPS System)

To show the information from Figure 6.11 more clearly, Table 6.2 and Table 6.3 show the average maximum value of position error during a 100-second GPS outage and the maximum residual position error during a 100-second GPS outage after RTS smoothing, using the HG1700/GPS and LN200/GPS systems, respectively.

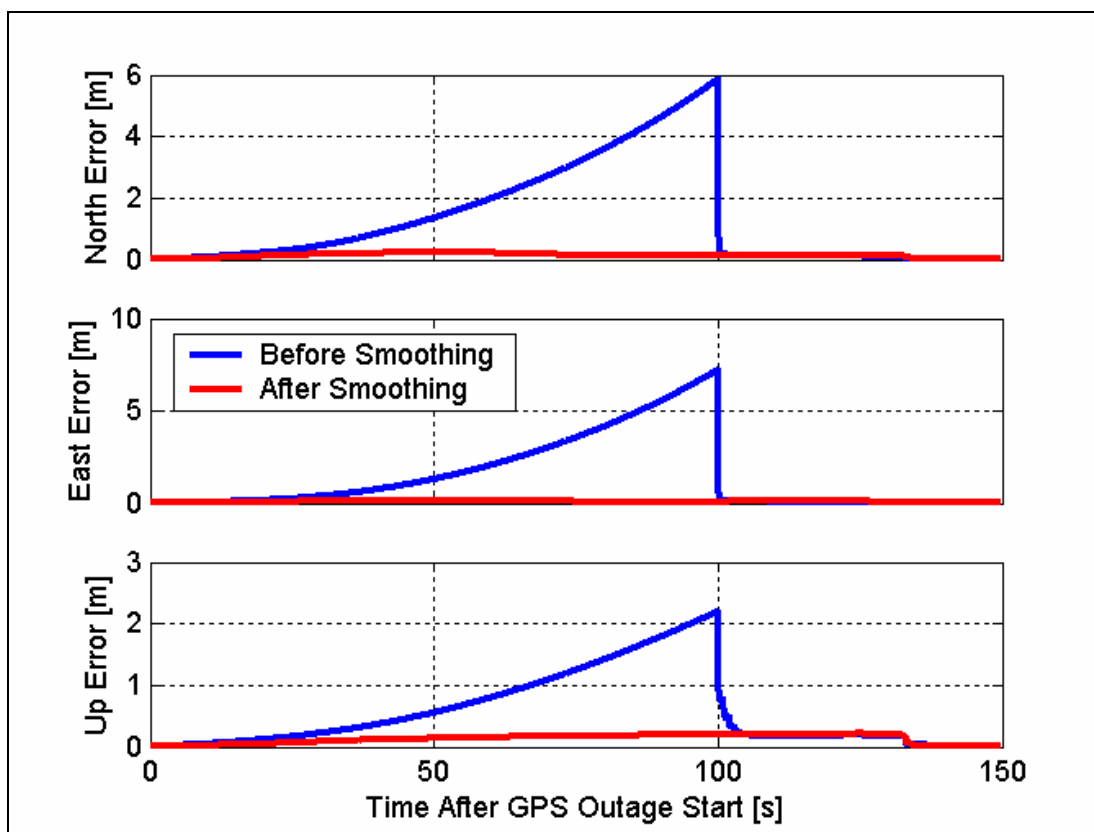


Figure 6.12 Average Absolute Position Error Across All 9 Simulated GPS Outages Before and After RTS Smoothing (LN200/GPS System)

It should be noted that start from 100 s (the end of the complete GPS outage) to about 130 s the solution during this period is a float solution. The ambiguities were generally fixed around 130 s. That is the reason why there is a step at about 130 s.

Table 6.2 Average Maximum Value of Position Error Cross all 9 Simulated 100-second GPS Outages Before and After RTS Smoothing (HG1700/GPS)

Average Maximum Position Error	Before Smoothing [m]	After Smoothing [m]	Improvements %
East	11.96	0.22	98.2
North	9.99	0.28	97.2
Up	2.35	0.26	89.0
Horizontal	15.59	0.35	97.7
3-D	15.76	0.40	97.5

Table 6.3 Average Maximum Value of Position Error Cross all 9 Simulated 100-seconds GPS Outages Before and After RTS Smoothing (LN200/GPS)

Average Maximum Position Error	Before Smooth [m]	After Smooth [m]	Improvements %
East Position Error	7.20	0.14	98.1
North Position Error	5.84	0.23	96.1
Up Position Error	2.20	0.21	90.3
Horizontal Error	9.27	0.27	97.1
3-D Position Error	9.53	0.30	96.8

The results show that improvements of greater than 96% in maximum position error after RTS smoothing in 3-D can be achieved using an RTS smoother. Results show that the RTS smoother shown as equation 4.13 is able to remove up to 97% of the 3-D position error in GPS outage cases. This confirms that backward smoothing is a very effective method of removing position error at the post-mission stage. The residual 3-D position errors after application of an RTS smoother are about 40 cm and 30 cm for the HG1700/CDGPS and LN200/CDGPS, respectively, in the case of a 100-second GPS outage.

Only the averaged absolute position error and absolute residual position error

were shown in this section. However, the position error and residual position error before and after smoothing of each particular GPS outage can be seen in Appendix B.

CHAPTER SEVEN - AMBIGUITY PROCESSING

STRATEGY PERFORMANCE COMPARISON

The long baseline data results are presented in this chapter to compare the performance of different ambiguity processing strategies in the presence of large differential errors in the position domain. The short baseline results focusing on the assessment of the ambiguity re-fixing time using different ambiguity processing strategies after GPS outages are presented as well. Since the inertial aiding to improve ambiguity resolution in the short baseline case was investigated in Chapter Six using the L1 only strategy as an example, only GPS-only, which provides longest ambiguity re-fix time, solutions are presented in this chapter for the short baseline scenario. As mentioned in Chapter Two, the ionospheric error will become to be the dominant error source in long baseline case. This means that the ionospheric error can be up to 20 centimetres for the 80 km baseline with a typical 2ppm ionospheric error (Table 2.2 in Chapter Two), indicating that ambiguity resolution is difficult. In this particular test, none of the integer ambiguities except the WL has been resolved in the long baseline case, so the comparison of different ambiguity resolution strategies is implemented only in the position domain. The same data was processed using the FLYKIN+ software as well in order to verify if the ambiguities are capable of resolution. FLYKIN+ is a differential GPS processing package developed by the PLAN

group, Department of Geomatics Engineering, University of Calgary (Liu, 2003). It can accommodate processes using L1, L2, or WL and IF frequency combinations. It also provides stochastic modelling of the ionosphere. Only WL ambiguities can be resolved when processing the data used herein using FLYKIN+.

The performance of the two systems is assessed in terms of position accuracy via using different ambiguity resolution strategies for the long baseline test, and in terms of ambiguity resolution using different ambiguity processing strategies for the short baseline test, as discussed in the following sections.

As mentioned in Chapter Six, using the GPS-only strategy the time to fix ambiguities after a GPS outage only depends on the quality of the GPS measurements but not the outage duration. Furthermore, as shown in Figure 6.5 and Figure 6.6, the time to fix ambiguities using a GPS-only strategy at each of the nine simulated GPS outages after different duration are very close. This means that the quality of the GPS measurements during these outages are very close. It doesn't make sense to simulate all GPS outages as shown Chapter Six, so only GPS outage durations of 9, 20, 50 and 100 seconds at the second GPS outage were simulated as examples for further investigation in this section.

The definition and characteristics of each ambiguity processing strategies are

first presented in this chapter.

7.1 DEFINITION OF EACH AMBIGUITY PROCESSING STRATEGIES

The definition of each ambiguity processing strategies is given in the following sub-sections (Liu, 2003):

7.1.1 STRATEGY 1 (L1)

This L1 only strategy uses the L1 carrier phase, code and Doppler measurements. As mentioned in Chapter Three, this is the simplest strategy, where only the L1 ambiguity is estimated. Compared to the L2 and WL, the L1 carrier has the shortest wavelength. That means to resolve the L1 ambiguity it needs the longest time with the same initial conditions. Since this strategy has low noise and ionospheric error characteristics compared to WL and L2, this strategy has the highest accuracy after its ambiguities have been resolved.

7.1.2 STRATEGY 2 (WL)

This WL only strategy uses the WL carrier phase observable and estimates WL ambiguities. As mentioned in Chapter Three, it is expected that this strategy

should have better ambiguity resolution performance than Strategy 1 considering the longer wavelength (86 cm). However, high noise and ionospheric error signature is expected when using this strategy since WL contains nearly six times the noise than L1 in metres.

7.1.3 STRATEGY 3 (L1L2)

In this strategy, the L1 and L2 carrier phase observables are used, and the L1 and L2 ambiguities are estimated in the filter. This strategy has more system redundancy than Strategies 1 and 2. Compared to Strategy 2, the carrier phase noise is kept to a minimum since no frequency combination is formed between L1 and L2. However, because the L2 carrier has more ionospheric error than either the L1 or the WL, it is expected that this strategy performs slightly better than Strategy 1 under very low ionospheric error and will perform poorer than Strategy 1 in high ionospheric activity. In very low ionospheric error conditions, the measurement noise level of Strategy 3 is similar to Strategy 1, thus it is expected to have same amount of time to fix ambiguities compared to Strategy 1 when starting from the same initial conditions.

7.1.4 STRATEGY 4 (L1WL)

This strategy is very similar to Strategy 3 except that the WL and L1 ambiguities

are estimated in the filter rather than the L1 and L2 ambiguities, although L1 and L2 observables are used. Like Strategy 3 this strategy has more system redundancy than Strategies 1 and 2. Since this strategy uses L1 and L2 observables to estimate L1 and WL instead of L1 and L2, the noise is kept to a minimum. It is therefore expected that this strategy has a similar accuracy as Strategy 3 in the position estimation. Furthermore, because the WL ambiguity is easier to resolve than both the L1 and L2 ambiguities, better position results can be achieved after the WL ambiguities are correctly fixed while L1 ambiguities are not fixed if L1 and WL ambiguities are estimated in the same filter, instead of L1 and L2 ambiguities. Since resolving the WL ambiguities can speed up the convergence speed of filters, this strategy is expected to have a faster time to fix L1 ambiguities compared to Strategy 1 when starting from the same initial conditions. Similar to Strategy 3, this strategy is expected to be at the same level of position estimation accuracy as Strategies 1 and 3 with low ionospheric error.

7.1.5 STRATEGY 5 (IF)

The IF ambiguities, which are floating values by definition, are estimated using the IF observations in this strategy. In this strategy, the ambiguities are estimated but need not be resolved to integers. One obvious advantage is that this strategy uses the ionosphere-free combination to cancel the ionospheric

error. This being said, if all other observation errors (e.g. tropospheric error, satellite orbital error, multipath) are properly accounted for, the float-valued IF ambiguities should be errorless. No ambiguities are needed to be resolved to their integer values. However, the amplification of the measurement noise (the IF observation is three times as noisy as L1 in metres) makes the IF solution noisy. So in very low ionospheric error conditions, this strategy performs the worst compared to Strategies 1, 3 and 4. Since the IF contains nearly three times the noise than L1 in metres (WL contains nearly 6 times than L1 in metres), it is expected to give better position estimation accuracy in very low ionospheric error conditions after filter convergence.

7.1.6 STRATEGY 6 (L1WL+I)

Similar to Strategy 4, this strategy now expands the filter's states to include the DD ionospheric error (Liu, 2002), which is modelled as a first order Gauss-Markov process. Given that the DD ionospheric error is modelled explicitly, the estimator in Strategy 6 is largely unbiased. Thus, it is expected that the position estimate will not be influenced by the ionospheric error. Similar to Strategy 4, it is expected that the time to fix L1 ambiguities is at the same level as Strategy 4, with Strategy 6 being slightly faster, when starting from the same initial conditions.

7.1.7 STRATEGY 7 (L1L2+I)

This strategy is very similar to the Strategy 6. The introduction of DD ionospheric error states makes the estimator in this strategy largely unbiased. This strategy has no frequency combination. Thus, better position estimation is expected compared to Strategies 5 and 6 if ambiguities are resolved correctly.

Summarised from above, the time to re-fix ambiguities using different strategies start from the same initial conditions as:

$$\text{TTF}_{\text{WL}} \leq \text{TTF}_{\text{L1WL+I}} \leq \text{TTF}_{\text{L1WL}} \leq \text{TTF}_{\text{L1L2+I}} \leq \text{TTF}_{\text{L1L2}} \leq \text{TTF}_{\text{L1}} \quad (7.1)$$

The position estimation accuracy after estimators which are using each ambiguity processing strategy have converged in very low ionospheric error case (e.g. short baseline) is as:

$$\sigma_{\text{WL}} \leq \sigma_{\text{IF}} \leq \sigma_{\text{L1}} \approx \sigma_{\text{L1WL+I}} \approx \sigma_{\text{L1L2+I}} \approx \sigma_{\text{L1WL}} \approx \sigma_{\text{L1L2}} \quad (\text{Short Baseline}) \quad (7.2)$$

where σ represents position accuracy.

The position estimation accuracy after estimators which are using each

ambiguity processing strategy have converged in the very high ionospheric error case (e.g. ionospheric error far greater than L1 carrier phase noise in long baseline) is:

$$\sigma_{WL} \leq \sigma_{L1} \approx \sigma_{L1WL} \approx \sigma_{L1L2} \leq \sigma_{L1WL+I} \approx \sigma_{L1L2I} \leq \sigma_{IF} \quad (\text{Long Baseline}) \quad (7.3)$$

It should be noted that the inequality represented by Equations (7.2) and (7.3) are affected by estimator convergence speed. The convergence speed of estimators using different ambiguity processing strategies can be summarized from above when starting from the same initial conditions as Table 7.1.

Table 7.1 Estimator Convergence Speed Comparison Using Each Ambiguity Processing Strategy

Ambiguity Processing Strategies	L1	WL	L1L2	L1WL	IF	L1L2+I	L1WL+I
Estimator Convergence Speed	slow	very fast	slow	fast	very slow	slow	fast

The inequality in Equations (7.2) and (7.3), when the position accuracy computed across a data run (before the estimator has converged and after) after taking the estimator convergence speed in to account, will change to be:

$$\sigma'_{WL} \leq \sigma'_{L1} \approx \sigma'_{L1WL+I} \approx \sigma'_{L1L2+I} \approx \sigma'_{L1WL} \approx \sigma'_{L1L2} \quad (7.4)$$

Inequality Equation (7.4) is adjusted form of Inequality Equation (7.2) under

short baseline when considering convergence speed. σ'_{IF} can be even worse than that of the WL in the short baseline case in the above inequality.

$$\sigma'_{L1L2} \approx \sigma'_{L1} \approx \sigma'_{L1L2+I} \leq \sigma'_{WL} \leq \sigma'_{L1WL} \approx \sigma'_{L1WL+I} \quad (7.5)$$

(Long Baseline considering estimator convergence speed)

Inequality Equation (7.5) is adjusted form of Inequality Equation (7.3) under long baseline when considering convergence speed. σ'_{IF} can be even the worst in above inequality since IF has slowest estimator convergence speed.

The above summarization of Equations (7.1), (7.4) and (7.5) and their relation to Table 7.1 is proven in the next section.

7.2 SHORT BASELINE TESTS AND RESULTS

7.2.1 AMBIGUITY PROCESSING STRATEGY DIFFERENCES IN POSITION DOMAIN

To compare the performance of different ambiguity processing strategies under short baseline condition results are first presented in this section with focusing on position accuracy. For kinematic positioning practice, the overall position

accuracy (right after initial alignments until the end of the run) is a very important criterion to evaluate the performance of the system. So the RMS of the position differences with respect to the reference trajectory investigated later is an RMS of the overall position difference. The short baseline data was processed using a tight coupling integration strategy, and different ambiguity processing strategies separately. Table 7.2 and Table 7.3 give the position differences using each ambiguity processing strategy in the short baseline case of the HG1700/CDGPS and LN200/CDGPS specifically. The comparison is preceded using the L1 tight coupling solution as the reference. Other tight coupling solutions using a corresponding ambiguity processing strategy are compared with the reference. The results during the initial alignment were discarded (e.g. only results in kinematic mode were compared). In the short baseline case, the DD ionospheric error and residual DD tropospheric error are small enough to be neglected. Refer to Appendix D for detailed information regarding stochastic DD ionospheric error modeling used in Strategies 6 and 7. In addition, Appendix D gives further information about the estimated double-differenced ionospheric delay for both short and long baseline conditions.

Table 7.2 RMS of Overall Position Difference Compare to Short Baseline
Tight Integration L1 Solution (HG1700/CDGPS system, Short Baseline)

Integration strategies	L1 (mm)	WL (mm)	L1L2 (mm)	L1WL (mm)	IF (mm)	L1L2+I (mm)	L1WL+I (mm)	
T¹	N²	0	32	6	6	44	7	6
	E³	0	41	3	3	49	4	4
	U⁴	0	39	7	7	154	7	7
	3-D⁵	0	64	10	10	168	10	10

¹ Tight coupling integration strategy

² North position difference

³ East position difference

⁴ Up position difference

⁵ 3-Dimention position difference

Table 7.3 RMS of Overall Position Difference Compare to Short Baseline Tight
Integration L1 Solution (LN200/CDGPS system, Short Baseline)

Integration strategies	L1 (mm)	WL (mm)	L1L2 (mm)	L1WL (mm)	IF (mm)	L1L2+I (mm)	L1WL+I (mm)	
T	N	0	32	6	6	44	7	6
	E	0	41	3	3	49	4	4
	U	0	39	7	7	154	7	7
	3-D	0	64	10	10	168	10	10

It should be noted that all ambiguities in Table 7.2 and Table 7.3 were fixed correctly and major ambiguities were kept to their integer values until the end of the run except for the IF ambiguities. As can be seen in the tables Strategies 1, 3, 4, 6, and 7 have a very similar position accuracy performance in short baseline case. Considering the 2-4 cm accuracy of the L1 tight coupling solution, the differences between ambiguity processing Strategies 1, 3, 4, 6 and 7 are neglectable.

As mentioned in Section 3.4, the WL contains nearly six times the noise than L1 and the IF contains nearly three times the noise. This being said, the position estimates using WL are expected to be noisier than that of using IF. However, as shown in Table 7.2 and Table 7.3, the position estimates using IF are worse than WL. This is because the estimator using the IF observable converges very slowly. Before the IF ambiguities converge to reasonable values, the position estimation has a very large bias. This makes the RMS of the position differences using Strategy 5, compared to Strategy 1, much larger than that of using Strategies 2 and 1. Generally, the results in Table 7.2 and Table 7.3 follow the rules of inequality (Equation (7.2)). The exception is that the position accuracy when using the IF processing strategy is the worst but not that of WL because the estimator when using the IF ambiguity processing strategy needs more time to converge.

Since the position accuracies of Strategies 1, 3, 4, 6, and 7 are very similar (1 cm RMS difference in 3-D), the time to re-fix ambiguities after a GPS outage is the other important criteria to compare the performance of different ambiguity processing strategies.

To better understand the short baseline results in the position domain, position differences between the reference solution and solutions obtained with the use of each strategy, as well as under short baselines, are as presented in Figures

7.1 to 7.6. It should be noted that the HG1700/GPS and LN200/GPS systems achieved the same results and, thus, only the HG1700/GPS results are given. As mentioned in Section 7.1, the L1 strategy (Strategy 1) which is used to compute the reference trajectory, the L1L2 strategy (Strategy 3), the L1WL strategy (Strategy 4), the L1L2+I strategy (Strategy 6) and the L1WL+I strategy (Strategy 7) are expected to deliver comparable position accuracies. As can be seen in Figures 7.1 to 7.4, and with reference to Table 7.2, the position difference of these strategies are at about the 1 cm level in the short baseline case and, thus, are negligible considering the 2 to 4 cm position accuracy of the reference trajectory.

However, due to its high noise measurements and 86 cm length wavelength, the position solution of the WL strategy (Strategy 2) is characterized by a distinct noise-like quality. Consequently, the position differences between the WL solution and the reference solution are about 6 cm (see Table 7.2).

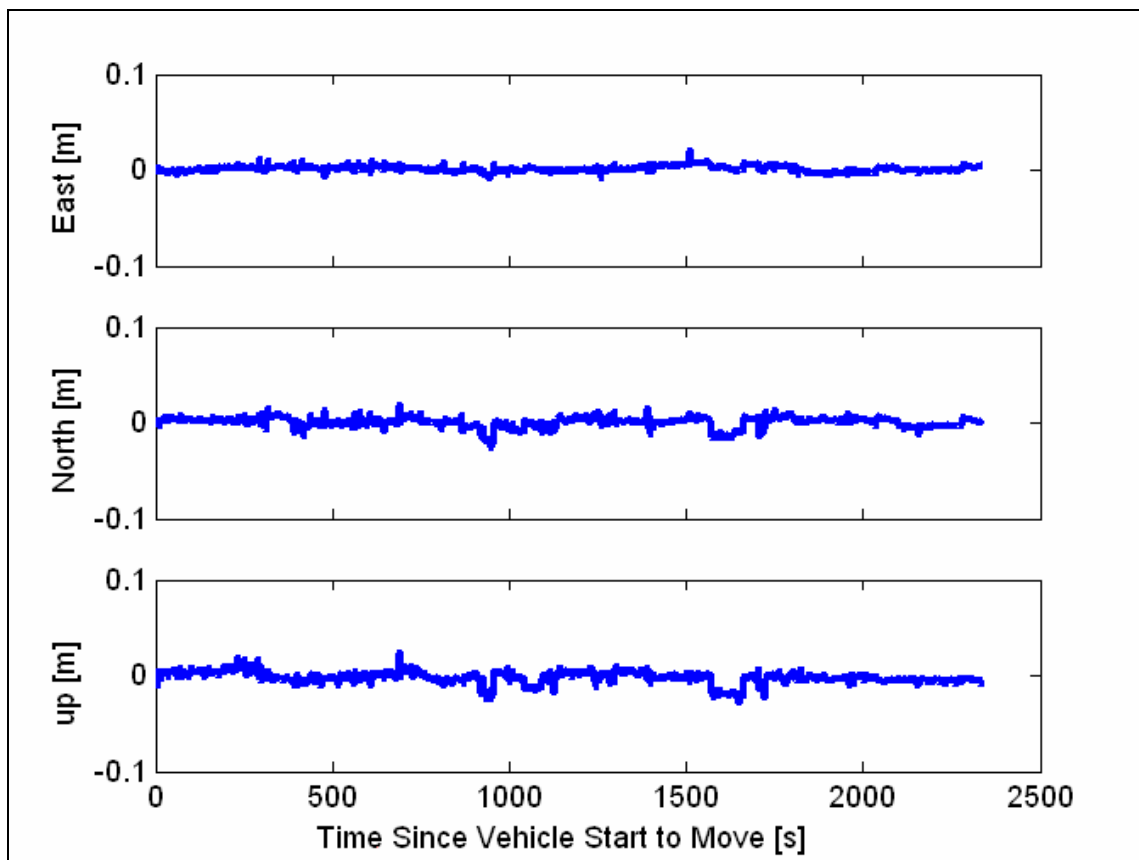


Figure 7.1 Position Difference L1L2 strategy Compared to Reference Trajectory

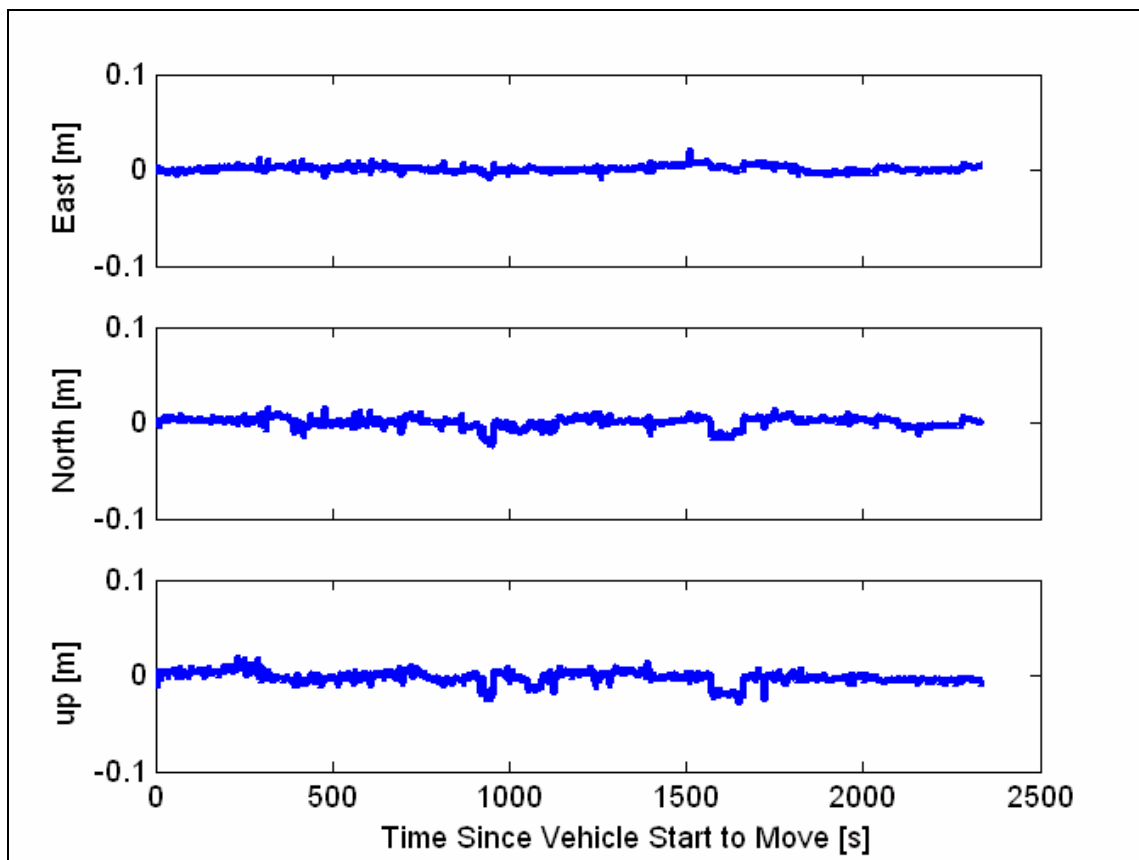


Figure 7.2 Position Difference L1WL strategy Compared to Reference Trajectory

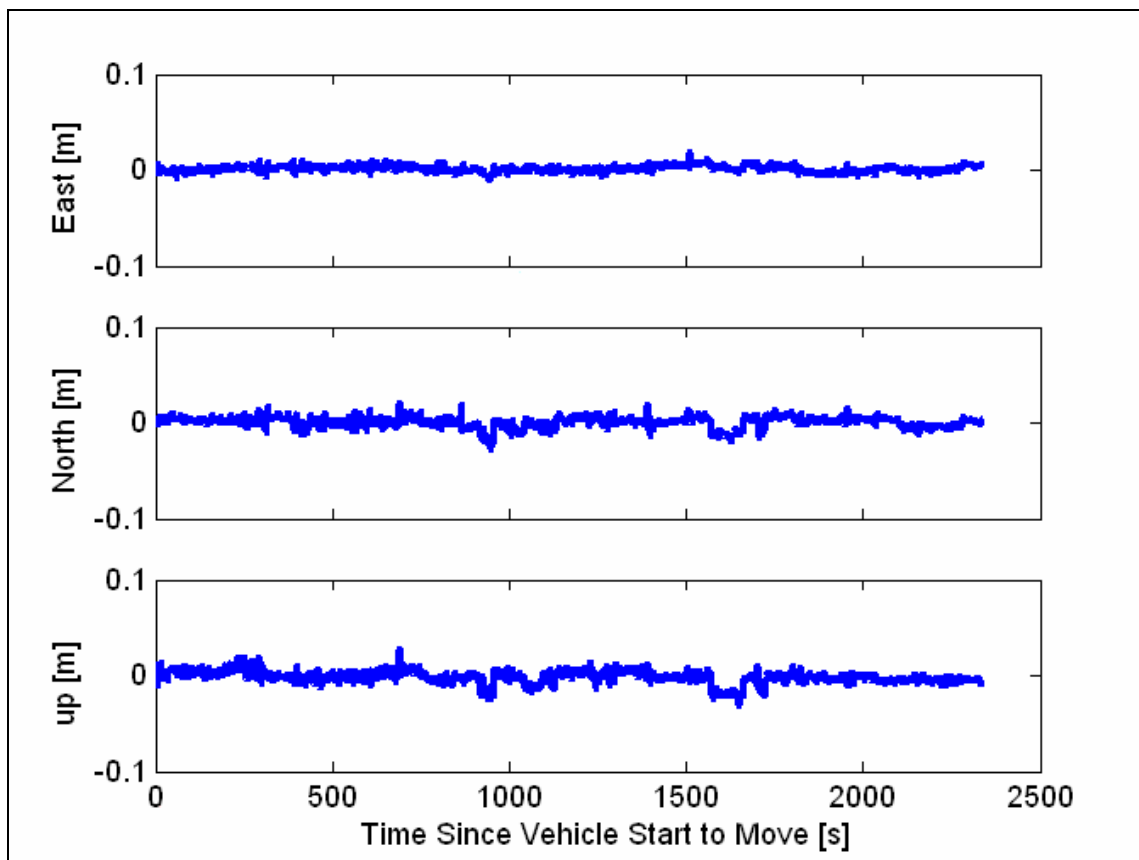


Figure 7.3 Position Difference L1L2+I strategy Compared to Reference Trajectory

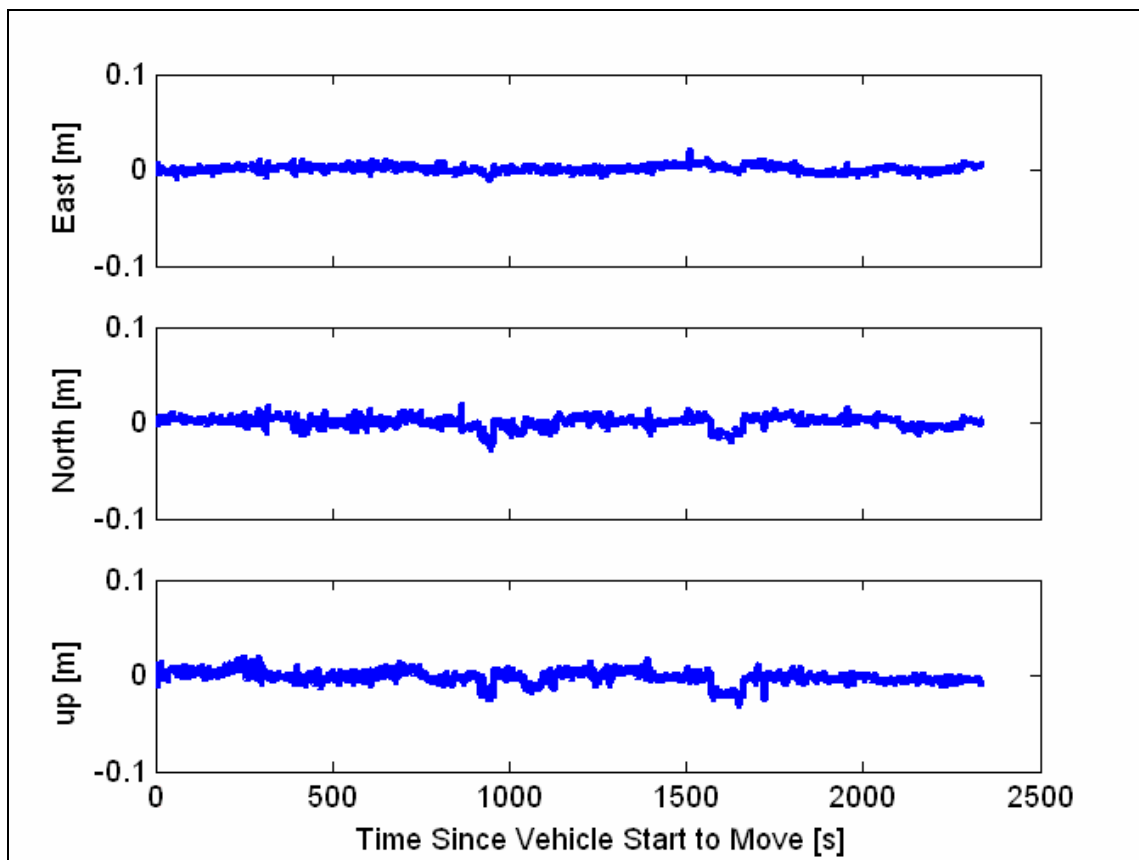


Figure 7.4 Position Difference L1WL+I strategy Compared to Reference Trajectory

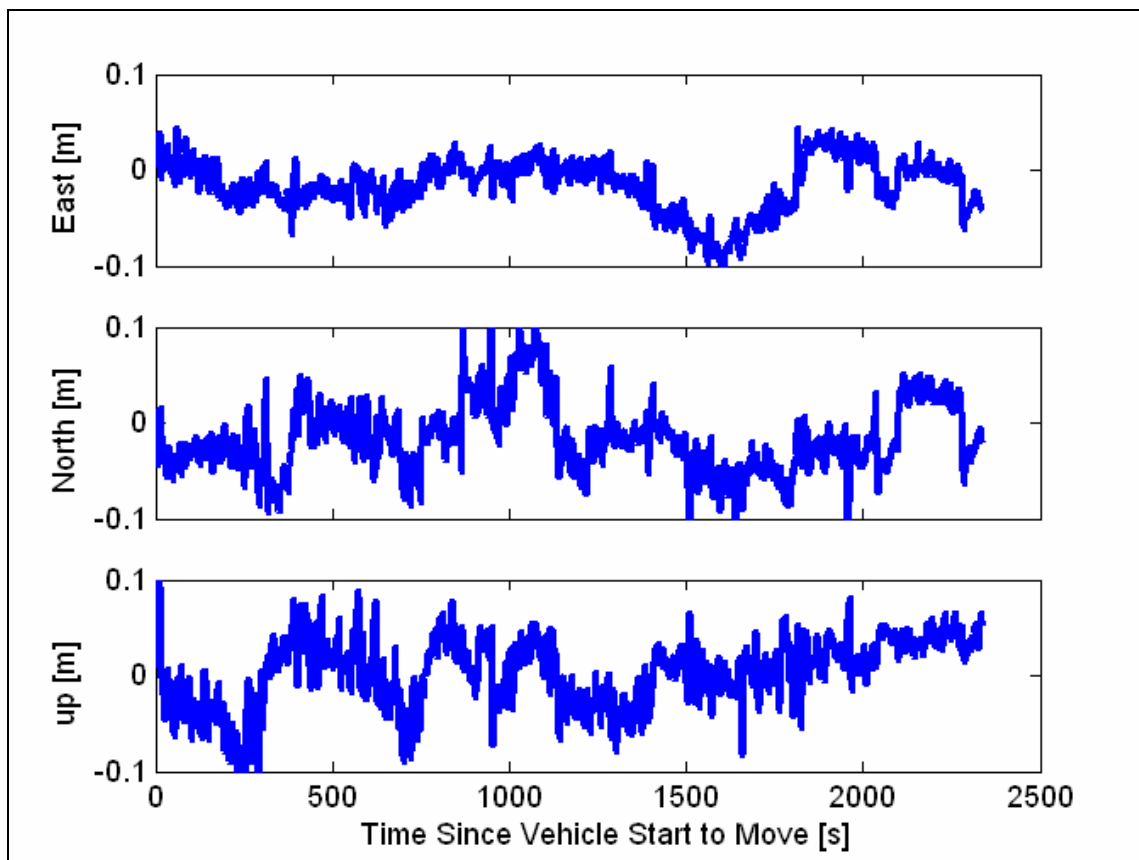


Figure 7.5 Position Difference WL strategy Compared to Reference Trajectory

The IF strategy (Strategy 5) solution demonstrates a very different position performance, as compared to the other strategies, as seen in Figure 7.6. As discussed in Section 7.1, the IF strategy ambiguities are characteristically float, having a wavelength of 48 cm. In addition, using the IF strategy amplifies the noise by almost three times, and the use of the IF strategy results in a very slow convergence. As can be seen in Figure 7.6, as compared to the other strategies, the IF strategy position error takes a much longer time to converge to the centimetre level. It is this exorbitant time demand that makes the overall position

performance of the IF strategy the worst among all strategies.

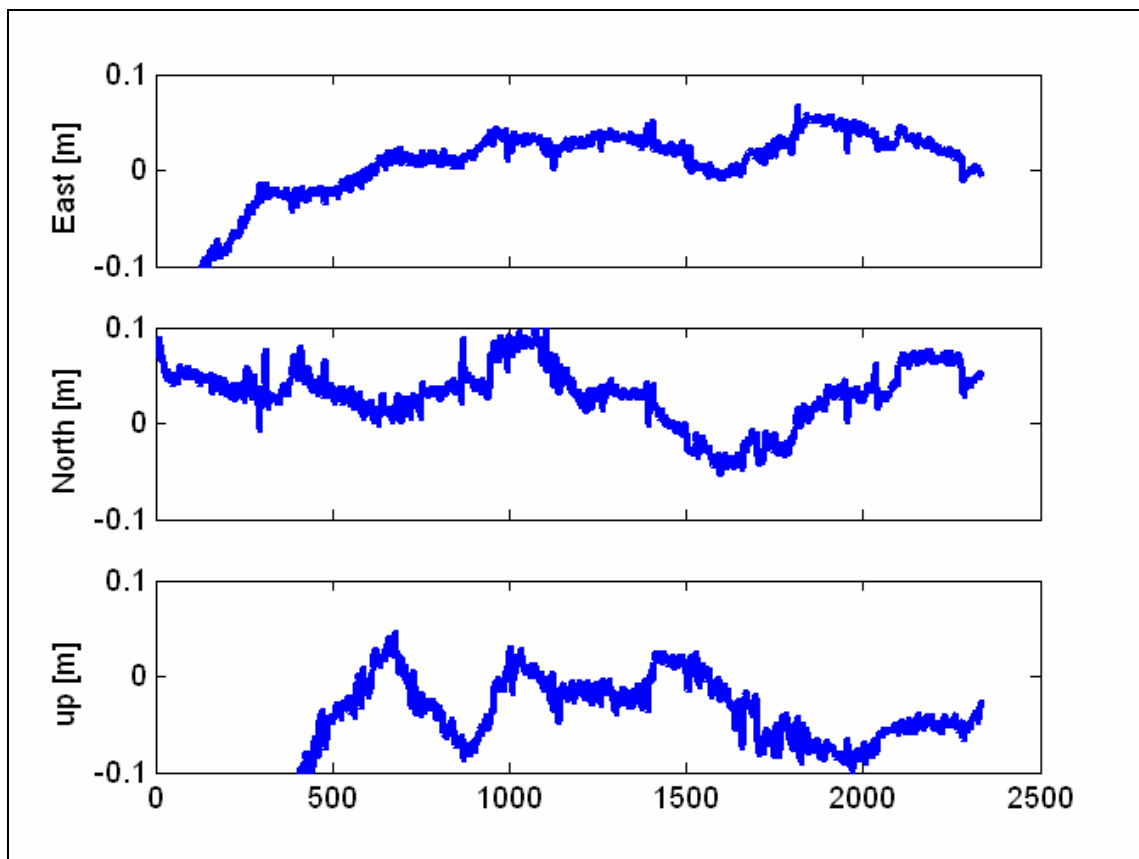


Figure 7.6 Position Difference IF strategy Compared to Reference Trajectory

7.2.2 AMBIGUITY PROCESSING STRATEGY DIFFERENCES IN THE AMBIGUITY DOMAIN

A GPS-only strategy provides the most basic criterion of how an ambiguity processing strategy is different. The performance with inertial aiding in ambiguity resolution is dependent on the GPS-only solution. So only the GPS-only ambiguity resolution solutions using different ambiguity processing strategies

are investigated in this section. Only one GPS complete outage is simulated - which is outage 2 shown in Chapter Five. Durations of 9, 20, 50 and 100 seconds are simulated specifically in the outage.

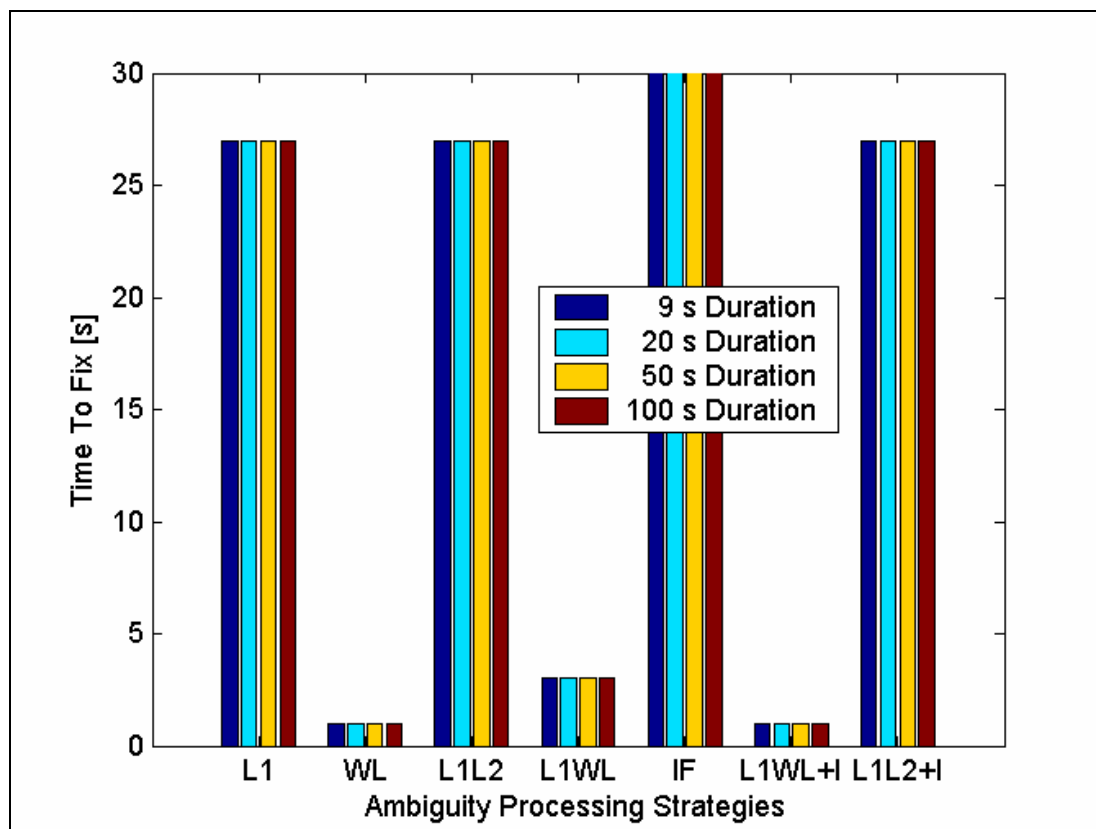


Figure 7.7 Time To Fix Corresponding Ambiguities after 9, 20, 50 and 100 seconds Outage at outage number 2 using different ambiguity processing strategies (HG1700/CDGPS system, GPS-only)

Figure 7.7 (HG1700/CDGPS system, using a GPS-only integration strategy) shows the time to fix the corresponding ambiguities after 9, 20, 50 and 100 second complete GPS outages at outage number 2 using different ambiguity processing strategies. The LN200/CDGPS results are exactly the same since

the two systems used the same GPS data, thus the results will not be shown.

It shows that the time to fix after a GPS outage with a GPS-only strategy is related to which processing strategy is used but not the length of the duration. Since the IF strategy has only a float solution, ambiguity fixing was not attempted.

Summarised from Section 7.1, the time to re-fix ambiguities using different strategies start from the same initial condition is as $TTF_{WL} \leq TTF_{L1WL+I} \leq TTF_{L1WL} \leq TTF_{L1L2+I} \leq TTF_{L1L2} \leq TTF_{L1}$; where TTF represents time to fix. Subscripts represent corresponding ambiguity processing strategies. Figure 7.7 shows this trend. This being said, in the short baseline case (which means low DD ionospheric and tropospheric errors), Strategies 4 and 6 (when properly modeling the ionospheric error factor) can give a near optimal position solution but the fastest time to re-fix ambiguities after a GPS outage.

7.3 LONG BASELINE TESTS AND RESULTS

The performance in the position domain is presented in this section. The analysis will be conducted according to the ambiguity processing strategy. In this scenario, the entire long baseline data set is processed with SAINTTM using

different ambiguity processing strategies with the positions being estimated at each epoch. The integration position solution is compared to the short baseline tightly coupled L1 solution as discussed in Chapter Five, which is used as a reference trajectory. The RMS of the position differences is also computed. The purposes of this section are to:

- 1) Determine the position error level of each ambiguity processing strategy in the long baseline case;
- 2) Assess the position accuracy of each ambiguity processing strategy in the long baseline case; and what is the difference between (1) and (2)
- 3) Assess the filter convergence speed affecting the position accuracy using different ambiguity processing strategies.

In conjunction with these objectives, this investigation will also help determine whether fixing WL first can reduce the position errors even if the L1 ambiguities cannot be fixed, although the ultimate goal is to fix the L1 ambiguities. Fixing the L1 and L2 ambiguities was not tried during processing to prevent the introducing of fixing wrong errors.

Table 7.4 RMS of Overall Position Difference Compare to Short Baseline
Tight Integration L1 Solution (HG1700/CDGPS system, Long Baseline)

Integration strategies	L1 (cm)	WL (cm)	L1L2 (cm)	L1WL (cm)	IF (cm)	L1L2+I (cm)	L1WL+I (cm)	
T	N	8	7	8	4	5	8	4
	E	9	6	7	3	4	6	4
	U	32	5	28	7	34	17	5
	3-D	34	11	30	8	34	19	7

The same results as Table 7.4 can be achieved using the LN200/CDGPS system, but thus will not be presented herein. It should be noted that in Table 7.4, all WL ambiguities were resolved across the data and the integer values were kept until the end of the data set. It is expected in the long baseline case, which means high ionospheric error, the inequality in Equation (7.5) - $\sigma'_{L1L2} \approx \sigma'_{L1} \approx \sigma'_{L1L2+I} \leq \sigma'_{WL} \approx \sigma'_{L1WL} \approx \sigma'_{L1WL+I}$ when considering estimator convergence speed - can be proved by Table 7.4. Because the IF strategy estimator has the slowest convergence speed (IF ambiguities did not converge to a reasonable value until the end of the data run), the overall position accuracy of the IF strategy is the worst in this particular case. This proves the inequality in Equation (7.5). Therefore, in the long baseline case, L1WL+I (Strategy 7) is expected to give the best position estimates if the ionospheric error is properly modeled. L1WL (Strategy 4) estimation results are except the same level of accuracy as Strategy 7. To better understand the performance of each strategy in the position domain, a comparison is given with the reference trajectory in each case, producing the position differences for each ambiguity processing

strategy. Referring to Section 7.1, the performance of each ambiguity processing strategy in the position domain depends not only on the quality of the measurements but also on the convergence speed of the corresponding estimator in the long baseline case. The L1 and L1L2 strategies demonstrate comparable position performance since they are based on very similar noise levels associated with measurements as well as similar convergence speeds. As compared to the L1 and L1L2 strategies, the L1L2+I strategy took the ionospheric delay into account and produced estimates for those values. Apart from other considerations, it is expected to have superior performance in terms of position accuracy if the ionospheric delay is properly modeled in the Kalman filter.

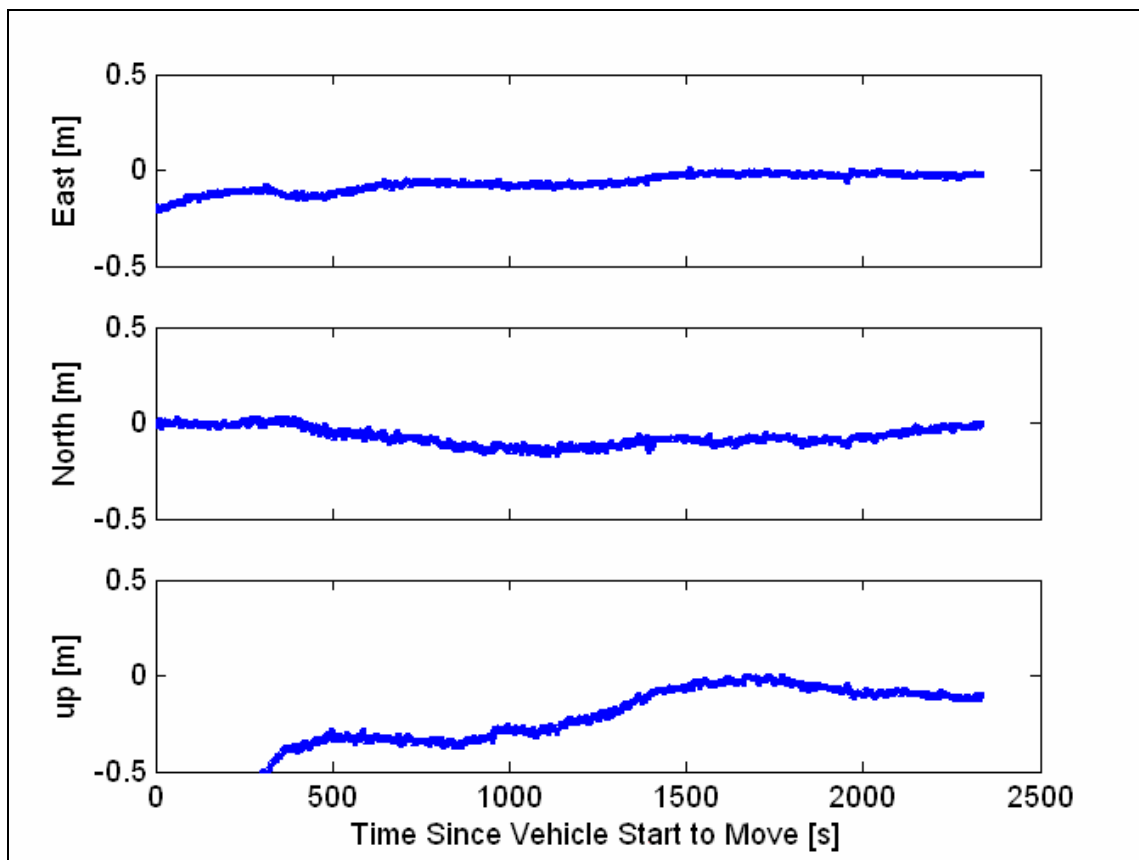


Figure 7.8 Position Difference L1 Strategy Compared to Reference Trajectory

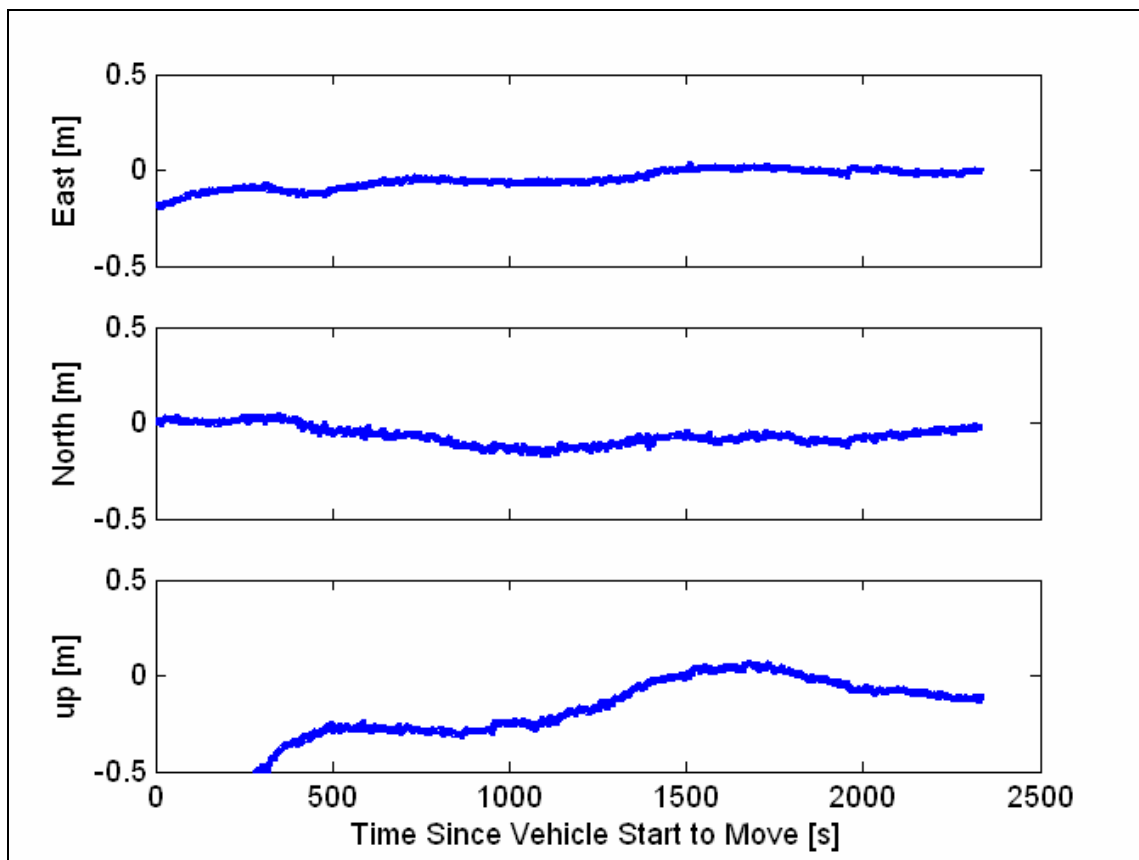


Figure 7.9 Position Difference L1L2 Strategy Compared to Reference Trajectory

As can be seen in Figures 7.8 and 7.9, the L1 and L1L2 strategies display similar patterns in convergence, with the L1 strategy solution being slightly noisier. The estimation of the ionospheric delay in the Kalman filter using the L1L2+I strategy slightly improves the position accuracy, as compared to that produced via the L1L2 strategy, as shown in Figure 7.10.

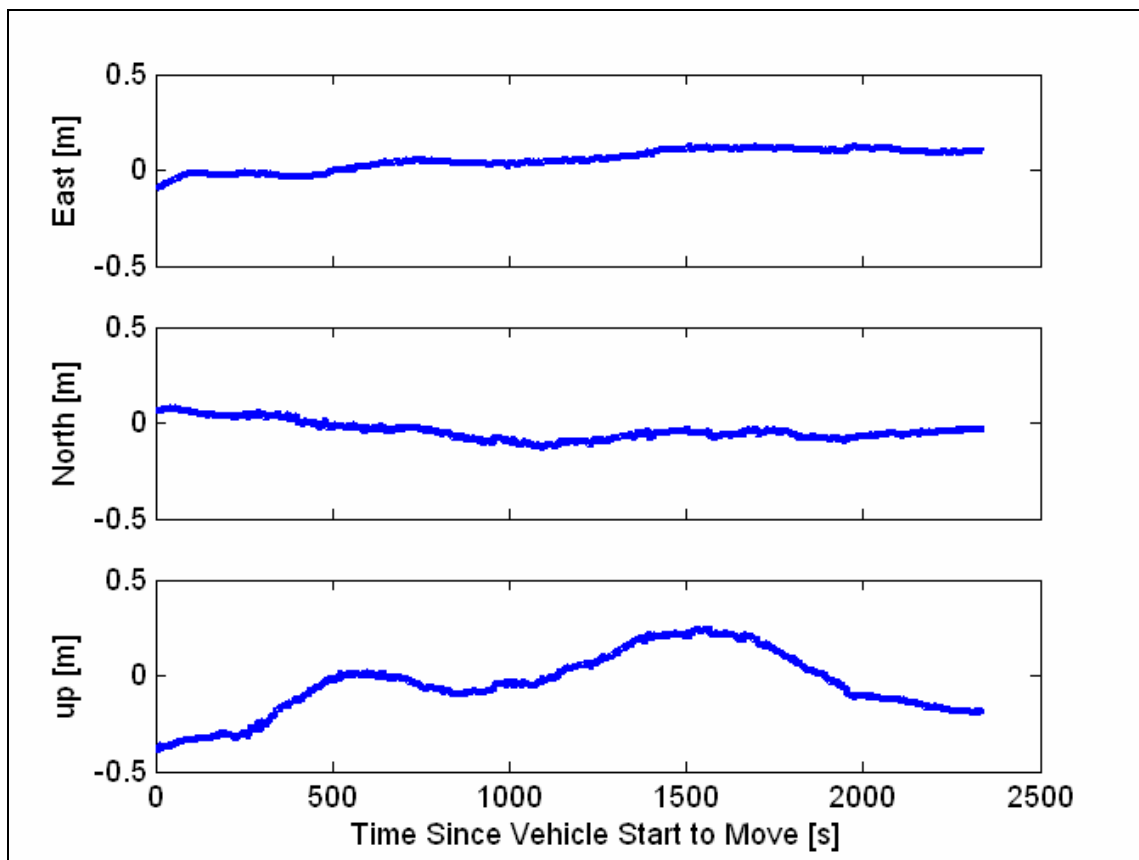


Figure 7.10 Position Difference L1L2+I Strategy Compared to Reference Trajectory

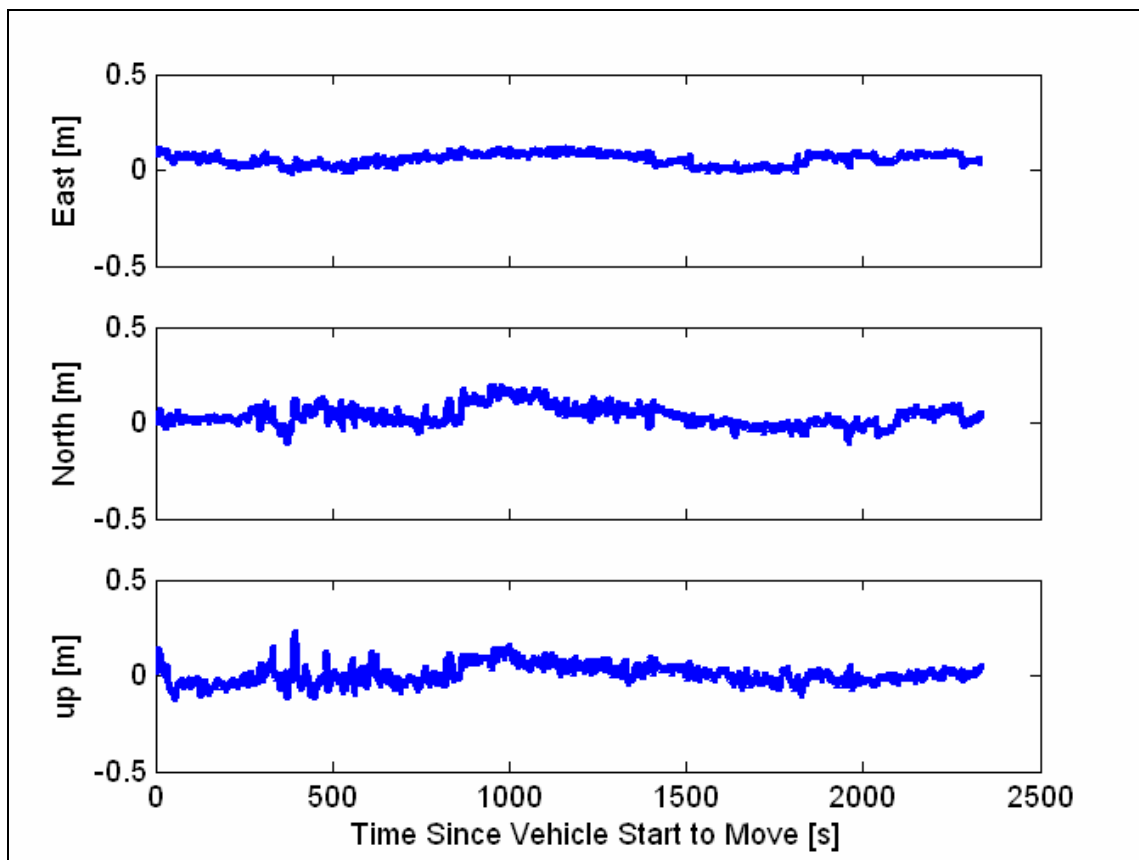


Figure 7.11 Position Difference WL Strategy Compared to Reference Trajectory

The WL strategy is used in the long baseline case because the WL ambiguities are more easily resolved as compared to either L1 or L2 ambiguities; consequently, the position accuracy rapidly converges to a reasonable value, as can be seen in Figure 7.11. Although the WL strategy solution is very noisy, the resolution of the WL ambiguities makes the solution robust and thus the overall position accuracy reasonably high, as compared to the L1, L1L2 and L1L2+I strategies.

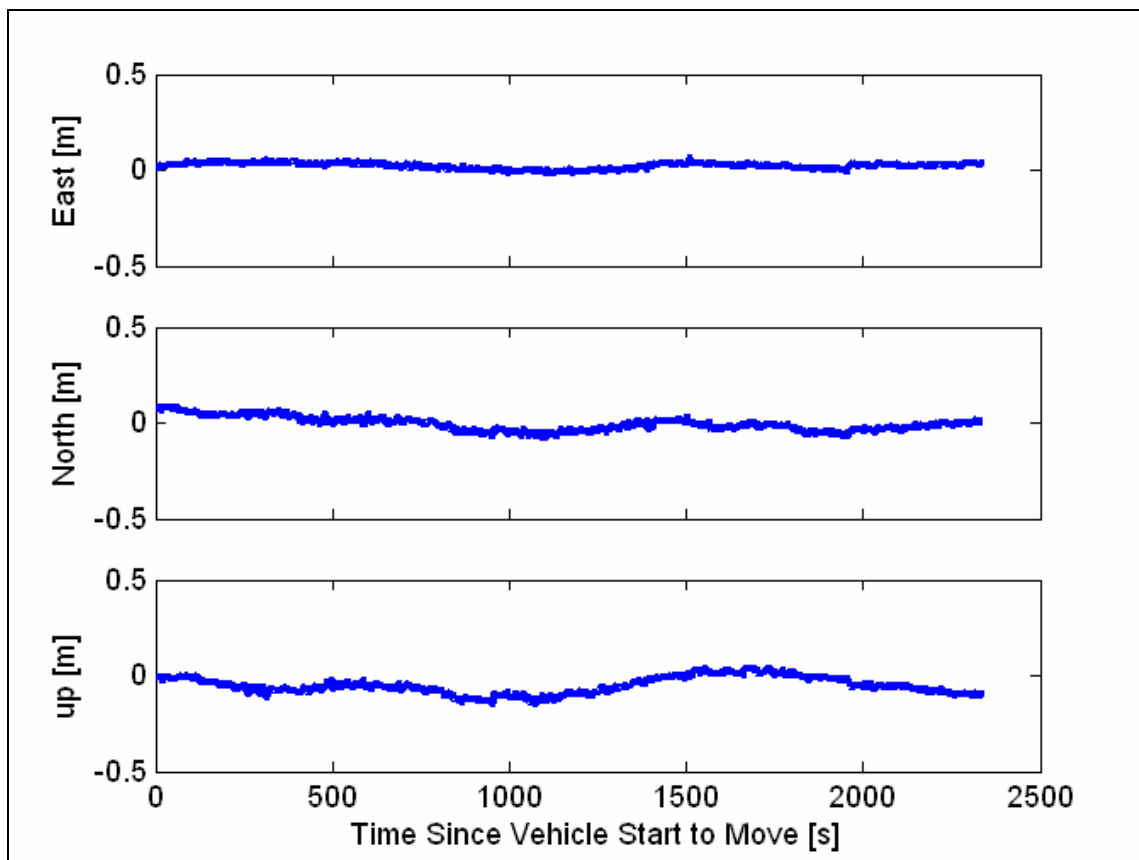


Figure 7.12 Position Difference L1WL strategy Compared to Reference Trajectory

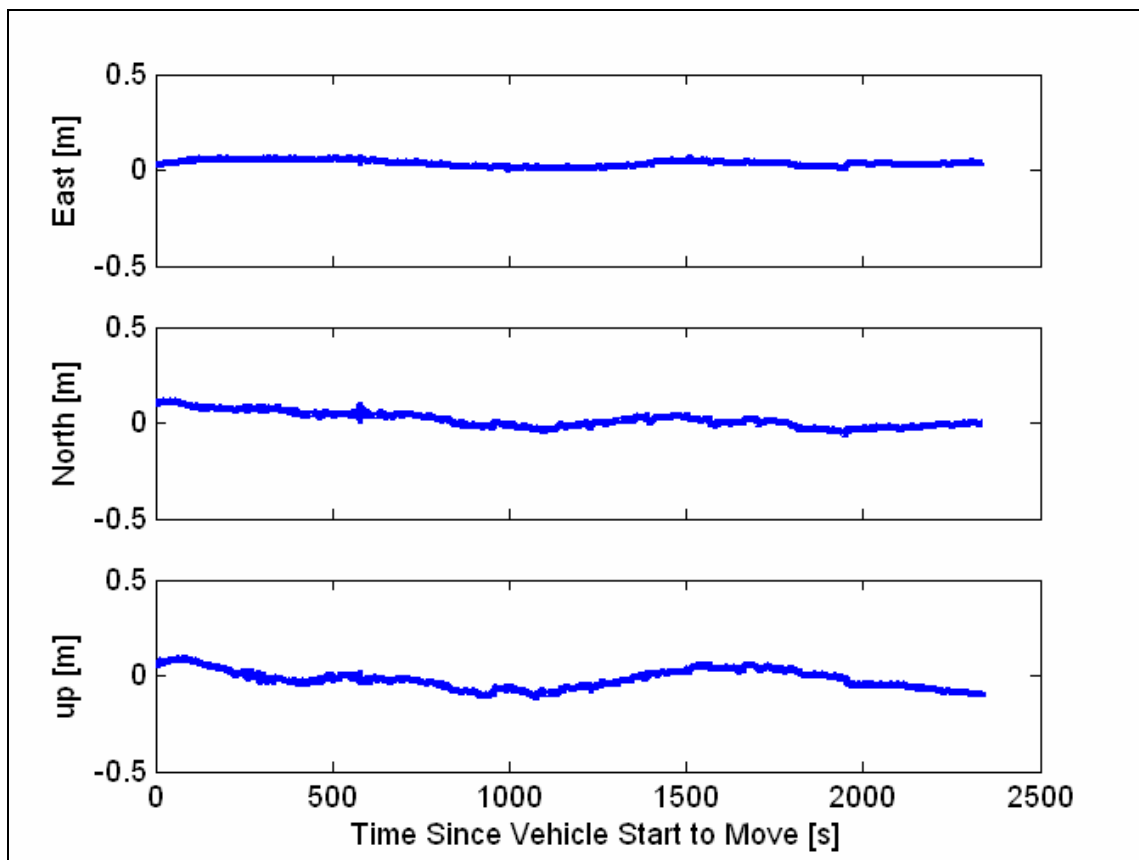


Figure 7.13 Position Difference L1WL+I Strategy Compared to Reference Trajectory

As can be seen in Figure 7.12 and 7.13, the L1WL and L1WL+I strategy solutions have the same pattern of convergence as the WL strategy solution, but are much less noisy. Because the WL ambiguity is easier to resolve than both the L1 and L2 ambiguities, better position results can be achieved after the WL ambiguities are correctly fixed, while L1 ambiguities are not fixed if L1 and WL ambiguities are estimated in the same filter, instead of L1 and L2 ambiguities. Also, the estimation of ionospheric delay can improve the position performance

slightly in this case, since the ionospheric delay is not as severe as discussed in Appendix D.

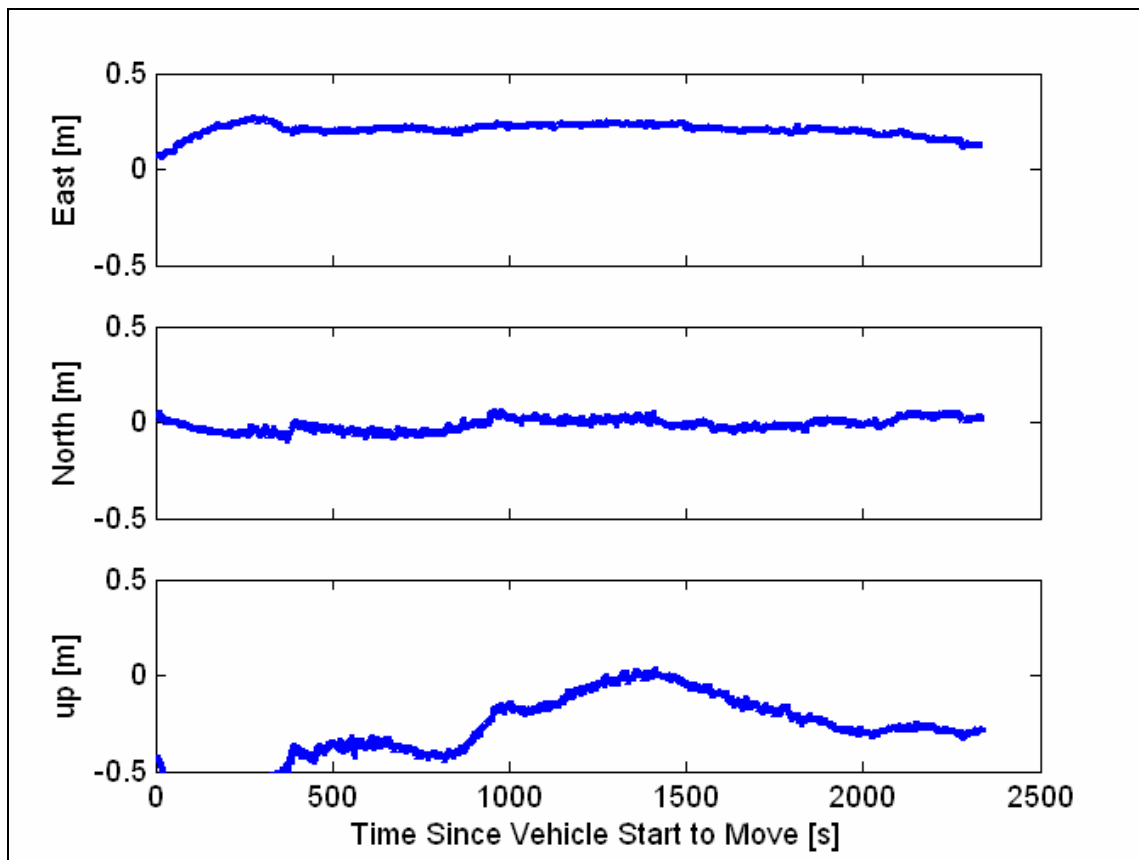


Figure 7.14 Position Difference IF Strategy Compared to Reference Trajectory

Compared to the WL strategy, the IF solution is less noisy; however, since it has the slowest convergence speed among all the strategies makes this strategy's overall performance the lowest due to the small ionospheric error. As can be seen, the IF strategy estimator cannot converge to 10 cm until the end of the data run.

CHAPTER EIGHT - CONCLUSIONS AND RECOMMENDATIONS

Essentially, this research investigated three topics. 1) Side-by-side testing of tactical-grade inertial measurement units, the HG1700 and the LN200, to assess whether comparable improvements can be achieved. Furthermore, an analytical equation was tested to compute the improvement in ambiguity resolution can be realized when kinematic carrier phase double differenced GPS is integrated with a generic IMU; 2) The effectiveness of the RTS smoothing technique in bridging position error during GPS outage; and 3) A detailed analysis of the impact of different ambiguity processing strategies on carrier phase ambiguity resolution and position accuracy under operational conditions.

This thesis began with a thorough investigation into ambiguity resolution improvements produced with the aid of inertial data. To verify the analytical equation, 9 complete GPS outages with duration from 2 to 100 seconds were simulated when processing the test data using SAINT™ software package with L1 only ambiguity processing strategy; To examine the impact of the RTS smoothing technique in bridging the position error during GPS outages, the simulated 9 outages with 100 seconds duration was selected as an sample. Modified SAINT™ save all information during processing for the RTS smoothing

usages; to examine the impact of the different ambiguity processing strategies on ambiguity resolution and position accuracy, a total of seven ambiguities resolution strategies were implemented in the SAINT™ software package. All those seven strategies have been tested using two baselines kinematic data from Calgary as described in Chapter Five. The short baseline length ranges from 0 km to 8 km; and the long baseline length ranges from 71 km to 79 km. It should be noted that actual GPS outages have very different characteristics as compared to simulated outages of the type used in this research; thus, in the strictest sense, the conclusions below are applicable only in simulated GPS outage situations.

Based on the tests and results achieved, the following conclusions can be made:

1. The integrated system showed better performance than GPS-only in all cases. Furthermore, the tight integration strategy outperformed the loose integration approach. These differences in some cases, however, were not significant.
2. The HG1700 and LN200 systems are seen to provide 10 cm accuracy for approximately 6 and 8 seconds, respectively. Furthermore, the errors grow to 2 m after about 36 and 49 seconds, respectively. For longer data outages, the position errors grow quite rapidly to a maximum of 20 and 10 m after 100 seconds, respectively.

3. Regardless of how long the GPS outage lasts, the GPS-only filter needs, on average, approximately the same amount of time to resolve the ambiguities.
4. The GPS-only solution performs the poorest in ambiguity resolution, relative to either integrated solution. In some of the cases, a 100% improvement over GPS-only can be achieved using the integrated systems, meaning that instantaneous ambiguity resolution is possible. Specifically, for data outages up to 2 and 4 seconds for the HG1700 and LN200 systems, respectively, instantaneous ambiguity resolution is possible using either integration strategy.
5. For outage durations lasting approximately 12 to 40 s (depending on the IMU), there is also a noticeable improvement when using tight integration over loose integration with GPS seeding.
6. As the inertial position covariance increases over time during a data outage, the benefit to the ambiguity resolution process decreases accordingly, with the limit being the GPS-only case.
7. Equation (3.13) provides insight into the level of improvement that can be expected, in terms of ambiguity resolution, when using either a loose or tight coupling strategy after complete GPS outage. This conclusion is expected to be emulated by any chosen grade of IMU.
8. Improvements of greater than 96% in the sense of maximum position error after RTS smoothing in 3-D can be achieved using an RTS smoother.

9. The strategy 1, 3, 4, 6, and 7 has very similar position accuracy performance in short baseline case. Consider of 2-4 cm accuracy of L1 tight coupling solution, the difference of ambiguity processing strategy 1, 3, 4, 6 and 7 is neglectable.
10. WL ambiguities are both reliable and easy to resolve. Figure 7.7 shows that the time to fix the WL ambiguities is much shorter than the time to fix the L1 or L2 ambiguities.
11. Inequality (7.1) gives relation of time to fix corresponding ambiguities using different ambiguity processing strategies where start from same initial condition.
12. Inequality (7.2) gives expected position accuracy relation achieved by different ambiguity processing strategy in short baseline condition. However, considering of estimator of IF strategy (strategy 5) is very slow, the position accuracy of IF strategy overall may descend even worse than that of WL strategy (strategy 2).
13. In short baseline case, strategy 4 and strategy 6 (when properly modeling the ionospheric error factor) can give near optimal position solution but fastest time to re-fix ambiguities after GPS outage.
14. The system overall position accuracy is not only depending on the measurements noise but also the estimator convergence speed especially for kinematic navigation practice. Since no one can expect carrier has longer than 30 minutes static mode to wait the estimator

converging in practice.

15. Estimating L1 and WL ambiguities in the same filter, instead of L1 and L2 ambiguities, does help to resolve the L1 ambiguities faster in short baseline case. It was demonstrated in Figure 7.7 that the time to fix ambiguities using WL, L1WL, and L1WL+I (strategy 1, 4, 6) are comparable in short baseline case.
16. Estimating L1 and WL ambiguities in the same filter, instead of L1 and L2 can decrease the overall position errors if the WL is fixed correctly in long baseline case. It was demonstrated in Table 7.4 that overall RMS position error in strategies 4 and 6 are significantly better than the position errors in strategies 1, 3, and 7 when both L1 and L2 ambiguities are not fixed.
17. The strategy 1, 3, 4, 6, and 7 has very similar position accuracy performance in short baseline case. Table 7.2 and Table 7.3 has demonstrated that inequality (7.4) describe the position accuracy of each ambiguity processing strategy clearly. The convergence speed of IF estimator makes the overall position accuracy descend.
18. In short baseline case (which means low DD ionospheric error and DD tropospheric error), strategy 4 and strategy 6 (when properly modeling the ionospheric error factor) can give near optimal position solution but fastest time to re-fix ambiguities after GPS outage.
19. It is expected that L1WL+I (strategy 6) can achieve the best position estimate compare to all others in long baseline condition, since the

ionospheric error becomes the dominant error source. And the estimator has very fast convergence speed. The results in Table 7.4 have demonstrated that.

20. In long baseline case, it is expected that IF strategy can give the best position estimation. However, because IF strategy estimator has the slowest convergence speed (IF ambiguities did not converge to reasonable value till end of the data run), the position accuracy of IF strategy is the worst but not the best in this particular case.

Based on the results and conclusions above of this research, the recommendations regarding the use and further investigations of qualified ambiguity resolution improvement with aiding of inertial data; backward smoothing in improving reference trajectory accuracy; various ambiguity resolution strategies can be made as following:

1. The Equation (3.13) is an only analytical qualified ambiguity resolution improvement with aiding of inertial data. Chapter Six shows that this equation is more suitable for tight integration strategy. Further research can be done to explain this phenomenon.
2. RTS smoothing in Chapter Six has shown its capability to improve the position accuracy during GPS outage. More than 96% position error can be removed after applying RTS smoothing technique. Naturally, it is

expected that the after smoothed ambiguity states and corresponding VCV are more efficient to resolve the integer ambiguities compare to that of forward filter. Thus if a data run contains a long period of float ambiguity solution, it is expected the ambiguities can be resolved after backward smoothing then the position accuracy of the float solution can be improved.

3. The test results in Chapter Six and seven are based on certain input parameters (e.g. IMU gyro and accelerometer error model parameters, data rate, observation variances, the magnitude of the noise spectral density driving the velocity and position states, and the magnitude of the pseudo-ionosphere observable variance). The impact of these input parameters on the output is not investigated in this thesis.
4. The author tested the Equation (3.13), RTS smoothing improvements, and performance of each ambiguity processing strategy only with one data set. It is recommended that more data sets should be used to do so, and should be tested more extensively for RTK applications.

Overall, this thesis gives an quantitative relationship between the free-inertial positioning accuracy after GPS outage and the respective ambiguity resolution improvements with the aiding of inertial data is presented to compute how big ambiguity resolution improvement can be expected use a generic IMU; verifies the RTS smoothing technique performance; and clarifies the advantages and

disadvantages of all the introduced ambiguity resolution strategies in short baseline condition and long baseline condition. With these knowledge, the selection of IMU in different scenario and ambiguity resolution process can be better understood, and the optimal scheme of ambiguity processing strategy for an application can be chosen.

REFERENCES

- Abdullah, Q. (1997). *Evaluation of GPS-Inertial Navigation System for Airborne Photogrammetry*, Proceedings of the ASPRS/MAPPS Softcopy Conference, Arlington, Virginia, USA, July 27-30.
- Abidin, H.Z. (1993). *On the Construction of the Ambiguity Searching Space from One-The-Fly Ambiguity Resolution*, Navigation: Journal of The Institute of Navigation, Vol. 40, No. 3, pp. 321-338.
- Alves, P., (2004). *Development of Two Novel Carrier Phase-Based Methods for Multiple Reference Station Positioning*. Ph.D thesis, Department of Geomatics Engineering, the University of Calgary. Calgary, Alberta, Canada, UCGE Report No. 20203.
- Axelrad, P., Comp, C., and Macdoran, P. (1996). *SNR-Based Multipath Error Correction for GPS Differential Phase*, IEEE Transactions on Aerospace and Electronic Systems, Vol. 32, No. 2, pp. 650-660
- Böder, V., and Seeber, G. (1997). *Real-Time PDGPS Positioning, Attitude Determination and INS-Integration for Hydrographic Applications*, Proceedings of the International Symposium on Kinematic Systems in Geodesy, Geomatics and Navigation, Department of Geomatics Engineering, The University of Calgary, pp. 187-194.
- Brenner, M. (1995). *Integrated GPS/Inertial Fault Detection Availability*. Proceedings of GPS'95, The Institute of Navigation, Alexandria, VA., pp. 1949-1958.
- Bruton, A. (2000). *Improving the Accuracy and Resolution of SINS/DGPS Airborne Gravimetry*, PhD Thesis, Department of Geomatics Engineering, University of Calgary, Calgary, Alberta, Canada, UCGE Report No. 20145.
- Bye, C.T., Hartmann, G.L., and Killen, A. (1997). *Inertial and GPS Technology Advances on the GGP Program*, Proceedings of the Annual Meeting 1997, The Institute of Navigation, Alexandria, VA., pp. 639-648.
- Cannon, M.E. (1990). *High-accuracy GPS semi-kinematic positioning: Modeling and results*, Navigation: J. Inst. Nav., vol. 37, no. 1, pp. 53-64.
- Cannon, M.E. (1991). *Airborne GPS/INS with an Application to Aerotriangulation*. PhD Thesis, UCGE Report #20040, Department of Geomatics Engineering, University of Calgary.
- Carvill, J.J. (1993). *GPS Velocity Damping and its Effect on SINS Performance*. Proceedings of the Annual Meeting 1993, The Institute of Navigation, Alexandria, VA., pp. 655-664.

- Carson, N.A. (1988). *Federate Filter for Fault-tolerant Integrated Navigation System*, Proceeding of IEEE Position Location and Navigation Symposium, pp: 110-119.
- Chen, D. (1994). *Development of a Fast Ambiguity Search Filter (FASF) Method for GPS Carrier Phase Ambiguity Resolution*, PhD Thesis, UCGE Report #20071, Department of Geomatics Engineering, University of Calgary.
- Comp, C. and Axelrad, P. (1998). *Adaptive SNR-Based Carrier Phase Multipath Mitigation Technique*, IEEE Transaction on Aerospace and Electronic Systems. Vol. 34, No. 1, pp. 264-276
- Colombo, O.L., Bhapkar, U.V., and Evans, A.G. (1999). *Inertial-Aided Cycle-Slip Detection/Correction for Precise, Long-Baseline Kinematic GPS*, Proceedings of GPS'99, The Institute of Navigation, Alexandria, VA., pp. 1915-1921.
- Cramer, M., Stallmann D., and Haala, N. (2000). Direct Georeferencing Using GPS/Inertial Exterior Orientation for Photogrammetric Applications. Proceedings of the XIX Congress of the International Society for Photogrammetry and Remote Sensing (ISPRS), Amsterdam, The Netherlands, July 16-23.
- Dao, T.H.D., Alves, P., and Lachapelle, G., (2004). *Performance Evaluation of Multiple Reference Station GPS RTK for a Medium Scale Network*, Proceeding of International Symposium on GNSS/GPS Sydney, Australia 6–8 December 2004.
- Dao, T.H.D., (2005). Personal conversation.
- de Jong, C.D., Lachapelle, G., Skone, S., and Elema, I.A. (2002). *Hydrography*. Delft University Press.
- Ebert, W.J.M., Krieg, T., and Schnell, J. (1994). *An Autonomous Inertial Navigation System for Autonomously Guided Vehicles*, Proceedings of the National Technical Meeting 1994, The Institute of Navigation, Alexandria, VA., pp. 567-576.
- El-Sheimy, N. (2003). *Inertial Techniques and INS/DGPS Integration*, ENGO 623 Lecture Note, the University of Calgary.
- Farrell, J.A., Givargis, T.D., and Barth, M.J. (2000). *Real-Time Differential Carrier Phase GPS-Aided INS*, IEEE Transactions on Control System Technology, Vol. 8, No. 4, pp. 709-721.
- Fenton, R. and Mayhan, R. (1991). *Automated highway studies at the Ohio State University—An overview*, IEEE Trans. on Veh. Technol., vol. 40, pp. 100–113.

- Federal Aviation Administration, *Picture of GPS Control Segment Location*, retrieved 2005 from <http://gps.faa.gov/>.
- Garmin, *Picture of GPS Constellation*, retrieved 2005 from <http://www.garmin.com/>.
- Greenspan, R.L. (1995). Inertial Navigation Technology from 1970-1995, *Journal of the Institute of Navigation*, Vol. 42, pp. 165-185.
- Greenspan, R.L. (1996). *GPS and Inertial Integration. Global Positioning System: Theory and Applications, Volume II*, American Institute of Aeronautics and Astronautics, Washington, DC, pp. 187-220.
- Grejner-Brzezinska, D., Da, A.R., and Toth, C. (1998). *GPS error modeling and OTF ambiguity resolution for high-accuracy GPS/INS integrated system*. *Journal of Geodesy*, 72, pp. 626–638.
- Guldner, J., Tan, H.S., and Patwardhan, S. (1996). *Analysis of automatic steering control for highway vehicles with look-down lateral reference systems*, *Veh. Syst. Dynamics*, vol. 26, pp. 243–269.
- Han, S., and Rizos C. (1997). *Comparing GPS Ambiguity Resolution Techniques*, *GPS World*, Advanstar Communications, pp. 54-61.
- Hartman, R.G. (1988). *An Integrated GPS/IRS Design Approach*, *Navigation: Journal of The Institute of Navigation*. Vol 35, No. 1, Alexandria, VA., pp. 121-134.
- Hatch, R. (1990). *Instantaneous ambiguity resolution*, in Symp. 107, *Kinematic Systems in Geodesy, Surveying and Remote Sensing*, Springer Verlag, New York, pp. 299–308.
- Hatch, R. (1994). *Comparison of Several AROF Kinematic Techniques*, *Proceedings of GPS'94*, The Institute of Navigation, Alexandria, VA., pp. 363-370.
- Hein, G., and Werner W. (1995). *Comparison of Different On-The-Fly Ambiguity Resolution Techniques*, *Proceedings of GPS'95*, The Institute of Navigation, Alexandria, VA., pp. 1137-1144.
- Honeywell, (1997). *Document DS34468-01: Critical Item Development Specification HG1700AG Inertial Measurement Unit*.
- Hopfield, H.S. (1970), *Tropospheric Effect on Electromagnetically Measured Range: Prediction from Surface Weather Data*, Applied Physics Laboratory, Johns Hopkins University, Baltimore, MD.
- Hopfield, H.S. (1972), *Tropospheric Range Error Parameters-Further Studies*, Applied Physics Laboratory, Johns Hopkins University, Baltimore, MD.

- IGS (2005), IGS Product Table, International GPS Service, retrieved (2005) from <http://igscb.jpl.nasa.gov/components/prods.html>.
- Jekeli, C. (2000). *Inertial Navigation Systems with Geodetic Applications*, Walter de Gruyter, New York.
- Kalman, R.E., (1961), *New Methods and Results in Linear Filtering and Prediction Theory*, ASME Jour. Basic Engineering, Series D, V. 83
- Kaplan, D. (Editor) (1996). *Understanding GPS Principles and Applications*, Artech House Publishers, Boston, pp. 351.
- Lachapelle, G. (2003). *Advanced GPS Theory and Applications*, ENGO 625 Lecture Notes, Department of Geomatics Engineering, University of Calgary.
- Lanyi, G. (1984), *Tropospheric Delay Effects in Radio Interferometry*, Telecommunications and Data Acquisition Progress Rep., Jet Propulsion Lab, Pasadena, CA.
- Leach, B.W., Dillon, J., and Rahbari, R. (2003). *Operational Experience with Optimal Integration of Low-Cost Inertial Sensors and GPS for Flight Test Requirements*, the Canadian Aeronautics and Space Journal, Vol, 49, No., 2, pp. 41-54.
- Liu, J., Cannon, M.E., Alves, P., Petovello, M.G., Lachapelle, G. Macgougan, G., and deGroot L. (2003). *A Performance Comparison of Single and Dual-Frequency GPS Ambiguity Resolution Strategies*, GPS Solution, Vol. 7, pp. 87-100.
- Lockheed Martin Corporation, retrieved (2005), from <http://www.lockheedmartin.com/wms/findPage.do?dsp=fec&ci=17164&rsbci=0&fti=112&ti=0&sc=400>.
- Lu, G. (1995). *Development of a GPS Multi-Antenna System for Attitude Determination*, UCGE Report 20073, Department of Geomatics Engineering, The University of Calgary.
- Masson, A., Burtin, D., and Sebe, M. (1996). *Kinematic DGPS and INS Hybridization for Precise Trajectory Determination*. Proceedings of GPS'96, The Institute of Navigation, Alexandria, VA., pp. 965-973.
- Misra, P., and Enge, P. (2001). *Global Positioning System, Signals, Measurements, and Performance*.
- Grewal, H.S., Weill, L.R. and Andrews, A.P. (2001), *Global Positioning System, Inertial Navigation, and Integration*, John Wiley & Sons, Inc.
- Nassar, S., and Schwarz, K.P. (2001). *Bridging DGPS Outages in Kinematic Applications Using a Simple Algorithm for INS Bias Modeling*, proceedings of the International Symposium on kinematic Systems in Geodesy, Geomatics and Navigation (KIS 2001), Banff, Alberta, Canada.

- Nassar, S. (2002). Different Algorithms for Bridging Kinematic DGPS Outages Using SINS/DGPS Integration, Proceedings of ION GPS'02, Portland, OR, pp. 1474-1482.
- Nassar, S., Schwarz, K., Noureldin, A., and El-Sheimy, N. (2003). *Modeling Inertial Sensor Errors Using Autoregressive (AR) Models*, Proceedings of ION NTM'03, Anaheim, CA. January 2003.
- Nassar, S. (2003). *Improving the Inertial Navigation System (INS) Error Model for INS and INS/DGPS*, PhD Thesis, UCGE Report #20183, Department of Geomatics Engineering, University of Calgary.
- NovAtel Inc. *NovAtel DL4-Plus*, retrieved (2005) from <http://www.novatel.ca/Documents/Papers/DL4plus.pdf>.
- U.S. Naval Observatory, retrieved March, 2005 from <http://tycho.usno.navy.mil/gpscurr.html>.
- Petovello, M.G., Cannon, M.E., Lachapelle, G., Wang, J., Wilson, C.K.H., Salychev, O.S., and Voronov, V.V. (2001). *Development and Testing of a Real-Time GPS/INS Reference System for Autonomous Automobile Navigation*, Proceedings of ION GPS'01, Salt Lake City, UT, pp. 2634-2641.
- Petovello, M.G. (2003a). *Real-Time Integration of a Tactical-Grade IMU and GPS for High-Accuracy Positioning and Navigation*, Ph.D Thesis, University of Calgary.
- Petovello, M.G. (2003b). *SAINT™ Operating manual*, University of Calgary.
- Petovello, M.G., Cannon, M.E., and Lachapelle, G. (2003). *Quantifying Improvements from the Integration of GPS and a Tactical Grade INS in High Accuracy Navigation Applications*, Proceeding of ION NTM'03, Anaheim, CA.
- Petovello, M.G. Personal Conversation.
- Raquet, J.F. (1998). *Development of a Method for Kinematic GPS Carrier Phase Ambiguity Resolution Using Multiple Reference Receivers*, PhD Thesis, UCGE Report #20116, Department of Geomatics Engineering, University of Calgary.
- Raquet, J., Lachapelle, G., and Melgard, T.E. (1998). *Test of A 400km X 600km Network of Reference Receivers for Precise Kinematic Carrier Phase Positioning in Norway*. Proceedings of ION GPS'98, The 11th International Technical Meeting of the Satellite Division of the Institute of Navigation, Nashville, Tennessee, September 15-19, pp. 407-416.
- Ray, J.K. (2000). *Mitigation of GPS Code and Carrier Phase Multipath Effects Using a Multi-Antenna System*, PhD Thesis, UCGE Report #20136, Department of Geomatics Engineering, University of Calgary.

- Rauch, H.E., Tung, F., and Striebel, C.T., (1965). *Maximum likelihood estimates of linear dynamic systems*, J. Amer. Inst. Aeronaut, Astronauts, vol. 3, no. 8, pp. 1445–50.
- Savage P (2000) *Strapdown Analytics*, Strapdown Associates, Inc., Minnesota
- Sasstamoinen, J. (1972), *Atmospheric Correction for the Troposphere and Stratosphere in Radio Ranging of Satellites*, Geophysical Monograph 15, American Geophysical Union, Washington DC.
- Scherzinger, B.M. (2000). *Precise Robust Positioning with Inertial/GPS RTK*, Proceedings of GPS-2000, The Institute of Navigation, Alexandria, VA., pp. 155-162.
- Scherzinger, B.M. (2002). *Robust Positioning with Single Frequency Inertially Aided RTK*, Proceeding of ION NTM'02, San Diego, CA, pp. 911-917.
- Scherzinger, B.M. (2004). *Estimation with Application to Navigation*, Engo 699.11 Lecture note, Department of Geomatics Engineering, the University of Calgary.
- Schwarz, K.P., El-Sheimy, N., and Liu, Z. (1994a). *Fixing GPS Cycle Slips by INS/GPS*. Proceedings of the International Symposium on Kinematic Systems in Geodesy, Geomatics and Navigation, Department of Geomatics Engineering, The University of Calgary, pp. 265-275.
- Schwarz, K.P., Chapman, M., Cannon, M., Gong, P., and Cosandier, D. (1994b). *A Precise Positioning/Attitude System in Support of Airborne Remote Sensing*. Proceedings of The GIS/ISPRS Conference, Ottawa, Canada, June 6-10, 1994.
- Sennott, J. and Senffner, D. (1997). *Robustness of Tightly Coupled Integrations for Real-Time Centimeter GPS Positioning*, Proceedings of GPS'97, The Institute of Navigation, Alexandria, VA., pp. 655-663.
- Shin, E. and El-Sheimy, N. (2002). *Optimizing Smoothing Computation for Near Rear-Time GPS Measurement Gap Filling in INS/GPS Systems*, Proceeding of ION GPS'02, Portland, OR, pp. 1434-1441.
- Shladover, S.E., Desoer, C.A., Hedrick, J.K., Tomizuka, M., Walrand, J., Zhang, W.B., McMahan, D.H., Peng, H., Sheikholeslam, S., and McKeown, N. (1991). *Automatic vehicle control developments in the PATH program*, IEEE Trans on Veh. Technol., vol. 40, pp. 114–130.
- Škaloud, J. (1998). *Reducing the GPS Ambiguity Search Space By Including Inertial Data*. Proceedings of GPS'98, The Institute of Navigation, Alexandria, VA., pp. 2073-2080.

- Škaloud, J. (1999). *Optimizing Georeferencing of Airborne Survey Systems by INS/GPS*. PhD Thesis, Department of Geomatics Engineering, University of Calgary, Calgary, Alberta, Canada, UCGE Report No. 20126.
- Skone, S. (1998). *Wide Area Ionospheric Grid Modelling in the Auroral Region*, PhD Thesis, UCGE Report #20123, Department of Geomatics Engineering, University of Calgary.
- Skone, S. and Hoyle, V., (2005). *Eye on the Ionosphere: Canadian GPS Network for ionospheric monitoring*, GPS solution, Vol 9(1), pp 59-62.
- Söhne, W., Heinze, O., and Mathes, A. (1994). *The Potential of the LASERNAV II Inertial Navigation System for Supporting Ambiguity Resolution During Motion*, Proceedings of the International Symposium on Kinematic Systems in Geodesy, Geomatics and Navigation, Department of Geomatics Engineering, The University of Calgary, pp. 147-153.
- Spilker, J.J. (1994), *GPS Navigation Data, Overview of GPS Operation and Design, Global Positioning System: Theory and Applications*, Vol. I, ed. B.W. Parkinson and J.J. Spilker, American Institute of Aeronautics and Astronautics, Inc., Washington, DC, pp. 121-176.
- Spilker, J.J. (1996). *GPS Signal Structure and Theoretical Performance, Global Positioning System: Theory and Applications*, Volume I, American Institute of Aeronautics and Astronautics, Washington, DC, pp. 57-119.
- Tan, H.S., Rajamani, R., and Zhang, W.B. (1998). *Demonstration of an automated highway platoon system*, in Amer. Cont. Conf., Philadelphia, PA, pp. 1823–1827.
- Teunissen, P.J.G. (1993). *Least-squares Estimation of the Integer GPS Ambiguities*, Invited lecture, Section IV Theory and Methodology, IAG General Meeting, Beijing, China, August 1993.
- Teunissen, P.J.G. (1994). *A New Method for Fast Carrier Phase Ambiguity Estimation*, Proceedings of IEEE PLANS'94, Las Vegas, NV, April 11-15, pp. 562-573.
- Teunissen, P.J.G. and Tiberius, C.C.J.M. (1994). *Integer Least-Squares Estimation of The GPS Phase Ambiguities*, Proceedings of the International Symposium on Kinematic Systems in Geodesy, Geomatics and Navigation, Department of Geomatics Engineering, The University of Calgary, pp. 221-231.
- Teunissen, P.J.G., de Jonge, P.J., and Tiberius, C.C.J.M. (1996). *The Volume of the GPS Ambiguity Search Space and its Relevance for Integer Ambiguity Resolution*, Proceedings of ION GPS'96.

- Wei, M., and Schwarz, K.P. (1989). A Discussion of Models for GPS/INS Integration, Presented at the IAG General Meeting, Edinburgh, Aug. 3-12.
- Wells, D., Beck, N., Delikaraoglou, D., Kleusberg, A., Krakiwsky, E.J., Lachapelle, G., Lamgley, R.B., Nakiboglu, M., Schwar, K.P., Tranquilla, J.M., and Vanicek, P. (1987). *Guide to GPS Positioning*, Canadian GPS Associates, Fredericton, New Brunswick, Canada.
- Wiener, N. (1949) *Extrapolation, Interpolation, and Smoothing of Stationary Time Series*. MIT Press.
- Zhang, H.T., (2003), *Multipath: Theory, Influence and Mitigation*, ENGO 625 Lead Discussion, The University of Calgary
- Zhang, H.T., Petovello, M.G., and Cannon, M.E. (2005). *Performance Comparison of GPS Integrating with Different Tactical Level IMU*, Proceedings of NTM 2005, The Institute of Navigation, Fairfax, VA, pp.243-254.,
- Zhang, J. (1999). *Investigations into the Estimation of Residual Tropospheric Delays in a GPS Network*, MSc. Thesis, UCGE Report #20132, Department of Geomatics Engineering, University of Calgary.

APPENDIX A

The DOP (Dilution of Precision) value during the test and the elevation angle of each satellite during the test are given in Figure A.1 and Figure A.2.

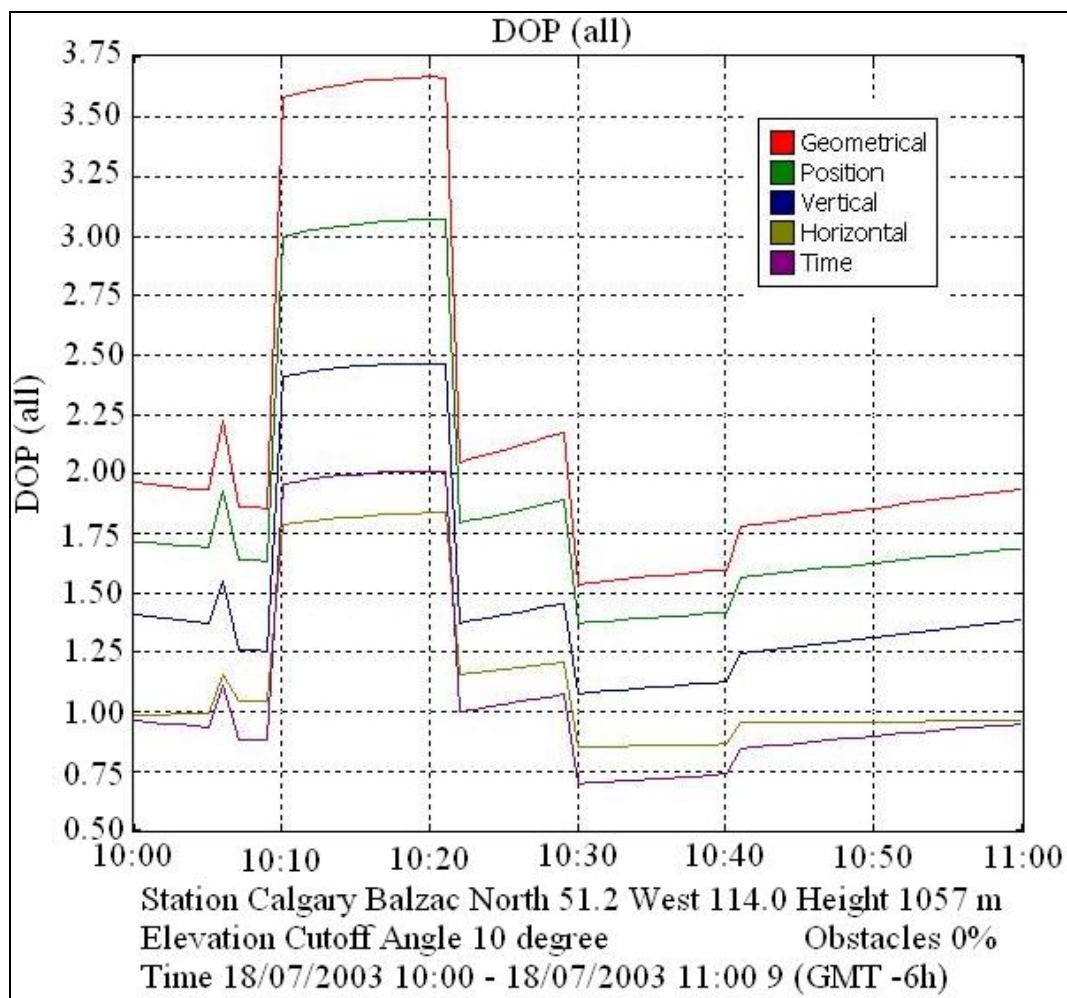


Figure A.1 DOP Value During Data Collection

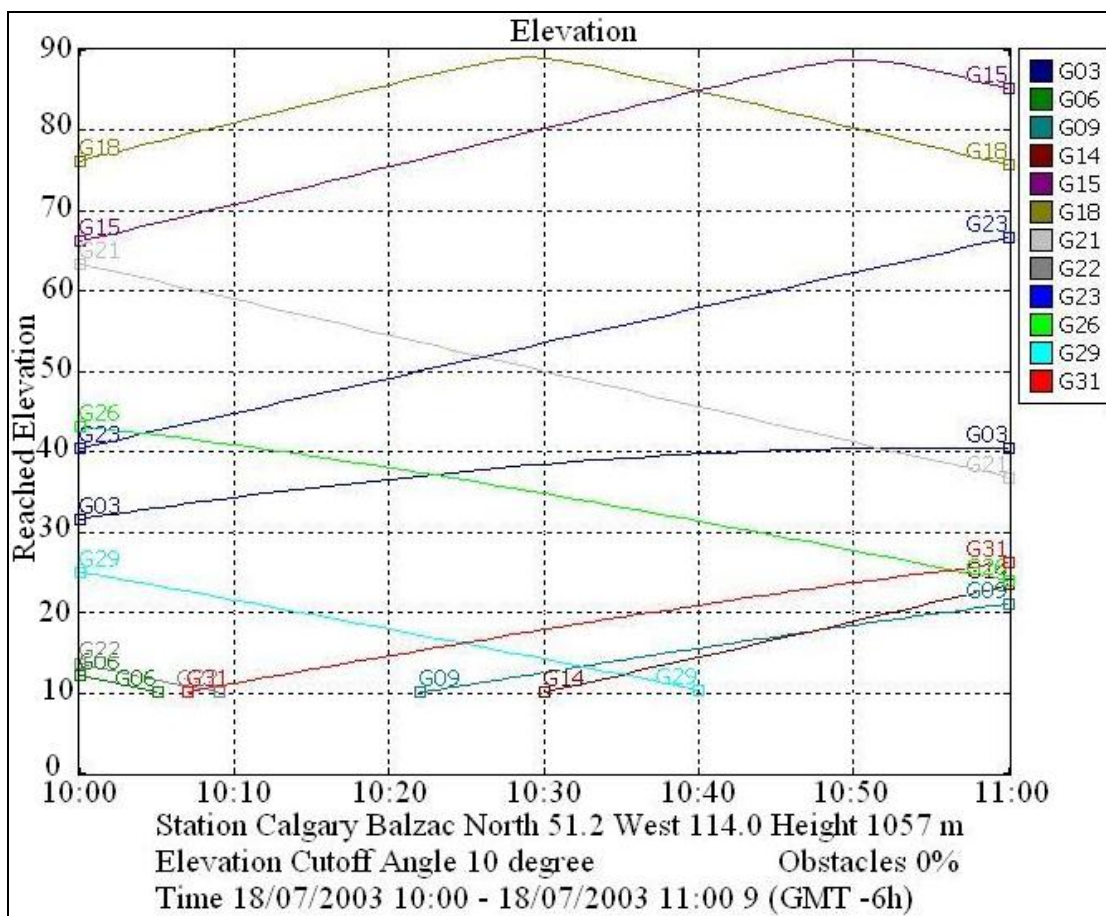


Figure A.2 Satellite Elevation Angle during Data Collection

APPENDIX B

The position error difference comparisons before and after smoothing are given in Appendix B. The following Figure B.1 to Figure B.18 shows that the difference in each of the simulated outages. The blue line represents the position error before smoothing, and the red line represents the position error of smoothed results. For the sake of clarity, only the 100-second data outage results for HG1700/CDGPS and LN200/CDGPS systems are shown herein.

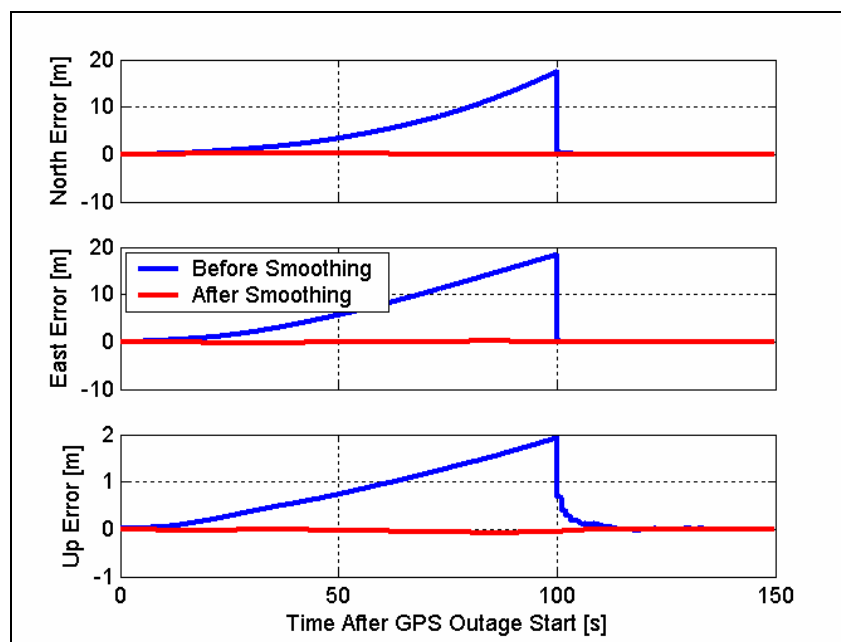


Figure B.1 Position Error at GPS Outage #1 (HG1700/CDGPS)

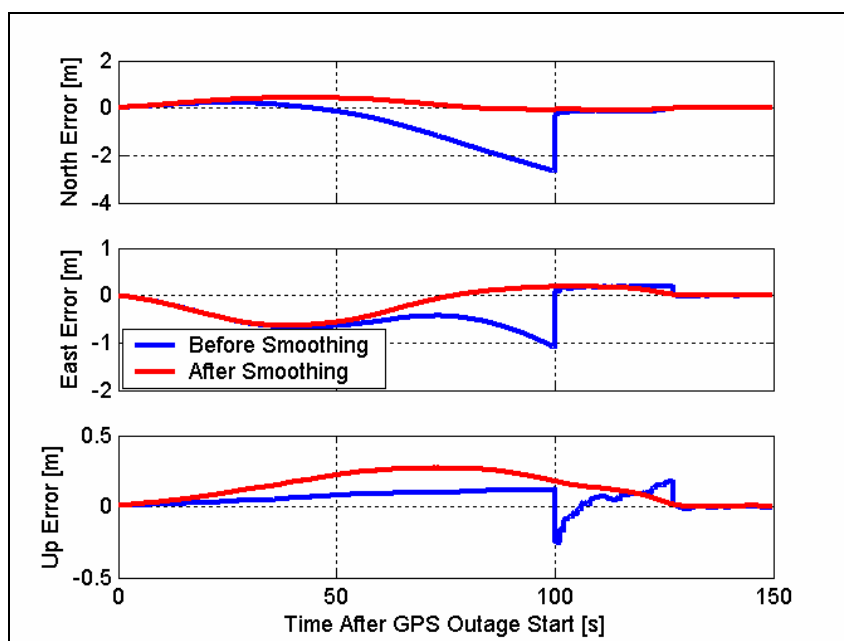


Figure B.2 Position Error at GPS Outage #2 (HG1700/CDGPS)

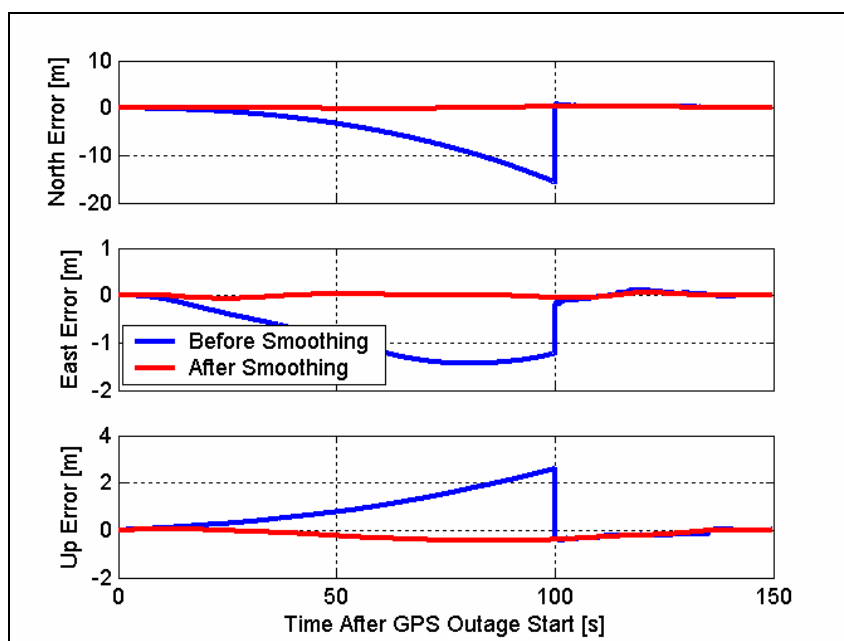


Figure B.3 Position Error at GPS Outage #3 (HG1700/CDGPS)

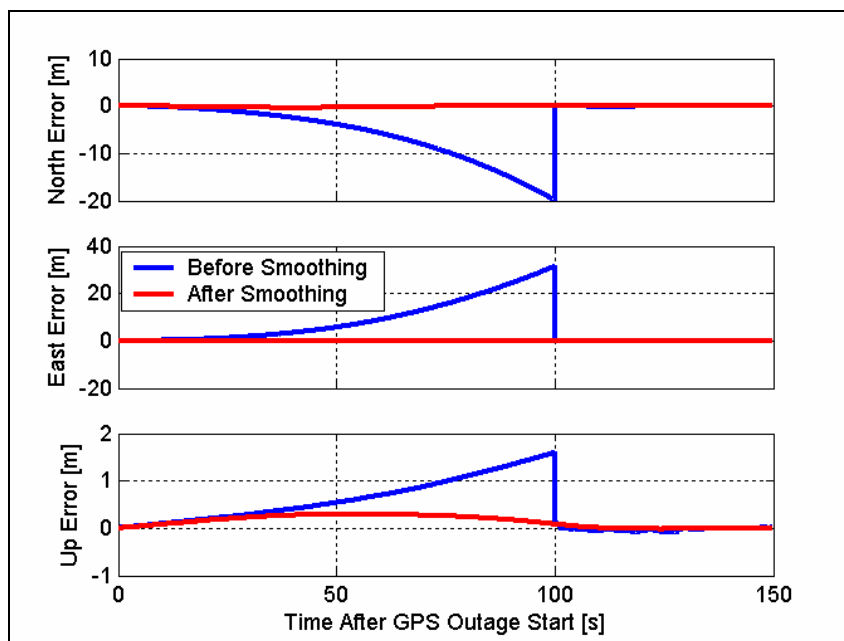


Figure B.4 Position Error at GPS Outage #4 (HG1700/CDGPS)

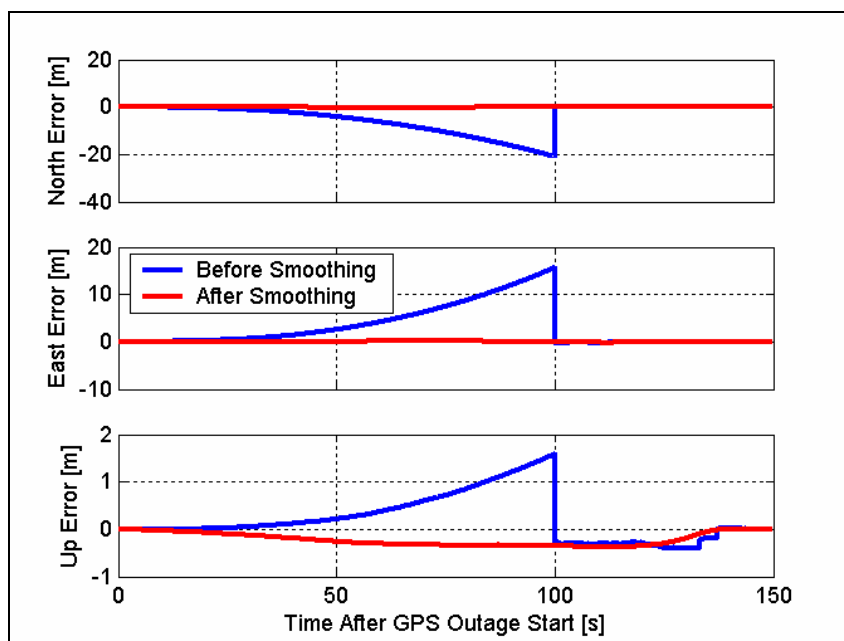


Figure B.5 Position Error at GPS Outage #5 (HG1700/CDGPS)

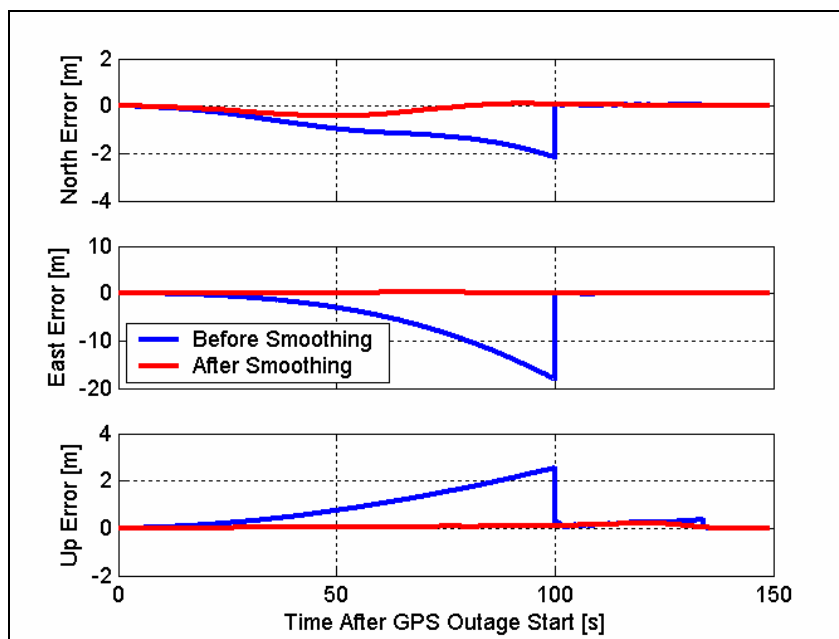


Figure B.6 Position Error at GPS Outage #6 (HG1700/CDGPS)

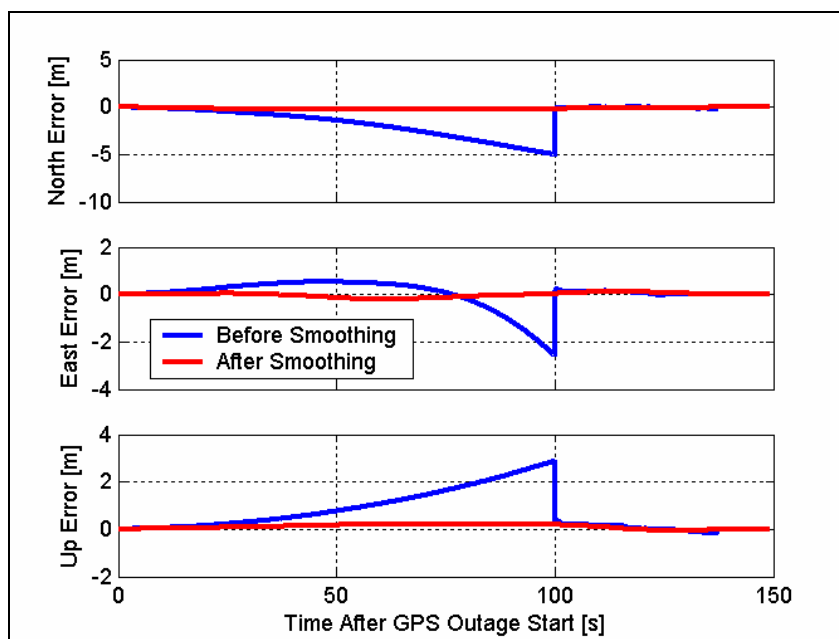


Figure B.7 Position Error at GPS Outage #7 (HG1700/CDGPS)

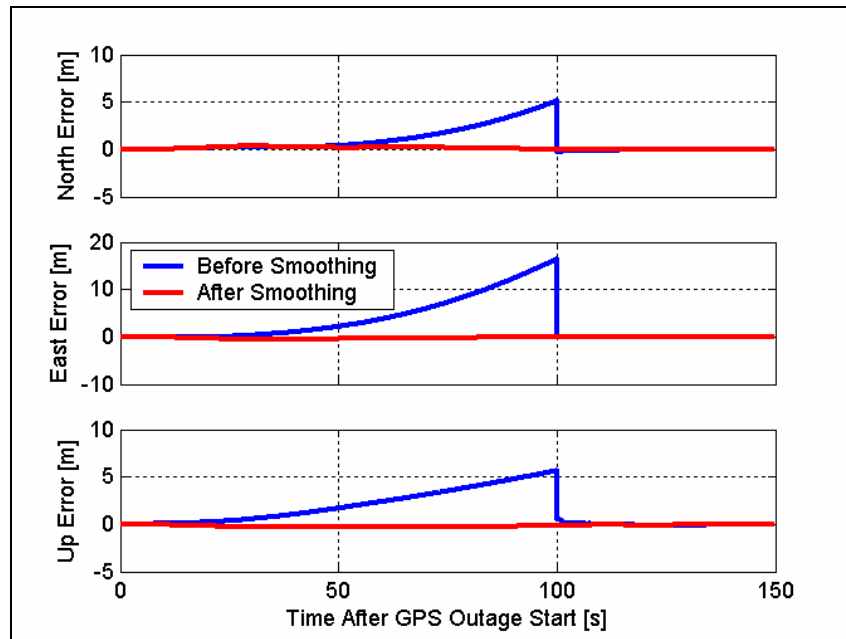


Figure B.8 Position Error at GPS Outage #8 (HG1700/CDGPS)

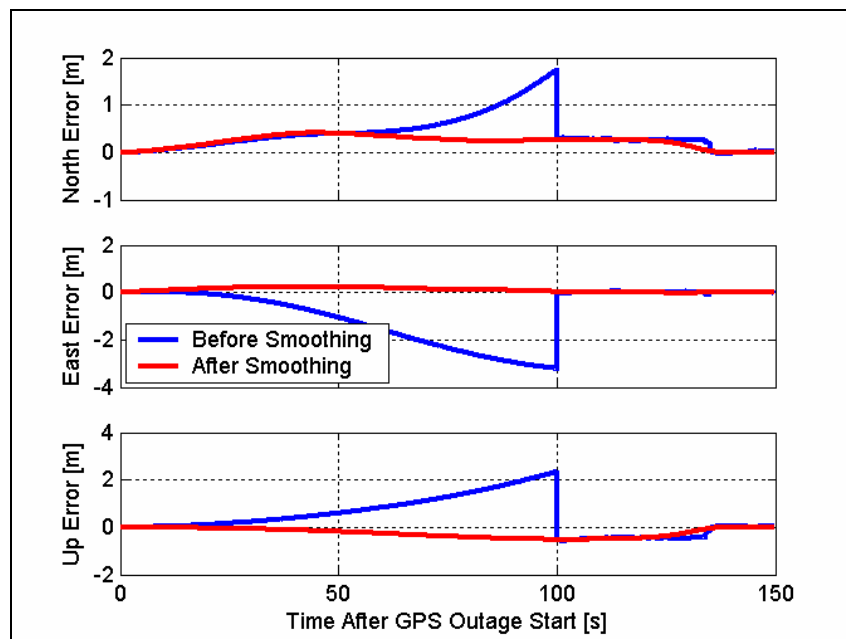


Figure B.9 Position Error at GPS Outage #9 (HG1700/CDGPS)

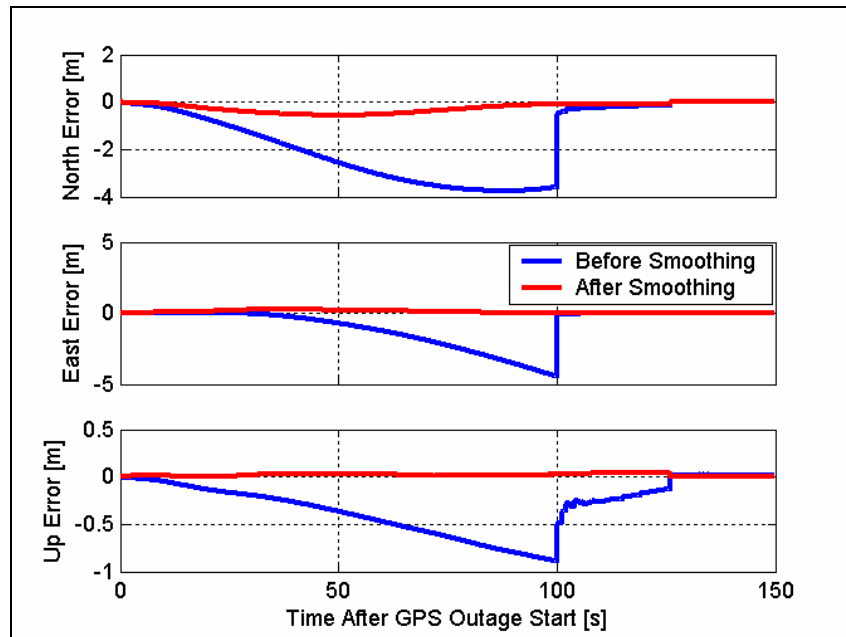


Figure B.10 Position Error at GPS Outage #1 (LN200/CDGPS)

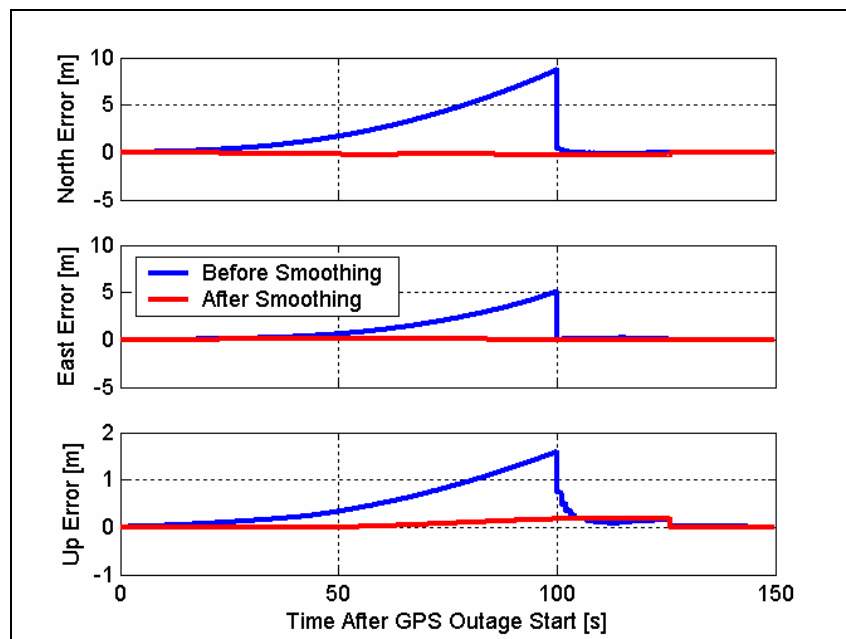


Figure B.11 Position Error at GPS Outage #2 (LN200/CDGPS)

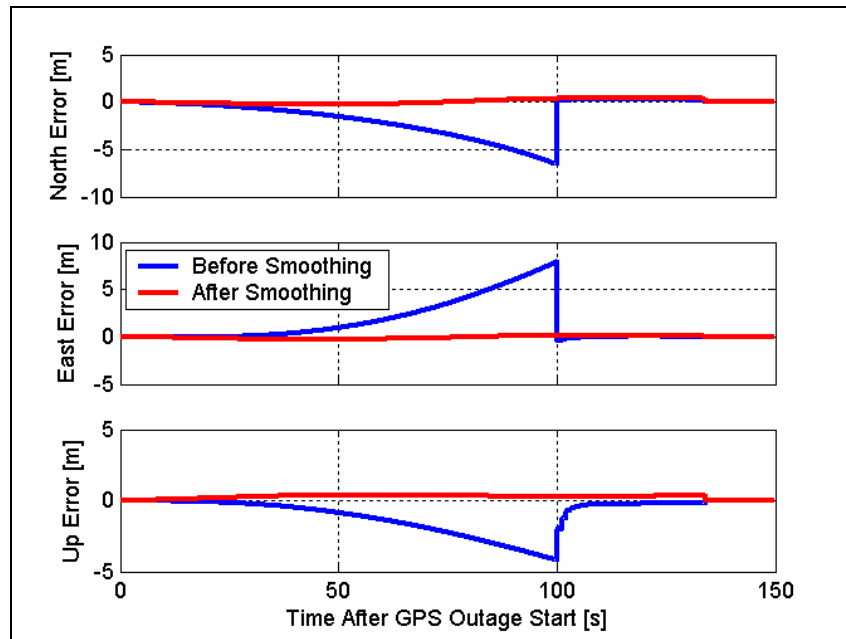


Figure B.12 Position Error at GPS Outage #3 (LN200/CDGPS)

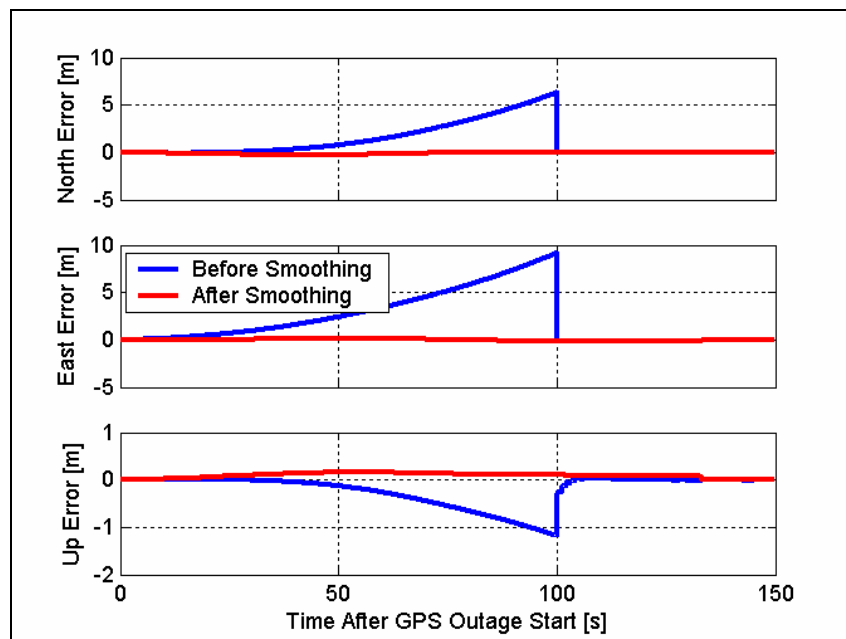


Figure B.13 Position Error at GPS Outage #4 (LN200/CDGPS)

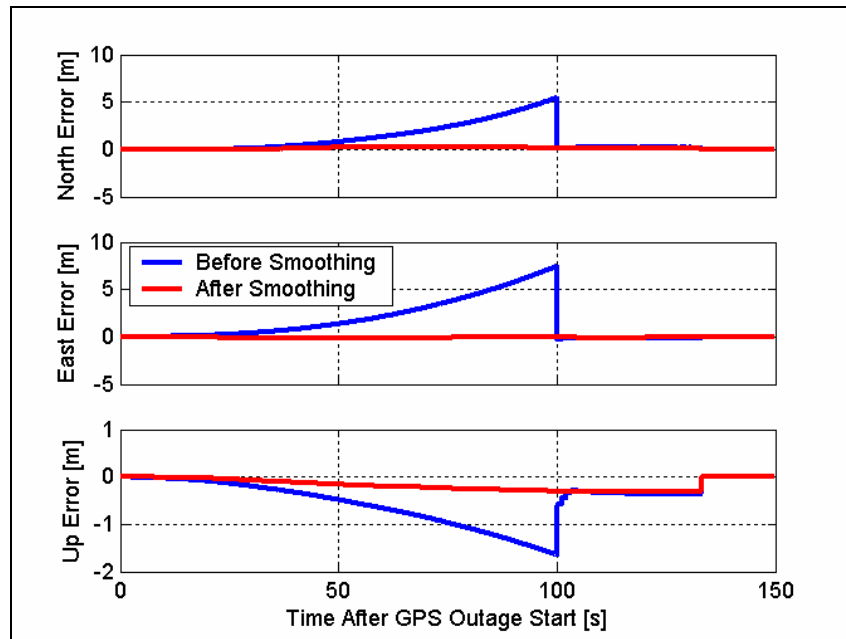


Figure B.14 Position Error at GPS Outage #5 (LN200/CDGPS)

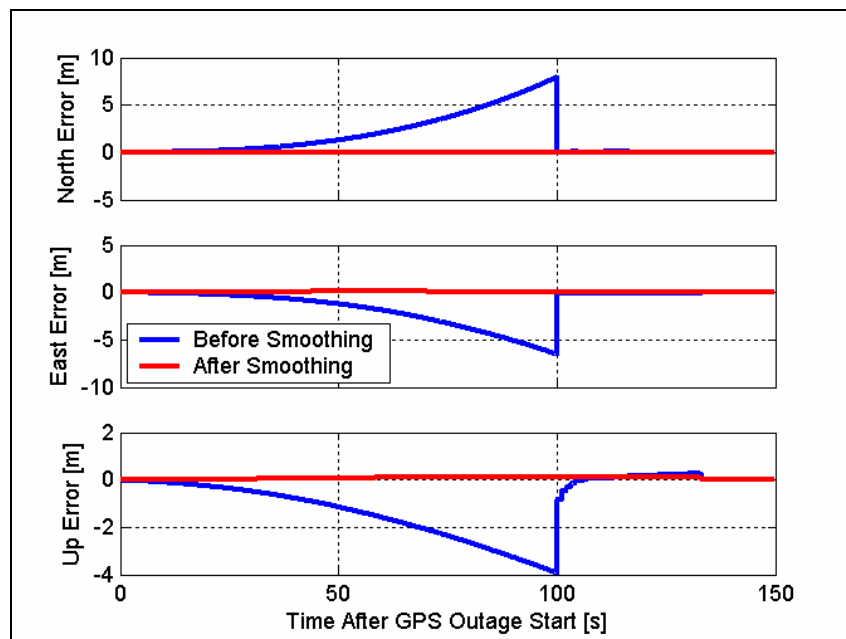


Figure B.15 Position Error at GPS Outage #6 (LN200/CDGPS)

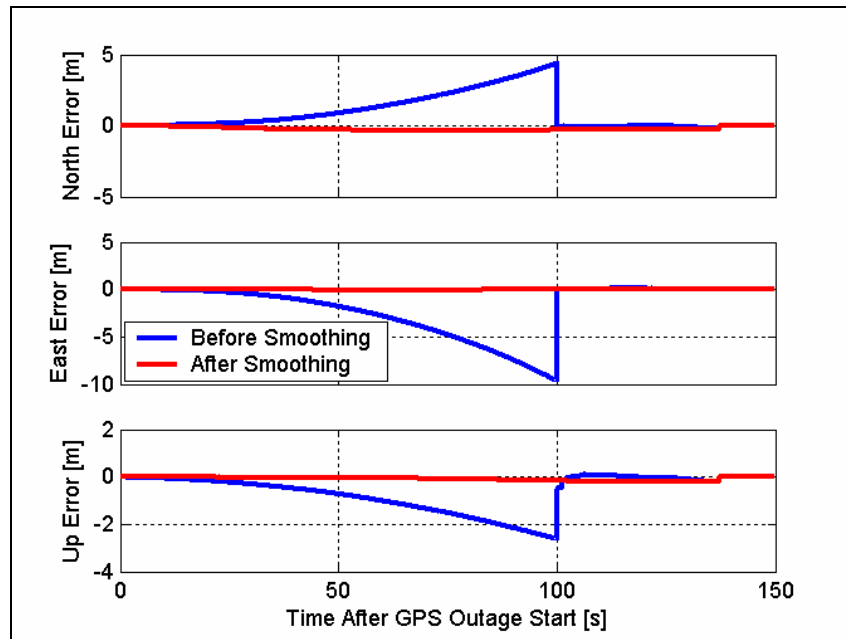


Figure B.16 Position Error at GPS Outage #7 (LN200/CDGPS)

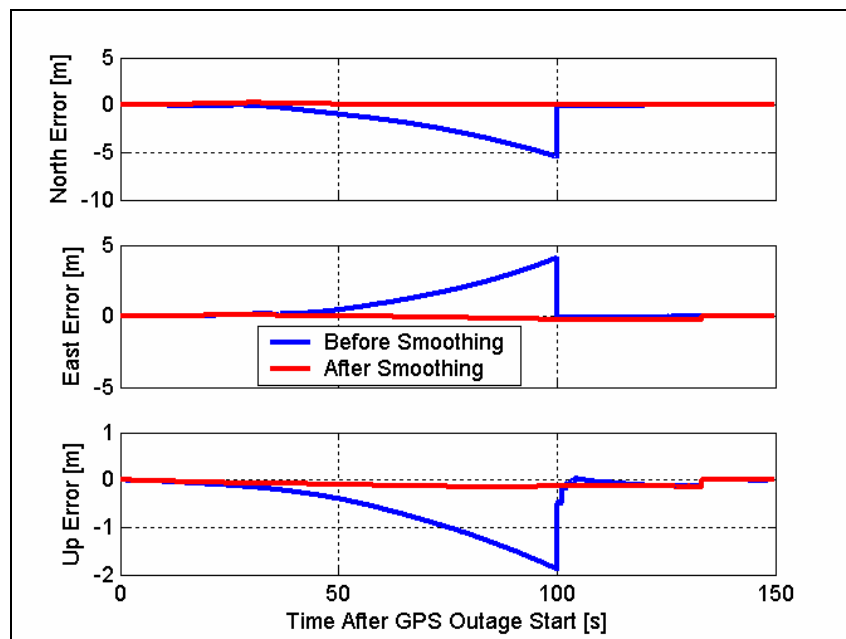


Figure B.17 Position Error at GPS Outage #8 (LN200/CDGPS)

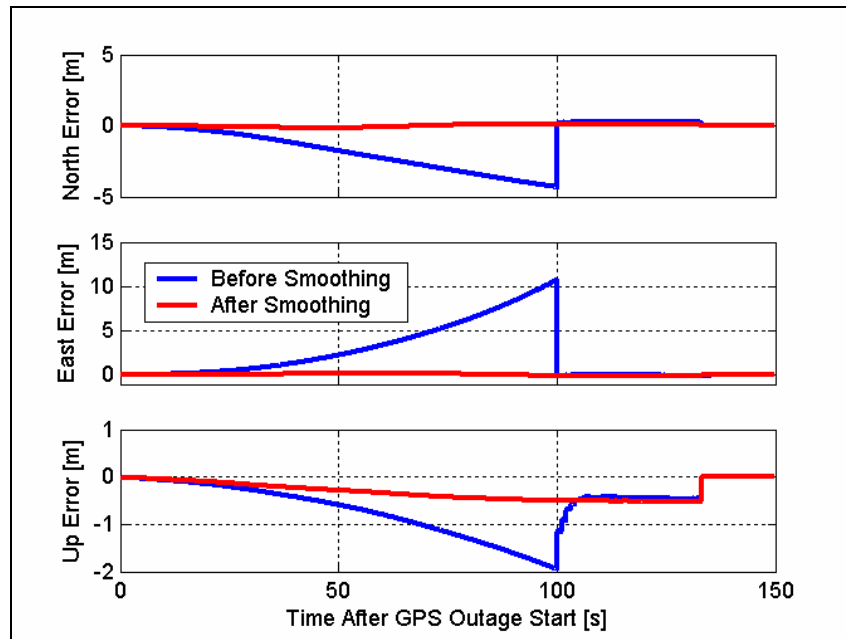


Figure B.18 Position Error at GPS Outage #9 (LN200/CDGPS)

APPENDIX C

The INS error model parameters and other parameters regarding the parameters which have been used to process GPS and INS test data in this particular research are given in Appendix C.

C.1 PROCESSING STRATEGY AND GPS MEASUREMENTS PARAMETERS

C/A code and Doppler measurements were always used to update the system. The carrier-phase measurements were L1 and L2. The selection of ambiguity processing strategy will ultimately decide which observation or observations will be selected based on Table 5.2. The variances of the different observations used in the processing of each strategy for all two baselines are given in Table C.1. For the comparison consistency, the variances given to the pseudorange for all strategies are the same. The L1 and L2 carrier-phase observation standard deviations are the same for Strategies 1 to 5. The L1 and L2 carrier-phase observation standard deviations for Strategies 6 and 7 are the same, however, lower than that of Strategies 1 to 5, because Strategies 6 and 7 models the DD ionospheric error explicitly. The standard deviation σ_0 for the short baseline is 10 cm and 50 cm for the long baseline because the long baseline has a much higher ionospheric error than that of short baseline.

Table C.1 Observation Standard Deviations

Strategy	Observation Standard Deviations			
	P (m)	CP ₁ (Cycle)	CP ₂ (Cycle)	l ₀ (m)
1	0.5	0.050	0.050	N/A
2	0.5	0.050	0.050	N/A
3	0.5	0.050	0.050	N/A
4	0.5	0.050	0.050	N/A
5	0.5	0.050	0.050	N/A
6	0.5	0.025	0.025	σ_0
7	0.5	0.025	0.025	σ_0

C.2 INS ERROR MODEL PARAMETERS

A first-order Gauss-Markov model is commonly used as error model to be included in the INS Kalman Filter. And a white noise power spectral density is needed to construct the noise distribution matrix as well. By studying the auto correlation sequences of the noise components at the output of initial sensors after wavelet de-noising and the standard variation of the noise components at the raw measurements of the initial sensors, we determined that a re-estimated first-order Gauss-Markov model and an estimated white noise spectral density can efficiently model such noise behavior for tactical grade IMU.

The detailed information about the method to estimate the first-order Gauss-Markov model parameters and a method to estimate the white noise power spectral density was given by Lachapelle *et, al.* (2003). The parameters of HG1700 and LN200 which were applied in this research were presented in this

section in following Table C.2.

Table C.2 Estimated Error Model Parameters

HG1700	X Gyro	Y Gyro	Z Gyro	X Acc	Y Acc	Z Acc
White noise SD	10^1 deg/hr/sqrt(Hz)			$7.8e-3^1$ m/s/s/sqrt(Hz)		
Bias GM σ	0.2605 (deg/hr)	0.2607 (deg/hr)	0.2613 (deg/hr)	3.411e-5 (m/s/s)	5.397e-5 (m/s/s)	7.231e-5 (m/s/s)
Bias τ (s)	392.9	392.9	397.7	397	382	432
LN200	X Gyro	Y Gyro	Z Gyro	X Acc	Y Acc	Z Acc
White noise SD	5.6 deg/hr/sqrt(Hz)			3.0e-3 m/s/s/sqrt(Hz)		
Bias GM σ	0.0139 (deg/hr)	0.0196 (deg/hr)	0.0204 (deg/hr)	4.894e-5 (m/s/s)	6.207e-5 (m/s/s)	7.070e-5 (m/s/s)
Bias τ (s)	337.8	265.9	336.2	365.7	292.0	315.3

¹ The white noise spectral density of each axis was considered to equal to the average value of three axis's variances

C.3 GPS DYNAMIC MODEL PARAMETERS

With respect to the DD carrier phase based GPS Kalman filter, for most navigation problems, the dynamics of the system are modeled using a random walk. Considering a random walk model for the velocity states $[v_x \ v_y \ v_z]^T$ with corresponding driving noise vector $[w_x \ w_y \ w_z]^T$, the equation relating the

$$v_x = w_x$$

white driving noise and the three velocity states are as $v_y = w_y$. The spectral

$$v_z = w_z$$

density for the driving noise vector $[sp_x \ sp_y \ sp_z]^T$ were set to $100 \text{ m}^2/\text{s}^3$.

APPENDIX D

The estimated double-differenced ionospheric delay for both the short and long baseline cases is given in this appendix. It begins with a discussion of the stochastic modeling of the DD ionospheric error.

Based on the very good temporal characteristics of the ionospheric error, Skone (1998) showed that a first order Gauss-Markov process is consistent with the observed temporal correlations in TEC. The following system model was employed to describe the evolution of the TEC:

$$VTEC(t_{j+1}) = e^{\frac{-\delta t}{T_0}} VTEC(t_j) + w(t_j)$$

where VTEC is the TEC component in the zenith direction, T_0 is the correlation time and $\delta t = t_{j+1} - t_j$. This property allows estimation of the ionospheric error through a Kalman filter. A Gauss-Markov process was used to model the ionospheric delay. The DD ionospheric error I_i in metres between the i^{th} satellite-receiver pair was modeled as a Gauss-Markov process with a driving noise w_i of spectral density σ_i in units of m^2/s , and a time constant T_0 in seconds. The discrete state-space equation for I_i is derived as $I_i^{k+1} = e^{\frac{-\delta t}{T_0}} I_i^k + w_i^k$;

the variance of the discrete white noise w_i^k is $\frac{\sigma_i T_0}{2} \left(1 - e^{\frac{-2\delta t}{T_0}} \right)$. The DD

ionospheric error state vector ($I_1, I_2, I_3 \dots$ and I_n) is then expanded into the Kalman filter.

Figure D.1 shows the estimated double-differenced ionospheric delay of all double difference satellite pairs versus baseline length using GPS-only, L1WL+I strategy for the short baseline case.

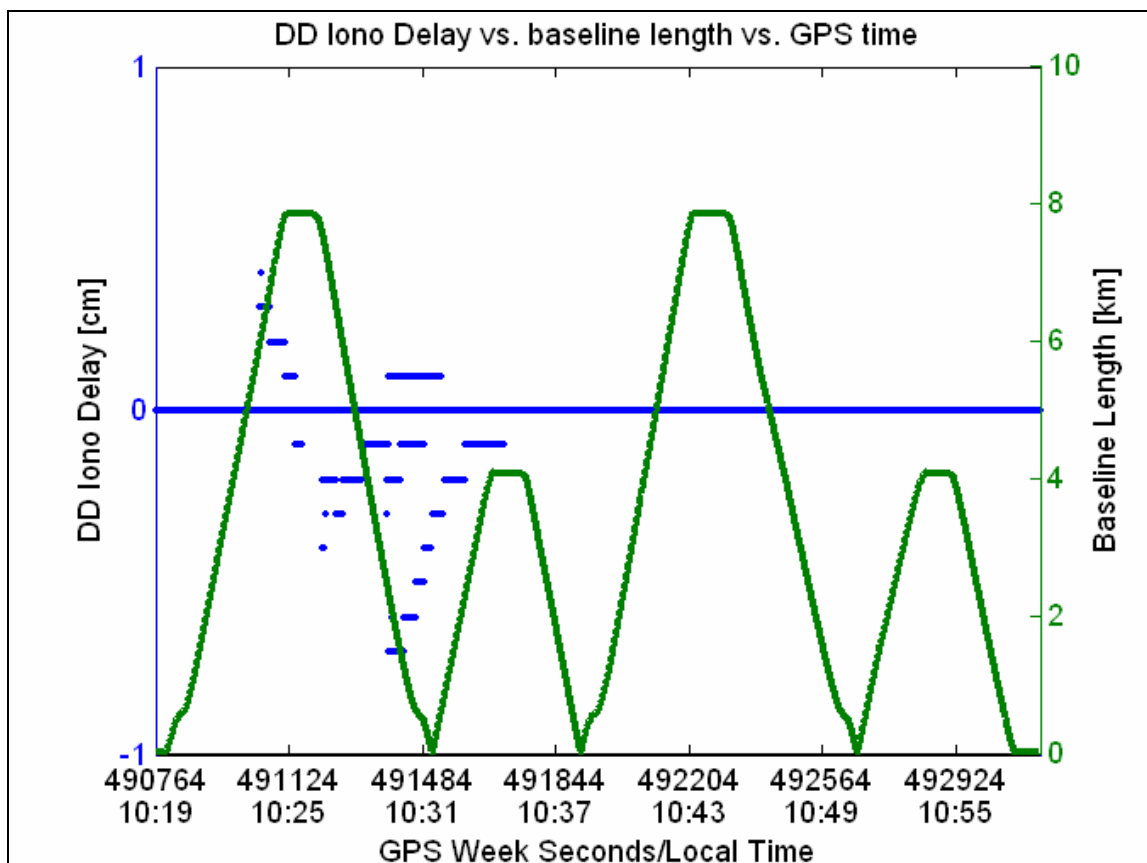


Figure D.1 Estimated DD Ionospheric Delay vs. Baseline Length vs. GPS Time

As can be seen, the double-differenced ionospheric delay, in the short baseline case, is less than 1 ppm.

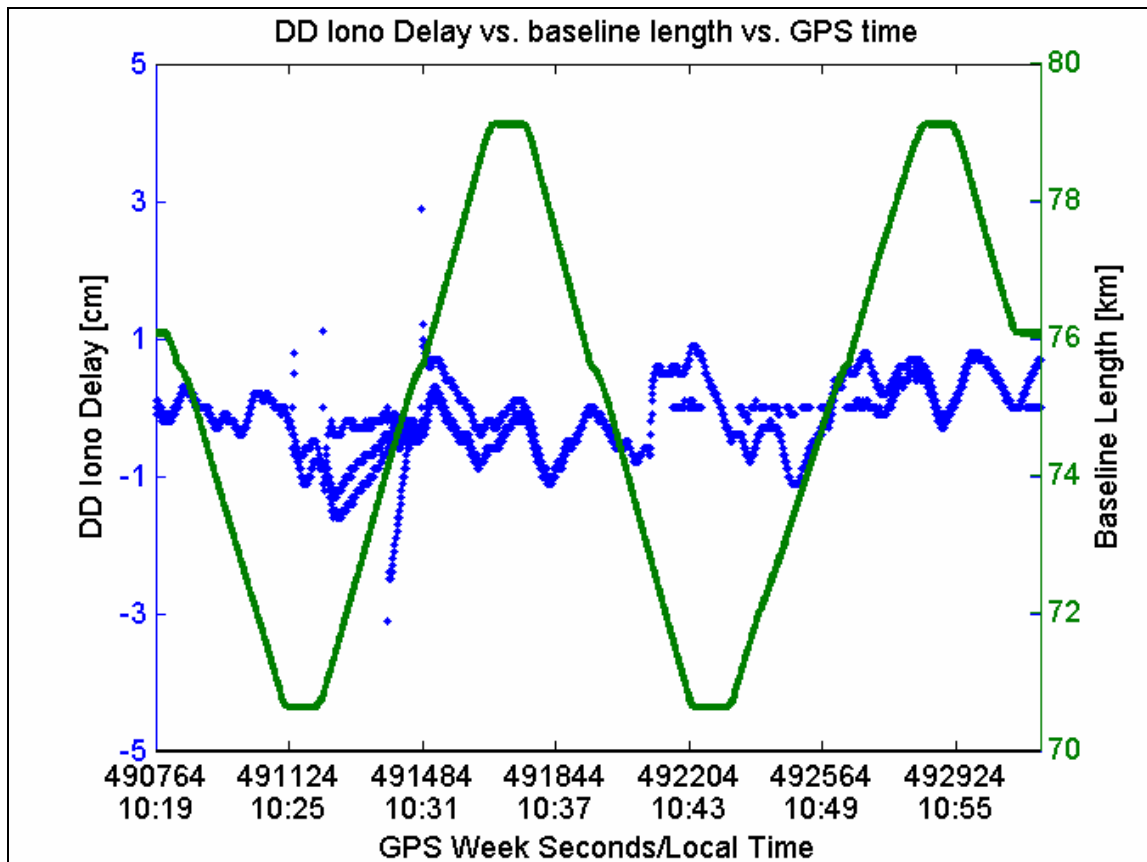


Figure D.2 Estimated DD Ionospheric Delay vs. Baseline Length vs. GPS Time

Figure D.2 shows the estimated double-differenced ionospheric delay of all double difference satellite pairs versus baseline length using GPS-only, and an L1WL+I strategy for the long baseline case. This means that the ionospheric error is not considered to be significant for the data set used herein.

APPENDIX E

The dynamics matrix of the 15 state Kalman filter linearized SINS error model in the local level and ECEF frames corresponding to Equation 2.12 are given in this appendix. The dynamics matrix in local level frame is as following.

$$\mathbf{F} = \begin{bmatrix}
 0 & 0 & F_{1,3} & | & 0 & F_{1,5} & 0 & | & 0 & 0 & 0 & | & 0 & 0 & 0 & | & 0 & 0 & 0 \\
 F_{2,1} & 0 & F_{2,3} & | & F_{2,4} & 0 & 0 & | & 0 & 0 & 0 & | & 0 & 0 & 0 & | & 0 & 0 & 0 \\
 0 & 0 & 0 & | & 0 & 0 & F_{3,6} & | & 0 & 0 & 0 & | & 0 & 0 & 0 & | & 0 & 0 & 0 \\
 - & - & - & + & - & - & - & + & - & - & - & + & - & - & - & + & - & - & - \\
 F_{4,1} & 0 & 0 & | & F_{4,4} & F_{4,5} & F_{4,6} & | & 0 & F_{4,8} & F_{4,9} & | & F_{4,10} & F_{4,11} & F_{4,12} & | & 0 & 0 & 0 \\
 F_{5,1} & 0 & 0 & | & F_{5,4} & F_{5,5} & F_{5,6} & | & F_{5,7} & 0 & F_{5,9} & | & F_{5,10} & F_{5,11} & F_{5,12} & | & 0 & 0 & 0 \\
 F_{6,1} & 0 & 0 & | & F_{6,4} & F_{6,5} & 0 & | & F_{6,7} & F_{6,8} & 0 & | & F_{6,10} & F_{6,11} & F_{6,12} & | & 0 & 0 & 0 \\
 - & - & - & + & - & - & - & + & - & - & - & + & - & - & - & + & - & - & - \\
 0 & 0 & F_{7,3} & | & 0 & F_{7,5} & 0 & | & & F_{7,8} & F_{7,9} & | & 0 & 0 & 0 & | & F_{7,13} & F_{7,14} & F_{7,15} \\
 F_{8,1} & 0 & F_{8,3} & | & F_{8,4} & 0 & 0 & | & F_{8,7} & & F_{8,9} & | & 0 & 0 & 0 & | & F_{8,13} & F_{8,14} & F_{8,15} \\
 F_{9,1} & 0 & F_{9,3} & | & F_{9,4} & 0 & 0 & | & F_{9,7} & F_{9,8} & & | & 0 & 0 & 0 & | & F_{9,13} & F_{9,14} & F_{9,15} \\
 - & - & - & + & - & - & - & + & - & - & - & + & - & - & - & + & - & - & - \\
 0 & 0 & 0 & | & 0 & 0 & 0 & | & 0 & 0 & 0 & | & F_{10,10} & 0 & 0 & | & 0 & 0 & 0 \\
 0 & 0 & 0 & | & 0 & 0 & 0 & | & 0 & 0 & 0 & | & 0 & F_{11,11} & 0 & | & 0 & 0 & 0 \\
 0 & 0 & 0 & | & 0 & 0 & 0 & | & 0 & 0 & 0 & | & 0 & 0 & F_{12,12} & | & 0 & 0 & 0 \\
 - & - & - & + & - & - & - & + & - & - & - & + & - & - & - & + & - & - & - \\
 0 & 0 & 0 & | & 0 & 0 & 0 & | & 0 & 0 & 0 & | & 0 & 0 & 0 & | & F_{13,13} & 0 & 0 \\
 0 & 0 & 0 & | & 0 & 0 & 0 & | & 0 & 0 & 0 & | & 0 & 0 & 0 & | & 0 & F_{14,14} & 0 \\
 0 & 0 & 0 & | & 0 & 0 & 0 & | & 0 & 0 & 0 & | & 0 & 0 & 0 & | & 0 & 0 & F_{15,15}
 \end{bmatrix}$$

$$F_{1,3} = -\frac{\dot{\varphi}}{M+h}$$

$$F_{1,5} = \frac{1}{M+h}$$

$$F_{2,1} = \dot{\lambda} \tan \varphi$$

$$F_{2,3} = -\frac{\dot{\lambda}}{N+h}$$

$$F_{2,4} = \frac{1}{(N+h)\cos\varphi}$$

$$F_{3,6} = 1$$

$$F_{4,1} = 2\omega_e(v^U \sin\varphi + v^N \cos\varphi) + \frac{v^N \dot{\lambda}}{\cos\varphi}$$

$$F_{4,4} = \frac{-v^U + \dot{\varphi} \tan\varphi(M+h)}{N+h}$$

$$F_{4,5} = (2\omega_e + \dot{\lambda})\sin\varphi$$

$$F_{4,6} = -(2\omega_e + \dot{\lambda})\cos\varphi$$

$$F_{4,8} = f^U$$

$$F_{4,9} = -f^N$$

$$F_{4,10} = R_{11}$$

$$F_{4,11} = R_{12}$$

$$F_{4,12} = R_{13}$$

$$F_{5,1} = 2\omega_e v^E \cos\varphi - \frac{v^E \dot{\lambda}}{\cos\varphi}$$

$$F_{5,4} = -2(\omega_e + \dot{\lambda})\sin\varphi$$

$$F_{5,5} = -\frac{v^U}{M+h}$$

$$F_{5,6} = \dot{\varphi}$$

$$F_{5,7} = -f^U$$

$$F_{5,9} = f^E$$

$$F_{5,10} = R_{21}$$

$$F_{5,11} = R_{22}$$

$$F_{5,12} = R_{23}$$

$$F_{6,1} = -2\omega_e v^E \sin\varphi$$

$$F_{6,3} = \frac{2\gamma^U}{R_e}$$

$$F_{6,4} = 2(\omega_e + \dot{\lambda})\cos\varphi$$

$$F_{6,5} = 2\dot{\varphi}$$

$$F_{6,7} = f^N$$

$$F_{6,8} = -f^E$$

$$F_{6,10} = R_{31}$$

$$F_{6,11} = R_{32}$$

$$F_{6,12} = R_{33}$$

$$F_{7,3} = -\frac{\dot{\varphi}}{M+h}$$

$$F_{7,5} = \frac{1}{M+h}$$

$$F_{7,8} = (\omega_e + \dot{\lambda})\sin\varphi$$

$$F_{7,9} = -(\omega_e + \dot{\lambda})\cos\varphi$$

$$F_{7,13} = R_{11}$$

$$F_{7,14} = R_{12}$$

$$F_{7,15} = R_{13}$$

$$F_{8,1} = \omega_e \sin \varphi$$

$$F_{8,3} = \frac{\dot{\lambda} \cos \varphi}{N + h}$$

$$F_{8,4} = -\frac{1}{N + h}$$

$$F_{8,7} = -(\omega_e + \dot{\lambda}) \sin \varphi$$

$$F_{8,9} = -\dot{\varphi}$$

$$F_{8,13} = R_{21}$$

$$F_{8,14} = R_{22}$$

$$F_{8,15} = R_{23}$$

$$F_{9,1} = -\omega_e \cos \varphi - \frac{\dot{\lambda}}{\cos \varphi}$$

$$F_{9,3} = \frac{\dot{\lambda} \sin \varphi}{N + h}$$

$$F_{9,4} = -\frac{\tan \varphi}{N + h}$$

$$F_{9,7} = (\omega_e + \dot{\lambda}) \cos \varphi$$

$$F_{9,8} = \dot{\varphi}$$

$$F_{9,13} = R_{31}$$

$$F_{9,14} = R_{32}$$

$$F_{9,15} = R_{33}$$

$$F_{10,10} = -\beta_{b^x}$$

$$F_{11,11} = -\beta_{b^y}$$

$$F_{12,12} = -\beta_{b^z}$$

$$F_{13,13} = -\beta_{d^x}$$

$$F_{14,14} = -\beta_{d^y}$$

$$F_{15,15} = -\beta_{d^z}$$

where the superscripts E, N, and U denote East, North and upwards (zenith) respectively; M is the Earth's Meridian radius of curvature; N is the Earth's Prime vertical radius of curvature; φ , λ , h are latitude, longitude and height, respectively; ω_e is the angular rate for Earth rotation; v^E , v^N , v^U are velocity components represented in the local level frame; f^E , f^N , f^U are

accelerometer-specific force components in the local level frame; γ^U is normal gravity in the local level frame; β_{b^x} , β_{b^y} , β_{b^z} are gyro bias first order Gauss-Markov model coefficients for each axis; β_{d^x} , β_{d^y} , β_{d^z} are accelerometer drift first order Gauss-Markov model coefficients for each axis; and

$\mathbf{R}_b^l = \begin{bmatrix} R_{11} & R_{12} & R_{13} \\ R_{21} & R_{22} & R_{23} \\ R_{31} & R_{32} & R_{33} \end{bmatrix}$ is a rotation matrix between the IMU body frame and the

local level frame.

For the sake of clarity, the dynamics matrix in the ECEF frame was separated into 25 3 by 3 dimensional matrix and is represented as follows:

$$\mathbf{F} = \begin{bmatrix} \mathbf{0} & \mathbf{I} & \mathbf{0} & \mathbf{0} & \mathbf{0} \\ \mathbf{N}^e & -2\boldsymbol{\Omega}_{ie}^e & -\mathbf{F}^e & \mathbf{0} & \mathbf{R}_b^e \\ \mathbf{0} & \mathbf{0} & -\boldsymbol{\Omega}_{ie}^e & \mathbf{R}_b^e & \mathbf{0} \\ \mathbf{0} & \mathbf{0} & \mathbf{0} & -\boldsymbol{\beta}_b & \mathbf{0} \\ \mathbf{0} & \mathbf{0} & \mathbf{0} & \mathbf{0} & -\boldsymbol{\beta}_d \end{bmatrix}$$

where $\mathbf{R}_b^e = \begin{bmatrix} R_{11} & R_{12} & R_{13} \\ R_{21} & R_{22} & R_{23} \\ R_{31} & R_{32} & R_{33} \end{bmatrix}$ represents the rotation matrix between the IMU

body frame and the ECEF frame; $\mathbf{F}^e = \begin{bmatrix} 0 & f_z & -f_y \\ -f_z & 0 & f_x \\ f_y & -f_x & 0 \end{bmatrix}$ is the skew-symmetric

matrix for the specific force vector given in the ECEF frame; the coefficient

matrix

$$\mathbf{N}^e = \begin{bmatrix} N_{11} & N_{12} & N_{13} \\ N_{21} & N_{22} & N_{23} \\ N_{31} & N_{32} & N_{33} \end{bmatrix} = \frac{kM}{r^3} \begin{bmatrix} -1 + \frac{3x^2}{r^2} & \frac{3xy}{r^2} & \frac{3xz}{r^2} \\ \frac{3yx}{r^2} & -1 + \frac{3y^2}{r^2} & \frac{3yz}{r^2} \\ \frac{3zx}{r^2} & \frac{3zy}{r^2} & -1 + \frac{3z^2}{r^2} \end{bmatrix} + \begin{bmatrix} \omega_e^2 & 0 & 0 \\ 0 & \omega_e^2 & 0 \\ 0 & 0 & 0 \end{bmatrix},$$

where r is the length of the geocentric position vector and kM is the product of

the Newtonian gravitational constant, and the Earth's mass; $\boldsymbol{\Omega}_{ie}^e = \begin{bmatrix} 0 & -\omega_e & 0 \\ \omega_e & 0 & 0 \\ 0 & 0 & 0 \end{bmatrix}$

is the skew-symmetric matrix for the Earth rotation rate; \mathbf{I} is a 3 x 3 identity

matrix; $\boldsymbol{\beta}_b = \begin{bmatrix} \beta_{b^x} & 0 & 0 \\ 0 & \beta_{b^y} & 0 \\ 0 & 0 & \beta_{b^z} \end{bmatrix}$ is a diagonal matrix of 1/(correlation time) of the

first order Gauss-Markov process describing the accelerometer bias, and the

1/(correlation time) of the first order Gauss-Markov process describing the gyro

drifts is represented by $\boldsymbol{\beta}_d = \begin{bmatrix} \beta_{d^x} & 0 & 0 \\ 0 & \beta_{d^y} & 0 \\ 0 & 0 & \beta_{d^z} \end{bmatrix}$; and $\mathbf{0}$ is a 3 by 3 zero matrix.